

UCSF

UC San Francisco Electronic Theses and Dissertations

Title

Melanocytes, Melanocytic Nevi, and Progression to Melanoma

Permalink

<https://escholarship.org/uc/item/0t7438c4>

Author

McNeal, Andrew Scott

Publication Date

2020

Peer reviewed|Thesis/dissertation

Melanocytes, Melanocytic Nevi, and Progression to Melanoma


by
Andrew Scott McNeal

DISSERTATION
Submitted in partial satisfaction of the requirements for degree of
DOCTOR OF PHILOSOPHY

in
Biomedical Sciences

in the
GRADUATE DIVISION
of the
UNIVERSITY OF CALIFORNIA, SAN FRANCISCO

Approved:

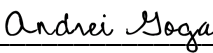
DocuSigned by:

BC645044B450408... K. Mark Ansel
Chair

DocuSigned by:

Robert Judson-Torres

DocuSigned by:

Alan Ashworth

DocuSigned by:

2582F8BD11124B6... Andrei Goga

Committee Members

Acknowledgments:

In many ways, it is difficult to imagine the end of graduate school. Perhaps it was easy at the beginning when the road appeared well-traveled, well-marked, and more or less straightforward. Having experienced this journey for myself, however, I now know this path to be filled with unexpected setbacks, detours, and occasional wonders. Fortunately, I have had the pleasure of meeting many people on the journey to my PhD, and I have many of them to thank for my success along the way.

First, I would like to thank Robert Judson-Torres, my PI, mentor, and fellow melanocyte enthusiast. Rob taught me to examine data in ways that helped uncover truths that were otherwise hidden or overlooked. He encouraged me to explore, to trust my instincts, and gave me a new appreciation for the complexity of biological systems. Rob's tireless work kept the lab running smoothly, freeing us to search and discover. I thank him for his continued guidance and support. Additionally, I want to thank the members of the Judson-Torres Lab including Hanlin, Apama, Rachel B, Helen, Ursula, and Rodrigo, and Rachel P for being wonderful co-workers who taught me a great deal, challenged my preconceived notions, and entertained my wild ideas.

Second, I would like to thank Alan Ashworth and the members of his lab for welcoming me into their group and continuing to support my research after my primary lab moved away. They are an exceptional group of scientists, always looking for opportunities to teach and learn, and they are steadfastly committed to improving the lives of those fighting cancer.

Alongside my two labs, I would like to thank the remaining members of my thesis committee, Mark Ansel and Andrei Goga for providing critical feedback and new perspectives on biology. Special thanks, as well, to my graduate cohort, especially Ton, Phi, Kim, Drew, Emily, and Tina, the members of the informal Mission Bay Lunch Club, for their emotional support, venting, and camaraderie.

Outside of UCSF, I owe many thanks to the San Francisco running community and most especially to the members of WeRunSF. Wednesday night runs were essential outlets that renewed my spirit and creativity. Special thanks to Sam, Leana, Jay, Frank, Joyce, Shimei, Paul, Anna, Marie, Victor, Vincent, Anant, Henry, Patrick, and Erin. You inspire me to better myself by setting goals and working to achieve them. Your determination, perseverance, and your fun-loving attitudes are infectious!

Most importantly, I would like to thank my family. Thank you, Mom and Dad, for everything you've done for me over the years. I could never have achieved what I have without your love and support. Thank you, Erin, Eric, and Emma, for being rays of sunshine enlivening the gloomiest San Francisco days.

Contributions

This manuscript contains data originally published in the following reports:

Background reports:

Chapter 2 Part 2 of this thesis was published in *Cancer Discovery* under the title “CDKN2B loss promotes progression from benign melanocytic nevus to melanoma.” *Cancer Discovery* 5, 1072-85 (2015). Co-authors of this manuscript include McNeal AS, Liu KL, Nakhate V, Natale CA, Capell BC, Dentchev T, Berger SL, Herlyn M, Seykora JT, Ridky TW.

Conception and Design: McNeal AS, Ridky TW, Seykora JT, Herlyn M. Development of methodology: McNeal AS, Ridky TW, Herlyn M. Data acquisition: McNeal AS, Liu K, Nakhate V, Natale CA, Duperret EK, Capell BC, Berger SL, Seykora JT, Ridky TW. Data analysis and interpretation: McNeal AS, Liu K, Nakhate V, Natale CA, Duperret EK, Capell BC, Seykora JT, Ridky TW. Writing, review, and/or revision of manuscript: McNeal AS, Liu K, Nakhate V, Natale CA, Duperret EK, Capell BC, Dentchev T, Seykora JT, Ridky TW. Administrative, technical or material support: McNeal AS, Liu K, Ridky TW. Study supervision: Berger SL, Ridky TW.

Reports reflecting thesis work:

Chapter 2 Part 3 of this dissertation was published in *Cancer Cell* under the title “Bi-allelic loss of CDKN2A initiates melanoma invasion and metastasis via E2F1-BRN2 axis.” *Cancer Cell* 56:68-84, (2018). Co-authors of this manuscript include Zeng H, Jorapur A, Shain AH, Lang UE, Torres R, Zhang Y, McNeal AS, Botton T, Lin J, Donne M, Bastian IN, North JP, Pincus L, Joseph NM, Yeh I, Bastian BC, Judson RL.

H.Z. conducted engineering, cell, and molecular assays in Figures 3, 5, 7, S1–S4, and S6. A.J. conducted cell, molecular, and mouse studies in Figures 3D,3E, 4, 5E, and S4. A.H.S. conducted genome and RNA analyses in Figures 1F, 4A–4C, and 6A. U.E.L. contributed to

case identification and analyses in Figures 6, 7I, 7J, S5, and S6. R.T. conducted RNA analysis in Figures 5A and 7A. J.L. conducted telomere length assay in Figure S2B. Y.Z., T.B., A.S.M., M.D., I.N.B., and R.Y. assisted in molecular, mouse, and computational work. J.P.N., L.P., and B.S.R. provided histopathology and diagnosis for cases in Figure 6. N.M.J. provided histopathology, diagnosis, and microdissection for cases in Figure 6. I.Y. and B.C.B. contributed to case identification, histopathology, diagnosis, and analyses for cases in Figure 6, and provided significant intellectual contribution. R.L.J. conceived of and directed all experiments and conducted engineering, cell and molecular assays in Figures 1, 2, 7, S1, S2, and S6. R.L.J., B.C.B., H.Z., T.B., and A.H.S wrote the paper.

Chapter 3 of this dissertation is currently in submission to *Cancer Discovery* under the manuscript title: “microRNAs Restrain Proliferation in BRAF^{V600E} Melanocytic Nevi.” Co-authors of this manuscript include McNeal AS, Belote RL, Zeng H, Barker K, Torres R, Shain AH, Andtbacka R, Holmen S, Lum DH, McCalmont TH, Van Brocklin, MW, Wei M, Lang UE, Ashworth A, Judson-Torres RL.

McNeal AS: Investigation, Formal analysis, Writing – original draft, Visualization, Funding acquisition; Belote, RL: Methodology, Resources, Writing – review & editing; Hanlin Zeng: Methodology, Investigation, Validation; Barker, K: Investigation; Torres,R: Formal analysis; A. Hunter Shain: Data curation; Robert Andtbacka: Resources; Holmen S, Lum DH, Van Brocklin MW: Conceptualization; Timothy H McCalmont, Wei M: Resources; Lang, UE: Investigation, Resources, Writing – review & editing; Judson-Torres RL: Conceptualization, Formal analysis, Investigation, Writing – original draft, Visualization, Supervision, Funding acquisition.

Chapter 4 of this dissertation is currently being developed into a manuscript with the working title: “Primary Cilia Loss is Consistent Across Multiple Genomic and Transcriptomic Pathways in

Melanoma Progression”. Co-authors of this manuscript include McNeal AS, Jankowski T, Shain AH, Joseph NM, Judson-Torres RL, Lang UE.

McNeal AS: Investigation, formal analysis, writing, visualization; Jankowski T: Methodology, writing, reviewing and editing; Shain AH: Data curation; Joseph NM: Data curation, resources; Judson-Torres RL: Formal analysis, writing, reviewing and editing; Lang UE: Conceptualization, Formal analysis, Investigation, Writing – original draft, Visualization, Supervision, Funding acquisition.

Abstract

Melanocytes, Melanocytic Nevi, and Progression to Melanoma

Andrew S. McNeal

Benign melanocytic nevi form when melanocytes that acquire a BRAF^{V600E} mutation undergo a period of rapid proliferation followed by subsequent growth-arrest. Constitutive activation of MAPK signaling downstream of BRAF drives the initial proliferative phenotype. However, the factors that establish and maintain growth-arrest in nevi remain elusive.

Here we investigate the contributions of several potential mediators of BRAF^{V600E}-induced growth arrest in nevus melanocytes. These mediators include the gene products of the CDKN2A-CDKN2B genetic locus, nevus-enriched microRNAs MIR211-5p and MIR328-3p, as well as transcriptional networks associated with primary cilia expression.

p16^{INK4A}, the cyclin dependent kinase inhibitor encoded by CDKN2A, has historically been associated with nevus formation. CDKN2B's gene product, p15^{INK4B}, remained under-studied in the context of nevus formation. Using primary melanocytes isolated directly from human nevi and naturally expressing the BRAFV600E-activating mutation, nevi progressing to melanoma, and normal melanocytes engineered to inducibly express BRAF^{V600E}, we showed that p15^{INK4B} expression is required for growth arrest in nevi and that loss promotes progression to melanoma. Investigating the role of the p16^{INK4A} tumor suppressor in nevus formation and progression to melanoma, we found that loss of p16^{INK4A} contributes to melanocyte hypermotility *in vitro* and increases invasive and metastatic behavior of melanoma cell lines *in vivo*. Using CRISPR-Cas9 to engineer a cellular model of melanoma initiation from primary human melanocytes, we determined that E2F1 upregulation as a consequence of CDKN2A loss drives these new phenotypes.

Additional acquired genetic alterations do not distinguish proliferating BRAF^{V600E} melanocytes from their growth-arrested nevus counterparts, suggesting a role for regulatory

elements. We investigated the role of microRNAs in the initiation and maintenance of nevus growth arrest. Using primary human melanocytes, melanocytic nevi, and adjacent melanoma, we show that MIR211-5p and MIR328-3p are enriched in nevi compared to normal melanocytes, then subsequently downregulated in adjacent melanoma. Both MIR211-5p and MIR328-3p proved necessary effectors of BRAF^{V600E}-induced growth arrest in human melanocytes. We identified microRNA target networks which, when suppressed, phenocopy BRAF^{V600E}-induced growth arrest and converge on inhibition of AURKB to block cell cycle progression in primary human melanocytes.

Similarly, expression of the primary cilium organelle has been shown to differentiate nevi from malignant melanoma. Investigations of primary cilia-associated gene expression in matched nevus and melanoma cases demonstrates that transcriptional changes in core primary cilia genes and related signaling molecules accompanies loss of the organelle during progression to melanoma.

Taken together, these data suggest that the BRAFV600E mutation leads to a cascade of intracellular changes that establish and maintain of growth arrest in human melanocytic nevi.

Table of Contents

Chapter 1: Introduction	1
Part 1: Overview of Melanocyte Biology	1
Part 2: Melanoma Biology	5
Part 3: Melanocytic Nevus Biology	12
Part 4: microRNA Biology	16
Part 5: microRNAs in Melanoma	19
Chapter 2: BRAF^{V600E} Drives Nevus Formation in Human Melanocytes	20
Part 1: Theories of BRAF ^{V600E} -mediated growth arrest in melanocytes	20
Part 2: Role of CDKN2B in BRAF ^{V600E} -mediated growth arrest	24
Part 3: Role of CDKN2A in growth arrest and additional roles in invasion and Metastasis	37
Part 4: Potential Regulation Beyond Cyclin Dependent Kinase Inhibitors	48
Chapter 3: microRNAs Restrain Proliferation in BRAF^{V600E} Melanocytic Nevi	49
Part 1: microRNAs regulate a nevus-specific transcriptome	49
Part 2: Role of MIR211-5p and MIR328-3p in Human Melanocytes and Nevus Formation	51
Part 3: Role of AURKB and GPR3 in Progression from Nevus to Melanoma	59
Part 4: Discussion of the role of microRNAs in nevus formation and progression to melanoma	65
Chapter 4: Primary Cilia in Melanocytic Nevi and Melanoma	69
Part 1: Biomarkers to distinguish nevi from melanoma	69

Part 2: Primary Cilia Biology	71
Part 3: Primary Cilia Expression in Nevi and Melanoma	73
Part 4: Transcriptional Profiling of Primary Cilia-associated Genes in Nevi and Melanoma	74
Chapter 5: Discussion	80-81
Materials and Methods	82-106
References	107-134

List of Figures

Figure 2.1: BRAFV600E-driven melanocyte growth arrest	25
Figure 2.2: p15 Expressed in nevi is a key factor mediating BRAF growth arrest	27
Figure 2.3: Active CDK4 reverses BRAFV600E-mediated melanocyte growth arrest	27
Figure 2.4: p15 is necessary and sufficient to arrest melanocyte proliferation	30
Figure 2.5: BRAF-Induced p15 is Decreased in Melanoma	32
Figure 2.6: TGF β secretion Induces p15 and drives melanocyte growth arrest	34
Figure 2.7: p15 loss reverses nevus-mc growth arrest and promotes progression to melanoma	36
Figure 2.8: Engineering CDKN2A null melanocytes	38
Figure 2.9: CDKN2A loss promotes melanocyte motility and invasion	41
Figure 2.10: p16INK4A regulates motility independent of driver mutation	44
Figure 2.11: p16INK4A loss induces metastasis in WM793 melanoma line	46
Figure 3.1: Identification of nevus-enriched microRNAs	53
Figure 3.2: Screening and validation of MIR211-5p and MIR328-3p mimics	54
Figure 3.3: MIR211-5p and MIR328-3p induce growth arrest in human melanocytes	56
Figure 3.4: BRAFV600E induced growth arrest requires MIR211-5p and MIR328-3p	58
Figure 3.5: Identification of MIR211-5p and MIR328-3p mRNA targets	60
Figure 3.6: AURKB and GPR3 inhibition contribute to BRAFV600E-induced growth arrest	62
Figure 3.7: Melanoma Growth Requires AURKB Expression	64
Figure 4.1: Differentially expressed primary cilia-associated gene expression in nevi and melanoma	75
Figure 4.2: Nevus-enriched primary cilia gene expression distinguishes nevi from melanoma	76

Chapter 1: Introduction

Part 1. Overview of Melanocyte Biology

Melanocytes are dendritic, pigment-producing cells. Cytologically, they are characterized as having two or more dendritic processes that protrude from the main cell body (Fitzpatrick and Szabo, 1959). Melanocytes are found in the uvea of the eye, the inner ear, the meninges of the brain, as well as in the bones and heart, however, they are most commonly associated with the skin (Yamaguchi and Hearing, 2014). A defining feature of melanocytes is their ability to produce pigment, known as melanin, which contributes to the range of scale, feather, fur, and skin coloring that we observe in nature. Melanin has two forms, a red/yellow pigment called pheomelanin and a brown/black pigment known as eumelanin. In addition to their different coloration, eumelanin and pheomelanin also differ in their size, shape, and granule packaging (Lin and Fisher, 2007). Both types of melanin, however, are derived from the common precursor, tyrosine. To begin melanogenesis (the process of making melanin), tyrosine is hydrolyzed to dopaquinone. From here, the chemical synthesis pathways diverge for each type of melanin. Due to the potential chemical risks posed by both melanin synthesis pathways, melanin production occurs in specialized lysosome-like structures called melanosomes. Melanosomes are trafficked from melanocytes to adjacent keratinocytes where they provide protection against ultra violet radiation (UV) (Yamaguchi and Hearing, 2009).

The process of pigment production and trafficking from melanocytes to surrounding keratinocytes underlies the phenomenon known as “tanning”. UV light from sun rays damage keratinocytes in the upper layers of the skin. In response, keratinocytes secrete several molecules, the most well-studied of which is alpha melanocyte stimulating hormone or α -MSH. α -MSH binds to the melanocortin 1 receptor (MC1R), a G-protein coupled receptor (GPCR) expressed on the melanocyte cell membrane. Upon stimulation by α -MSH, MC1R activates

adenyl cyclase, which in turn activates cyclic AMP (cAMP). cAMP signaling activates Protein kinase A (PKA), which phosphorylates the transcription factor CREB. CREB, in turn, binds the MITF promoter and induces melanin synthesis (Westerhof, 2006). Although this is considered the primary pigmentation pathway, other peptides and hormones, such as estrogen, have been shown to stimulate pigment production in melanocytes (Natale et al., 2016). Diversity in human pigmentation and tanning responses is thought to arise from mutations in the melanin signaling and synthesis pathways. The balance of eumelanin and pheomelanin synthesis ultimately determines the pigmentation status of the individual.

Developmental lineage of melanocytes

Neural Crest Precursors

Melanocytes derive from neural crest cells which originate in the dorsal-most region of the neural tube. The neural crest precursors of melanocytes migrate from the embryonic trunk and also give rise to cells of the nervous system including neurons and glia (Mort et al., 2015). Models of chicken development demonstrated that the neural crest cells that become neurons and glia follow a ventral migration path through blocks of mesodermal cells that differentiate into the vertebral cartilage of the spine, while those that become melanocytes depart the trunk later and follow a path between the ectoderm and somites of the developing dermis (Erickson and Goins). In a seminal set of experiments, Henion and Weston isolated single migratory neural crest cells and allowed them to differentiate *in vitro*. Some cells gave rise to a mixture of neurons, glia, and melanocytes. Others gave rise to more restricted mixtures of neurons and glia or glia and melanocytes. Still others differentiated solely into a single lineage (Henion and Weston, 1997). While this study definitively showed that melanocytes derived from neural crest progenitors, the range of differentiation outcomes suggested that other extracellular factors were at work to determine the neural crest progenitor's ultimate cell fate.

Schwann Cell Precursors

In addition to late-migrating neural crest cells of the trunk, Dupin et al. showed that Schwann cells, a type of glial cell of the peripheral nervous system, could be de-differentiated in vitro to a precursor of glia and melanocytes. Today, there is a consensus that melanocytes originate from two distinct paths. First, they can differentiate from neural crest cells following a dorsolateral migration. Second, a Schwann cell glial/melanoblast progenitor migrating on the ventral path can also differentiate into melanocytes (Dupin et al., 2003).

Transcriptional regulation of melanocyte identity

Understanding of the developmental lineage of melanocytes is useful, but how are melanocytes defined at the molecular level? Melanocyte inducing transcription factor (formerly microphthalmia-associated transcription factor) or MITF is widely accepted as the master-regulator of melanocyte identity. Mice lacking MITF (Steingrímsson et al., 2004) or fish missing the *mitfa* ortholog (Lister et al., 1999) cannot make melanocytes. In 2003, Bejar et al. showed that expression of MITF in embryo-derived stem cells could induce melanocyte differentiation (Bejar, 2003). As further evidence, humans with Waardenburg Syndrome or Tietz Syndrome have specific loss-of-function mutations in the MITF gene and are characterized by a lack of pigment (Cortés-González et al., 2016).

Although MITF is required for melanocyte differentiation, it is part of a larger transcriptional program that defines melanocyte identity. In mammals, neural crest cells with active SRY-box transcription factor 10 (*SOX10*) expression become bi-potent progenitors of melanoblasts (a precursor of melanocytes) and glia. Specific expression of *SOX10* in conjunction with the paired box 3 (*PAX3*) gene has been shown to synergistically activate MITF (Potterf et al., 2000) (Watanabe et al., 2000). MITF activation results in downstream activation of the dopachrome tautomerase (*DCT*) (also known as *TRPM2*) and KIT proto-oncogene receptor tyrosine kinase (*KIT*) genes, which promote further differentiation to the melanocyte. Alternatively, MITF and KIT

can be inactivated in the melanoblast, while still retaining DCT expression, and these melanoblasts will form melanocyte stem cells (MSC) in the bulge of the hair follicle. From the hair follicle bulge, MSCs can differentiate into rapidly- dividing transit-amplifying cells in which MITF and KIT are re-activated and in turn replenish the differentiated melanocytes of the hair follicle and surrounding epidermis (Yoshida et al. 1996).

To colonize the epidermis and developing hair follicle, melanoblasts must proliferate and migrate. Failure to migrate can lead to un-pigmented patches seen in humans (Fleischman et al., 1991), numerous mouse mutants (Bennett and Lamoreux, 2003), and in selectively bred pie- bald horses (Hauswirth et al., 2012). Unexpectedly, in 2010, Li and colleagues demonstrated that crossing from the dermis to the epidermis is an active process that can occur without degradation of the basement membrane protein barrier (Li et al., 2010). During mammalian development, melanoblasts are thought to cross the epidermal/dermal membrane, although a melanoblast population persists in the dermis. Follicular melanocyte stem cells can act as an additional reservoir to replenish epidermal melanocytes (Nishimura, 2011). A separate MSC pool, identified in sweat glands, can also give rise to epidermal melanocytes (Okamoto et al., 2014). Furthermore, under wound healing conditions induced by UV-radiation, or mechanical wounding, MSCs have the potential to leave the bulge niche of the hair follicle and supply sources of epidermal melanocytes (Chou et al., 2013). Nevertheless, MSCs are a finite population and depletion of this population due to aging results in a failure to replenish follicular and epidermal melanocytes, leading to loss of hair pigmentation known as “greying” (Mort et al., 2015).

Part 2: Melanoma Biology

Melanoma is a dangerous skin cancer

Melanoma is a form of cancer arising from melanocytes. Cutaneous melanoma (melanoma arising from melanocytes of the skin) is the predominant form of melanoma, however, rarer forms exist, named for the originating melanocyte population. Non-cutaneous forms of melanoma include acral melanoma, which typically arises from melanocytes on the palms of hands or soles of feet as well as in the nail bed. Uveal melanoma, arises from melanocytes of the uvea of the eyes (Chattopadhyay et al., 2016), and mucosal melanoma develops from melanocytes of the mucous membrane (Ablain et al., 2018). Melanoma is the third most common form of skin cancer behind basal cell carcinoma (BCC) and squamous cell carcinoma (SCC), however it accounts for the largest number of skin cancer deaths world-wide (Siegel et al., 2017). The prevalence and mortality rate of melanoma make it a pressing issue for researchers and physicians to understand the etiology of the disease and for which to develop new and improved therapies.

Pathology of Melanoma

Melanoma arises when a melanocyte acquires a series of DNA mutations that allow it to clonally expand. Unchecked radial proliferation of melanocytes in the epidermis or at the basement membrane is referred to as melanoma *in situ*. When proliferative melanocytes descend through the basement membrane into the dermis, or in some cases, descend further into the dermis, the disease is referred to as invasive melanoma. Finally, malignant melanoma cells can acquire the ability to travel through the bloodstream and/or lymphatic system to colonize other organs, at which point the disease stage is referred to as metastatic melanoma.

According to The Cancer Genome Atlas (TCGA www.cancer.gov/about-nci/organization/ccg/research/structural-genomics/tcga), which collected DNA and RNA sequencing from 333 primary or metastatic melanomas arising in 331 patients, there are four

main genetic sub-types of cutaneous melanoma (Akbari et al., 2015). (Note: only 318 patients had matched tumor and germline tissue to determine the background mutation rate). B-RAF proto-oncogene (*BRAF*), the most commonly mutated gene in the cohort, was mutated in 52% (166/318) of the melanoma tumors sequenced. Among the *BRAF* mutations, the V600E (c.T1799A) mutation (124/166), which constitutively activates the kinase domain of the protein, occurred most frequently. V600K (18/166) and V600R, which similarly activate the kinase domain (3/166) were also present in the cohort. Activating mutations in the *NRAS* proto-oncogene (*NRAS*) were present in approximately 28% of the tumors and defined the second main sub-type. *NRAS* mutations were shown to be mutually exclusive of *BRAF* V600 mutations. Neurofibromin 1 (*NF1*) mutations defined the third main sub-type and accounted for approximately 14% of tumors. *NF1* mutations are thought to be loss of function mutations, which is consistent with its role as a GTP-ase activating protein known to suppress RAS activity. Inactivation of *NF1* could provide another means of activating RAS activity in the melanocyte. Mutations in *NF1* appear exclusive of tumors with *BRAF* V600 mutations, but can be found in tumors with activating *NRAS* mutations. The final melanoma sub-type is known as “Triple Wildtype” and is simply characterized by a lack of hotspot mutations in *BRAF*, *NRAS*, or *NF1*. *KIT*, *GNAQ*, *GNA11*, and *EZH2* are genes often mutated in this cohort.

Nearly all of the melanomas in this study (94%) had mutations that activated the MAPK signaling pathway strongly suggesting that MAPK signaling, which drives cell proliferation, plays an essential role in melanomagenesis. However, as I will discuss in the next section, MAPK activation alone is insufficient to drive melanocytes to malignant melanoma. The TCGA study further revealed that MAPK activation was frequently paired with inactivating mutations in tumor suppressors, the most common of which was loss of the *CDKN2A* locus, which encodes p14ARF and p16INK4A proteins. Additionally, mutations in the promoter of the *telomerase* (*TERT*) gene were common in melanoma (Akbari et al., 2015).

Working with paired samples of nevi (melanoma precursors) and adjacent melanoma, Shain and colleagues attempted to infer the order in which mutations are acquired in melanoma (Shain et al., 2015). They found that melanocytes are most likely to acquire MAPKinase activating mutations first. These mutations typically lead to a localized clonal expansion event known as a melanocytic nevus that I will discuss in the next section. Without additional mutations, however, the mutant melanocytes will enter a durable growth-arrest phase. Mutations in the *TERT* promoter, which constitutively activate TERT activity and enhance telomere maintenance, thus preventing replicative senescence, are thought to be acquired next and selected for upon transition to melanoma *in situ*. Loss of tumor suppressor genes, such as *p16INK4A*, *p15INK4B*, *p14ARF*, are thought to be selected for during transition to invasive melanoma. Shain and colleagues point out that no specific mutations have been shown to confer metastatic ability on melanocytes, however a host of additional mutations are found in invasive and metastatic melanomas that are not found in melanoma *in situ*. These include, additional activating mutations to the MAPKinase pathway, such as loss of heterozygosity, or copy number gains, of the BRAF locus, activating mutations in pathways also implicated in cell proliferation such as PI3Kinase pathway activating mutations in *AKT3* or loss of function mutations in AKT regulator *PTEN*, and mutation of SWI/SNF chromatin remodeling genes that lead to a shift towards the PRC2 complex. Additionally, later stage melanomas are characterized by increasing copy number variations (CNVs) and chromosomal instability (Shain et al., 2015).

Animal Models of Melanomagenesis

Mouse Melanoma Model

One of the most widely used mouse models of melanoma is the tri-allelic BRaf^{CA}, Pten^{loxP}, Tyr::CreER^{T2} model. These mice harbor a constitutively active *BRafV600E* allele and deletes *Pten* in a 4-hydroxytamoxifen dependent manner. Cre-ER^{T2} is expressed under tyrosinase promoter (tyrosinase is a melanin enzyme expressed in late melanoblast development and

differentiated melanocytes). BRAF mutation alone produced hyperpigmentation and benign melanocytic hyperplasia. Depending on level and duration of transgene expression, dermal melanomagenesis with long latency can also occur (Goel et al., 2009). If the BRAF transgenic mice are crossed with a mouse harboring genetic loss of p53 and/or CDKN2A, melanoma incidence greatly increases in the progeny. Similarly, PTEN deletion causes rapid initiation of melanoma (100% penetrance in 4-5 weeks) with accompanying metastasis to lymph nodes and surrounding organs. The introduction of degradation-resistant B-catenin further increased penetrance (Marsh Durban et al., 2013) (Pérez-Guijarro et al., 2017). The engineering of the BRaf^{CA}, Pten^{loxP}, Tyr::CreER^{T2} mouse model was an important step in understanding the etiology of melanoma. It provides a genetic platform for interrogating the effects of potential oncogenes or tumor suppressors on the penetrance and progression of BRAF^{V600E}-driven melanoma. However, this model has several caveats. First, unlike humans, mice do not natively have inter-follicular melanocytes in their epidermis, so the melanomas that arise in this model are from a follicular melanocyte pool. This raises questions about whether the melanocytic cell of origin of the melanoma influences the trajectory of the melanoma transformation and whether this model recapitulates human melanoma progression. Similarly, BRAF^{V600E} expression alone in these mouse follicular melanocytes leads to melanoma transformation with low penetrance, which has not been observed in humans. Likewise, BRAF^{V600E} is expressed under a tyrosinase promoter, which is expressed in late melanoblast development and can therefore affect cells of the central nervous system in addition to melanocytes.

Zebrafish Melanoma Model

The “*miniCoopR*” melanoma model in zebrafish was constructed by inserting an *mitfa*-driven intronless MITF zebrafish minigene into a vector containing a *mitfa* promoter driving an EGFP transgene, or other gene of interest (Ceol et al., 2011). The MITF minigene and transgene are flanked by Tol2 transposon arms then microinjected with the transposase into single cell zebrafish embryos, from (*mitfa:BRAF(V600E);p53^{-/-};mitfa^{-/-}* zebrafish. Because *mitfa* is essential for melanocyte differentiation, only cells that undergo successful incorporation of the *mitfa* minigene transposon will have viable melanocytes. This system ensures that every melanocyte in the zebrafish will express mutant BRAF(V600E) on a p53 null background, in addition to any oncogene of interest cloned into the miniCoopR vector. Ultimately, there is a mosaic rescue of neural crest cells, which will develop into patches of rescued melanocytes, some of which will develop melanoma (Heilmann et al., 2015). The advantage of this system is that different transgenes can easily be swapped into the transposon vector to determine which oncogenes may contribute to melanoma formation. However, a distinct disadvantage of the model is that BRAFV600E is driven by the *mitfa* promoter, indicating that not only melanocytes, but also cells of the nervous system will express the mutant oncogene. Likewise, the *mitfa* promoter can be activated to varying degrees depending on the differentiation state of the cell, which, depending on the cell or origin, may account for the mosaicism of BRAF^{V600E} expression and the inconsistent penetrance of melanoma progression. Furthermore, p53 is more often seen mutated to loss of function than fully deleted in melanomas and p53 mutations are typically seen in more advanced melanomas, so it is difficult to assess the role of this oncogene in the induction of melanoma *in situ*.

3D Reconstituted Human Skin Melanoma Model

Arguably the most human of the current melanoma models adapted a model of 3-dimensional organotypic human skin (Ridky et al., 2010), to culture primary human melanocytes in addition to primary human keratinocytes and primary human dermal fibroblasts. Human skin was obtained from skin banks and incubated in PBS. The epidermis was mechanically peeled, leaving a devitalized human dermis. The dermis was then reconstituted with human fibroblasts for 7 days, at which point, it was elevated on a stand in a culture dish forming an air-liquid interface. Primary human keratinocytes and melanocytes derived from human neonatal foreskin tissue were seeded onto the air interface of the dermis and allowed to reconstitute an epidermis over the following 4-5 days. At this point, the cultures could be studied *in vitro* for up to 2 weeks, or grafted onto the back of immunocompromised mice and studied continuously for the lifespan of the mouse. The ability to genetically manipulate the melanocytes *in vitro* before skin reconstitution allowed the researchers to directly characterize the effects of specific oncogenes on skin reconstitution and melanomagenesis in a human cellular context. Another advantage is that the researcher is not limited by time and cost necessary to breed genetic mouse variants. A disadvantage of this system is that melanomas do not form in a dish and only form when grafted onto an immunocompromised mouse, suggesting that murine factors contribute to the process of melanomagenesis in an uncontrolled manner.

Current Therapies

For patients with early stage melanoma, surgical excision is the most effective option and is often curative. For patients with unresectable, metastatic, or otherwise late-stage disease, small molecule drug and immunotherapies provide two current options for treatment. Drug treatment is based on the principle that MAPK pathway activation drives melanoma proliferation. In 2011 vemurafenib and dabrafenib, which specifically inhibit dimerization of mutant BRAF^{V600E} and render it incapable of phosphorylating MEK, were approved by the FDA for use in BRAF

mutant melanomas. Although RAF inhibition initially shrank melanomas, it was soon discovered that patients treated with BRAF inhibitors relapsed after several months of treatment as sub-populations of tumor cells developed resistance (Sharma et al. 2012) (Sharma et al., 2012). In an attempt to overcome this resistance, MEK inhibitors, such as cobimetinib and trametinib, were added to treatment. The combination of these two inhibitors produced response rates of approximately 70% and progression-free survival of approximately 12 months (Leonardi et al., 2018).

A second treatment modality emerged with the advent of immunotherapy. Research into tumor-immune system interactions found that although lymphocytes are often present in the tumor microenvironment, these cells were unable to mount an immune challenge to the tumor cells (Grivennikov et al., 2010). Studies of cytotoxic T Cells (CD8+ cells) uncovered the need for complex signaling to activate a T Cell response that was absent in most tumor microenvironments (Bouwhuis et al., 2010) (Francisco et al., 2009). This research resulted in the development of immune checkpoint inhibiting antibodies such as anti-programmed cell death protein 1 (anti-PD1) and anti-cytotoxic T-lymphocyte-associated antigen 4 (anti-CTLA4) (Topalian et al., 2012) (Hodi et al., 2010). Immune checkpoint inhibitor therapy has lower rates of response (~30%) in comparison to MAPKinase inhibitors, however, this treatment can confer more durable responses with some patients showing complete clearance of tumors and no recurrence several years post-treatment (Franklin et al., 2017).

Part 3: Melanocytic Nevus Biology

Melanocytic nevi, commonly known as “moles”, are comprised of clonal expansions of melanocytes and often present as pigmented lesions, or macules, on the surface of the skin (Bastian, 2014). Many forms of melanocytic nevi exist, each possessing unique histology and molecular genetics. Nevi are broadly divided into two categories: 1. Acquired nevi and 2. Congenital nevi. Congenital nevi are thought to form in-utero during development. These nevi typically grow larger than acquired nevi, in some cases covering 50% of an individual’s body (Roh et al., 2015). Acquired nevi arise after birth due to the acquisition of mutations and/or copy number changes to chromosomal segments. Acquired nevi can be further divided into three primary groups defined by the position of the constituent melanocytes in the skin. Junctional nevi comprise melanocytes confined to the epidermis. Intradermal nevi contain melanocytes in the dermis, and compound nevi have melanocytes spanning the epidermal and dermal compartments (Damsky and Bosenberg, 2017).

Melanocytic Nevus Types

An array of nevus types, each characterized by a unique histology, populate the junctional, intradermal, and compound nevus categories. These include, but are not limited to: common nevus, Spitz nevus, Hori’s nevus, Becker’s nevus, and blue nevus. Spitz nevi, named for the pioneering dermatopathologist Sophie Spitz (1910-1956), were once thought to be juvenile melanomas. Further research demonstrated that these lesions are typically benign lesions of vertically arranged melanocyte nests with spindled and epithelioid morphology. Spitz nevi are further characterized by multinucleate or mononucleate giant cells, large pigmented spindle cells, and pigmentation mainly in the superficial part of the lesion (Manchi and Canzonieri, 2019). Hori’s nevus is a pigmentation disorder reported most often in middle-aged Asian women and presents as multiple brown-grey or blue-brown macules (Kaur et al., 2019). Becker’s nevus, first reported by dermatologist Samuel W. Becker (1894-1964), typically affects males. This nevus is

characterized by a large area of hyperpigmentation and excessive hair growth (Happle, 2017). Blue nevi are rare, tend to be nodular, and present with blue-grey hues on the epidermis (Borgenvik et al., 2017). In contrast to the previously described nevus types, which occur at low frequency across the population, common nevi are the most prevalent form of melanocytic nevi and will be the subject of this work.

Common melanocytic nevi

Common melanocytic nevi generally appear as flat, uniformly pigmented, and symmetric spheres or ellipses in the epidermis with a radius of several millimeters (Damsky and Bosenberg, 2017). These nevi can arise at any time in a person's life, however, the greatest number are acquired from childhood to ~30 years of age. After 30 the rate of new common nevus acquisition typically decreases and nevus regression, a poorly understood process wherein nevi disappear from the skin, begins to occur (Stegmaier, 1959). Viewed in cross-section under the microscope, common nevi have two distinct histological features - nesting and maturation. Nesting describes the tendency of nevus melanocytes to form clusters of cells or "nests" within the tissue. Maturation occurs in nevi with a dermal component and describes the gradual and progressive change in nest architecture and cell shape. As nevi penetrate deeper into the dermis, nest size decreases along with the nuclear volume and pigment production of the constituent melanocytes (Damsky and Bosenberg, 2017). The complex nature of melanocyte cytology within nevi suggests that both cell intrinsic and extrinsic factors, such as the microenvironment, converge to dictate the ultimate dimensions and morphology of the nevus.

Mutations driving nevus formation

Considerable research has been conducted in an attempt to define the molecular processes that give rise to melanocytic nevi. DNA sequencing of nevi and surrounding normal tissue provided the first insights into genomic changes that underlie nevus formation. In 2003, Pollock and colleagues published work showing that 63 of 77 nevi they sequenced (82%) had activating mutations in the BRAF proto-oncogene, with c.T1799A (p.V600E) as the dominant

mutation (Pollock et al., 2003). Subsequent sequencing efforts confirmed Pollock's finding and found that activating mutations in NRAS proto-oncogene are commonly found in congenital nevi. Spitz nevi often have HRAS proto-oncogene mutations as well as chromosomal copy number alterations (Bastian et al., 2000), and GNAQ/GNA11 mutations are common in blue nevi (Roh et al., 2015). Importantly, BRAF, NRAS, HRAS, and GNAQ/GNA11 are all components of the MAPK signaling pathway, a central regulator of cellular proliferation (Dhillon et al., 2007) (Park et al., 2018). The prevalence of single, activating mutations in genes encoding key proteins of the MAPK signaling pathway suggests that melanocytic nevi arise from the rapid clonal expansion of a single mutant melanocyte.

Two main hypotheses exist to explain how melanocytes acquire these activating MAPK pathway mutations. The first implicates UV light from sun exposure, as many melanocytic nevi appear on sun exposed or sun damaged skin. Although melanomas have high UV signature mutation burdens, there is no direct evidence that UV light is the causative agent for the most common *BRAF*, *NRAS*, or *HRAS* mutations. Furthermore, the T>A transversion that results in the *BRAF(V600E)* mutation, the most common in melanocytic nevi, is not part of the canonical UV signature of C>T or CC>TT (cite). Likewise, individuals with Xeroderma Pigmentosa, who have a deficiency nucleotide excision repair pathways necessary to repair UV-induced DNA damage, rarely develop melanomas with *BRAF(V600E)* mutations (Masaki et al., 2014). The second hypothesis suggests that these mutations form as the product of oxidative stress, or as a combination of UV light and oxidative stress. In this model, reactive oxygen species interfere with normal DNA replication leading to adducts in the DNA, which if not properly repaired, give rise to mutations (Venza et al., 2015).

Why study BRAF^{V600E}-driven nevi?

While the specific mutagens remain unclear, the phenotype induced by activating mutations in the MAPK pathway is well described. Rapid clonal expansion leads to nests of

melanocytes and subsequent growth arrest establishes the boundaries of the melanocytic nevus. For the remainder of this work, I will focus on common melanocytic nevi driven by the *BRAF(V600E)* mutation. Unlike activating NRAS and HRAS mutations, which occasionally lead to nevi in human skin but more often lead directly to hyperproliferation and malignant disease, the activating V600E mutation of the BRAF proto-oncogene is thought to predominately induce nevus formation.

Common nevi driven by BRAF^{V600E} mutations are interesting for numerous reasons. First, approximately 50% of melanomas are also driven by BRAF^{V600E} and thought to arise when previously quiescent nevus cells re-enter the cell cycle and begin proliferating. Therefore, understanding how nevi form and how they can transition to melanoma becomes crucial to discovering more efficacious treatments for the disease. Second, because they are usually visible in the skin and because each defined stage of melanoma progression can be captured histologically, BRAF^{V600E} nevi provide a unique window into the entire process of tumorigenesis from acquisition of an initiating mutation to metastasis. Finally, since most BRAF^{V600E} nevi remain innocuous for the entirety of an individual's life, these lesions provide a fascinating opportunity to study the cell intrinsic and extrinsic factors that play a role in resisting oncogenic transformation.

Part 4: microRNA Biology

Overview of microRNA function

microRNAs are small non-coding RNAs approximately 20-22 nucleotides in length. They are found in extragenic sequences of the genome (Bartel, 2004), as well as in the exons or introns of genes (Rodriguez, 2004) (Okamura et al., 2007). microRNAs were first reported in a pair of 1993 papers by Lee and colleagues and Wightman and colleagues in *Caenorhabditis elegans* (*C. elegans*), a species of roundworm. These papers described *lin-4* as a 21 nucleotide RNA that could partially base pair with sequences in the 3' UTR of the mRNA of a gene called *lin-14*. This partial base-pairing activity ultimately caused the inhibition of LIN-14 protein expression. When measuring the effects of *lin-4* on *lin-14* mRNA, the authors found that LIN-14 mRNA expression was unaffected by *lin-4* binding, and that *lin-14* mRNA was still able to bind to the polyribosome (Lee et al., 1993) (Wightman et al., 1993). These findings therefore suggested a model whereby microRNAs regulated mRNA translation.

In 2000, two groups published work describing the activity of a second *C. elegans* microRNA named *let-7*, which post-transcriptionally inhibited *lin-41* mRNA by binding a pair of sequences in the *lin-41* 3' UTR (Pasquinelli et al., 2000) (Reinhart et al., 2000). Besides confirming the mechanism of microRNA regulation proposed by Lee and Wightman, the discovery of *let-7* precipitated the finding that this microRNA is conserved broadly among animal species, including in humans (Pasquinelli et al., 2000). Further research into animal microRNAs demonstrated that microRNAs could also directly regulate mRNA levels. Initially, experimental data showed that miRNA:target duplexes with imperfect base pairing resulted in inhibition of mRNA translation (Bartel, 2004). If, however, significant perfect pairing occurs between the miRNA and target mRNA (including the seed sequence of the miRNA), the target mRNA itself can be cleaved and degraded (Park and Shin, 2014). This mode of mRNA cleavage parallels that of small-interfering RNAs (si-RNAs), which had previously been described in plants (Elbashir et al., 2001). Research in *Drosophila* and mammalian cell systems identified Argonaute 2 (AGO2)

as the protein responsible for mRNA cleavage (Hammond, 2001). Finally, in 2005, Bagga et al. found that imperfect miRNA:mRNA base pairing of *let-7* and *lin-41* also led to the degradation of *lin-41* target mRNA (Bagga et al., 2005). This finding helped establish the current dogma that miRNAs can directly regulate mRNA transcript levels as well as regulate mRNA translation.

microRNA processing

In mammalian cells, microRNAs are initially transcribed from their genomic positions in the nucleus by Polymerase II (POLII) as hairpins known as pri-miRNAs often in the range of 80-100 nucleotides. The hairpin then complexes with the micro-processing unit composed of DGCR8 and DROSHA proteins. This unit trims the longer hairpin down to a hairpin of shorter length known as the pre-miRNA. The pre-miRNA is subsequently exported from the nucleus to the cytoplasm through a nuclear pore complex comprised of Exportin 5 (XPO5) and RanGTP. Once in the cytoplasm, the pre-miRNA hairpin is further cleaved by a protein complex including DICER1 and TRBP. This cleavage produces two independent microRNAs with the designations 5' or 3', depending on their position in the pre-miRNA hairpin. From here, the mature microRNA (now approximately 20-22 nucleotides) can be loaded into the binding pocket of Argonaute proteins (primarily AGO2 in mammalian cells) and bind complementary sequences in the 3' UTRs of target mRNAs. As previously described, miRNA:mRNA base pairing typically results in to both translational inhibition and mRNA degradation (Shukla et al., 2012).

microRNAs regulate multiple genes

The large number of potential miRNA binding sites found in the 3'UTR of genes suggests that individual miRNAs have the potential to regulate numerous genes simultaneously. Indeed, multiple groups have shown that overexpression of mature miRNA sequences (miRNA mimics) in cells induces changes in mRNA transcript levels across a wide range of genes (Guo et al., 2010) (Thomson et al., 2013). The advent of High Throughput Sequencing of RNA Isolated by Crosslinking Immunoprecipitation (HITS CLIP) enabled researchers to crosslink miRNA:mRNA complexes to AGO2 and the sequence mRNAs bound to immunoprecipitated AGO2 protein

(Darnell, 2010). This method further confirmed the finding that miRNAs simultaneously regulated many mRNAs through direct binding to their 3' UTRs and permitted the identification of miRNA specific mRNA targets at a fixed time point. Similarly, large-scale proteomic analyses of cells post-miRNA overexpression or knockdown led to the complementary finding that miRNAs had profound effects on translation of target mRNAs (Baek et al., 2008). The hunt for microRNA targets across the genome spawned the construction of several algorithms that follow defined sets of rules dictating which binding sites in the 3' UTR of mRNAs would result in target mRNA regulation (Lewis et al., 2003) (Agarwal et al., 2015). These computational methods of identifying potential miRNA targets resulted in the construction of target databases, most notably *TargetScan* (Lewis et al., 2005).

Despite the established rules for miRNA target prediction, the identification of functional miRNA targets remains highly context dependent. mRNAs targeted by a miRNA in one cell type may not be transcribed in another cell type. miRNA overexpression studies have shown that mRNA targets with a low score based on computational prediction may indeed be regulated when higher scoring targets are absent or in low abundance, or when the concentration of the miRNA exceeds a certain level. Additional studies have shown that mRNAs with miRNA target sequences in their 5' UTR (Lytle et al., 2007) or even the gene body may also be regulated by miRNA binding, however, the evidence supporting these claims remains controversial (Chi et al., 2009). These experimental findings argue strongly that potential transcript targets of the miRNA must be validated within the cell type of interest through measurements of mRNA and protein expression in response to miRNA manipulation. Furthermore, these observations raise a series of questions regarding the importance of both miRNA and potential target mRNA concentrations, as well as the availability of Argonaute protein occupancy in the cell when determining specific miRNA targets.

Part 5: Role of miRNAs in melanoma

Evolutionary history and experimental observation suggest that miRNAs contribute to cell differentiation and cell state maintenance by buffering against changes in target gene networks (Ebert and Sharp, 2012) (Berezikov, 2011) (Parchem et al., 2014). Transitions from differentiated cells to tumor cells can be viewed as a subversion of miRNA buffering capacity resulting in reprogramming of a cell's transcriptional networks (Schmiedel et al., 2015). Work by Lu et al. provides further evidence for this by showing that total miRNA diversity decreases in tumors versus normal tissue, suggesting that loss of miRNA expression might lead to remodeling of the intracellular environment thereby lowering the barrier to tumorigenesis (Lu et al., 2005).

Consistent with these observations, small RNA sequencing of human melanoma tumors or melanoma cell lines have identified miRNAs differentially expressed in comparison to human melanocytes, including miR-17 (Nemlich et al., 2013), miR-221 (Kanemaru et al., 2011), miR-146a (increased) (Forloni et al., 2014) and miR-211 (Levy et al., 2010), miR-125b (Wandler et al., 2017), miR-206 (decreased) (Georgantas et al., 2014). Moreover Ren et al. show that miR 143, miR-34a, and miR-29a are upregulated in human melanocytes transduced with lentiviral *BRAF(V600E)*, suggesting that these miRNAs are expressed in an effort to counter BRAF-induced hyperproliferation (Ren et al., 2012). Taken together, these findings support the hypothesis that microRNA expression is dysregulated during progression from normal melanocytes to malignancy. Furthermore, these results argue that a thorough understanding of the dynamics of microRNA expression and target regulation from normal melanocytes to melanocytic nevi and melanoma may be essential to understanding the early events that lead to melanoma initiation and progression.

Chapter 2: BRAF^{V600E} induces growth arrest in human melanocytes to form melanocytic nevi.

Part 1: Theories of BRAF^{V600E}-mediated growth arrest in melanocytes.

To develop more efficacious melanoma therapies, scientists and physicians sought to determine how nevus cells restrain mutant BRAF-driven proliferative signaling and discover which elements are lost in progression to malignant disease. Beginning in the early 2000s, researchers have inferred that the acquisition of the activating V600E mutation in the *BRAF* proto-oncogene is the founding genetic event that causes melanocytes to first proliferate and then undergo growth arrest. Numerous theories have emerged to explain BRAF^{V600E}-induced growth-arrest or “senescence”, as it is widely referred to in scientific literature, that forms the melanocytic nevus. Despite the plethora of explanations, nearly all converge on the principle that aberrant MAPK signaling downstream of BRAF^{V600E} expression induces a cascade of intracellular changes that contribute to the establishment and/or maintenance of cell cycle arrest. In this section, I will discuss several of these theories and their supporting evidence before detailing my own investigations into nevus formation.

In 2006, Uribe and colleagues sought to understand why MAPK signaling downstream of BRAF^{V600E} was repressed in nevi in comparison with primary melanomas if both lesions expressed the same mutation (Cohen et al., 2002) (Jørgensen and Holm, 2003). By staining formalin fixed cutaneous tissue sections, they found that whereas melanoma samples had increased phosphorylation of *extracellular signal regulating kinases 1/2* (ERK1/2), a downstream target of BRAF^{V600E} activity, nevi had low levels of phospho-ERK1/2. They posited that BRAF^{V600E} expression must induce negative feed-back loops that ultimately dampen MAPK signaling. This hypothesis was consistent with contemporaneous studies of MAPK signaling regulation in the presence or absence of BRAF^{V600E} expression (Uribe et al., 2006). Courtois-Cox et al. published

work suggesting that activation of RAS or RAF signaling induced negative feedback signals from RAS protein regulators including RasGAPs, RasGEFs, and SPROUTY proteins. Relieving RAS protein inhibition by introducing shRNAs against NF1 (itself a RasGAP), the authors showed that in primary diploid human fibroblasts, RAS signaling was transiently activated followed by proliferation arrest. They further identified a coordinated intracellular response wherein pro-mitogenic phosphoinositide 3-kinase (*PI3K*) signaling was downregulated in response to RAS activation and anti-mitogenic forkhead box (*FOXO*) family of transcription factors was upregulated (Courtois-Cox et al., 2006).

A second hypothesis suggested that DNA hyper-replication from oncogenic activation triggered DNA Damage Response (DDR) pathways. Di Micco and colleagues expressed a constitutively activated HRAS protein, HRAS^{G12V}, which was thought to drive cell proliferation in specific cases of squamous cell carcinoma and melanomas, in human diploid fibroblasts via lentiviral transduction. Rather than increasing cell proliferation, proliferation dramatically decreased. They further found that expression of HRAS^{G12V} led to increases in the numbers of active DNA replicons and led to asymmetric replication fork progression, damaging DNA. They also showed that HRAS activation increased expression of DDR pathway proteins including p53 and checkpoint kinase 2 (*CHEK2*) and that inhibition of the DDR pathway led to bypassing of senescence (Di Micco et al., 2006). Also working in HRAS mutant human fibroblasts, Aird and colleagues demonstrated that aberrant MAPKinase pathway activation depleted intracellular stores of deoxyribonucleotide triphosphates (dNTPs), which are required for DNA synthesis. They found that *ribonucleotide reductase unit M2* (RRM2) was a rate-limiting protein in DNA synthesis, specifically in S-phase, and that its suppression downstream of activated RAS signaling decreased nucleotide metabolism (Aird et al., 2013).

In parallel with gene expression changes and increased DNA damage, researchers identified differences in chromatin structure between nevi and malignant melanoma. Electron microscopy of fixed ultrathin sections of human nevus and melanoma tissue revealed a

compaction of chromatin, known as heterochromatin, that makes DNA less accessible to transcription factors. In malignant melanoma samples, however, the chromatin favored a more open structure known as euchromatin. These observations of differences in the chromatin structure between nevi and melanoma suggested that chromatin remodeling in nevi can silence key transcriptional targets stymying proliferation (Stolz et al., 1991) (Narita et al., 2003) (Bandyopadhyay et al., 2007).

One of the longest studied contributions to melanocytic nevus growth arrest is the relationship between BRAF^{V600E} and the upregulation of a family of cell cycle inhibitors known as cyclin dependent kinase inhibitors. The cyclin dependent kinase 2A (*CDKN2A*) gene encodes two tumor suppressor proteins, p16^{INK4A} and p14^{ARF}. *CDKN2A* expression is typically observed in nevi but regularly mutated to loss-of-function or deleted in melanoma. p16^{INK4A} functions by inhibiting Cyclin D- CDK4/6 complex phosphorylation of retinoblastoma (*Rb*), an event required for passage through the G1 phase of the cell cycle (McConnell et al., 1999). Meanwhile, p14^{ARF} inhibits mouse double minute 2 (*MDM2*), which in turn degrades p53, increasing p53 expression and activating the DDR pathway (Lohrum et al., 2000). Due to the upregulation of p16^{INK4A} and p14^{ARF} expression in human nevus sections, and their molecular functions, it was accepted that these proteins provided “an effective cellular brake against BRAF^{V600E}-mediated oncogenic signaling”.

Michaloglou and colleagues directly investigated the connection between BRAF^{V600E} and p16^{INK4A} expression in normal human diploid melanocytes (in this case foreskin-derived melanocytes) *in vitro*. To simulate the *BRAF(V600E)* mutation, they transduced human melanocytes with a lentiviral vector harboring the *BRAF(V600E)* transgene. They observed that BRAF^{V600E} expression induces growth-arrest in melanocytes. Likewise, BRAFV600E induced p16^{INK4A} expression in a mosaic pattern in growth-arrested melanocytes, but p14^{ARF} expression did not increase. They then expressed BRAF^{V600E} or p16^{INK4A} in human diploid fibroblasts and showed that expression of either transgene significantly reduced proliferation over the course of

11 days. Somewhat surprisingly, knockdown of p16^{INK4A} via shRNA could not rescue BRAFV600E-induced arrest in fibroblasts, suggesting that it was sufficient but not necessary for growth-arrest induction (Figure 1). Moreover, they argued that p16 regulation of RB rather than p14 induction of p53 contributed to growth arrest, as they failed to detect upregulation of p53 in nevus sections.

Finally, their work challenged a longstanding hypothesis in the field of nevus growth arrest which asserted that nevus melanocytes ceased to proliferate due to a critical shortening of their telomeres. Telomeres are repeating motifs of adenine and thymidine bases found at the termini of chromosomes and, in normal physiology, these repeats protect DNA integrity during replication. Hayflick et al. proposed that cells with critically shortened telomeres (those that had reached the “Hayflick Limit”) could not replicate their DNA, effectively inhibiting proliferation. Through telomere staining in sections of human nevi, Michaloglou et al., however, found no apparent loss of telomeres in nevi (Michaloglou et al., 2005) casting doubt on the validity of the telomere hypothesis.

In a 2009 study, Haferkamp and colleagues returned to the role of the *CDKN2A* locus genes in mediating growth-arrest downstream of aberrant MAPKinase signaling. The group transduced primary human melanocytes with a lentiviral NRAS^{Q61K} transgene and observed a strong upregulation of the DDR pathway including increased phosphorylation of CHK2 and p53, similar to that seen by DiMicco et al with HRAS^{G12V}. In concordance with Michaloglou et al., they also observed concurrent upregulation of p16^{INK4A} protein downstream of aberrant MAPKinase signaling. Overexpressing p16^{INK4A} transgene in WMM1175 melanoma cells, they found that p16 induced upregulation of senescence markers, such as Senescence-Associated Beta Galactosidase (SA-B-Gal) staining and senescence-associated heterochromatin foci (SAHF). Consistent with Michaloglou’s findings, Haferkamp ultimately concluded that regulation of RB phosphorylation by p16 contributed more to inducing growth arrest than did p53 upregulation (Haferkamp et al., 2009).

While these publications established relationships between activating mutations in RAS and BRAF and the growth arrest phenotype observed in nevi, as well as p16 expression, they raised further questions. What is the molecular connection between BRAF^{V600E} and the CDK inhibitors? Do the effects of exogenous BRAF^{V600E} or p16 overexpression change in different cell types such as melanocytes? How does exogenous BRAF^{V600E} overexpression affect proliferation in human melanocytes, the cell of origin of melanoma? To explore these unanswered questions we sought to isolate benign human nevi and test these hypotheses directly.

**Part 2: Role of CDKN2B in BRAFV600E-mediated growth arrest. (Pre-Thesis Contribution)
(Reproduced from McNeal et al. Cancer Discovery 2015).**

BRAFV600E Nevus Melanocytes are Growth-Arrested

To better understand the mechanisms promoting growth arrest in BRAF(V600E) nevi, we set out to first isolate nevus melanocytes. Melanocytes from clinically benign nevi were excised from 27 human donors (Fig. 2.1A). To ensure that our nevus cells were growth arrested and not contaminated with cells already progressing to melanomas, we specifically used long-standing nevi with benign appearance and no history of recent morphologic changes were collected. Interestingly, we found that cultured nevus-MCs were morphologically indistinguishable from melanocytes isolated from unremarkable skin (Fig. 2.1B). Sequencing BRAF cDNA from cultured nevus-MCs revealed overlapping, equal-intensity peaks at nucleotide 1799, corresponding to expression of both wild-type (1799T) and mutant V600E (1799T>A) BRAF alleles (Fig. 2.1C). Keratinocytes isolated from epidermis associated with the nevi expressed only wild-type BRAF (Fig. 2.1C). While nevus-MCs remained viable in vitro, they failed to proliferate, independent of cell plating density, reflecting their in vivo growth-arrest. Consistent with this, the Ki-67+ proliferative index of nevus-MCs was only 4%, compared to 38% for normal MCs, (Fig. 2.1D). To determine whether BRAF(V600E) expression was sufficient to drive MC proliferative arrest in the

absence of additional *in vivo* cues, we engineered normal primary melanocytes to express doxycycline-inducible BRAF(V600E) (diBRAF(V600E)). Consistent with a key role for BRAF(V600E) in nevus-MC growth arrest, doxycycline treated diBRAF-MCs ceased to proliferate, while untreated diBRAF cells proliferated normally (Fig. 2.1E).

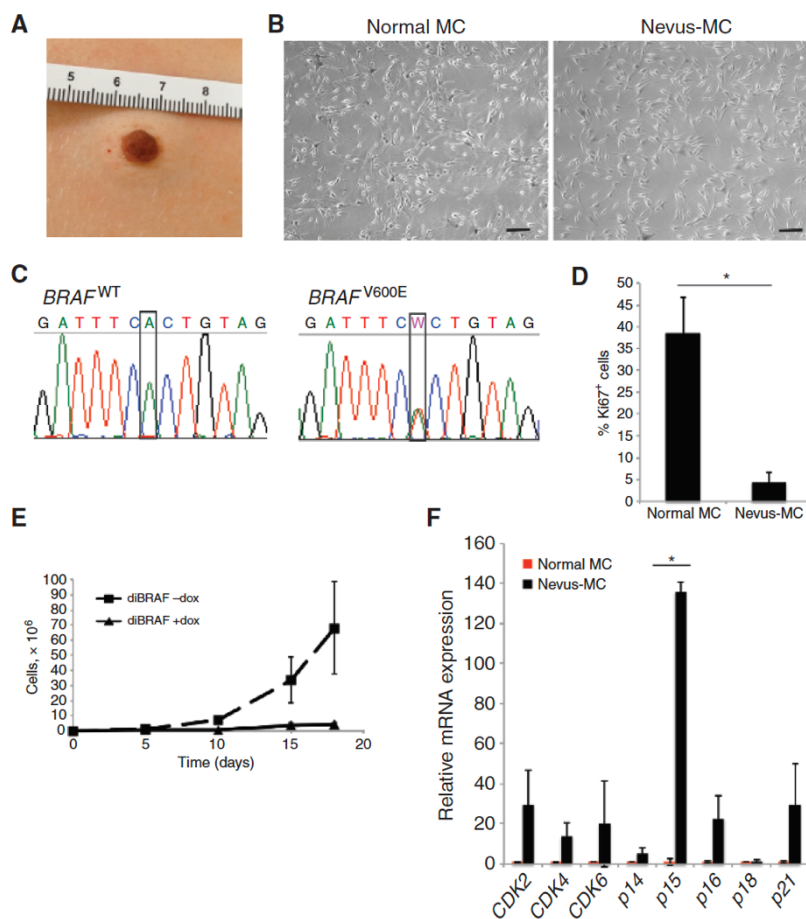


Figure 2.1: BRAFV600E-Driven Melanocyte Growth Arrest.

(A) Clinical image of a benign nevus used in this study.

(B) 10× brightfield images of representative normal-MCs (left) and nevus-MCs (right). Scale bars = 20µm.

(C) Sanger sequencing of nevus-associated keratinocytes expressing WT BRAF (left), and nevus-MCs expressing BRAF(V600E) (right).

(D) Ki-67 proliferation index of normal and nevus-MCs.

(E) Growth of diBRAF melanocytes +/- 0.25µg/mL doxycycline showing proliferation arrest in BRAF(V600E)-expressing MCs.

(F) Relative mRNA expression of cell cycle regulators in normal vs nevus-derived melanocytes. *P<0.05. n = 3 biological replicates of distinct normal and nevus melanocyte populations used in each experiment.

The Cyclin Dependent Kinase Inhibitor p15 is Induced in Nevi

To elucidate the mechanisms underlying BRAF(V600E)-induced growth arrest, we compared expression of cell cycle regulatory genes in nevus vs normal-MCs by quantitative reverse transcriptase polymerase chain reaction (qRT-PCR) analysis. This revealed increased expression of multiple cell CDKi cycle regulators, the most prominent being CDKN2B (p15) (Fig. 1F). We further confirmed that, benign human nevi *in vivo* also express high levels of p15 (Fig. 2.2A and 2.2B). Conversely, epidermal melanocytes in adjacent tissue, not associated with the nevus, appeared p15 negative (Fig. 2.2C and 2.2D). p15 has been shown to inhibit CyclinD-CDK4/6 complexes, and promote Rb-dependent maintenance of the G1-S cell-cycle checkpoint (Hannon et al. 1994) (Hannon and Beach, 1994). We therefore hypothesized that p15 may play a role in arresting nevus growth, potentially cooperating with other upregulated cell cycle regulators including p14, p16, and p21 to maintain proliferative arrest *in vivo*. To test the hypothesis that p15, and/or p16, induction is a necessary component for BRAF(V600E) growth arrest, and to determine whether the growth arrest is reversible, we first sought to circumvent p15/p16 function through expression of CDK4(R24C) in arrested nevus, and diBRAF(V600E) melanocytes (Wolfel et al., 1995) (Zuo et al., 1996). We found that the R24C mutation renders CDK4 resistant to p15/p16 inhibition, and restored proliferation in both nevus and engineered diBRAF(V600E) MC.

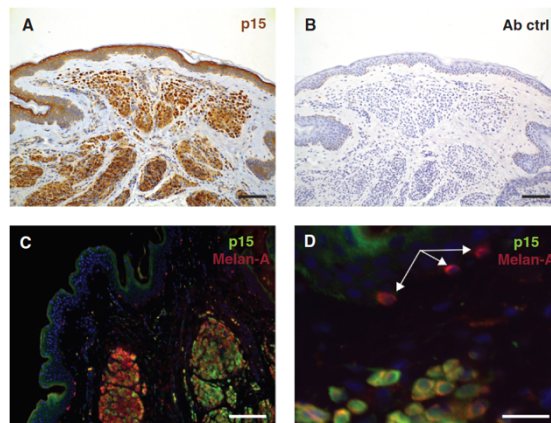


Figure 2.2: p15 Expressed in Nevi is a Key Factor Mediating BRAF Growth Arrest.

(A) p15 expression in a benign intradermal nevus and (B), antibody control (C), Co-Immunofluorescence of p15 and Melan-A in a representative intradermal benign nevus. Scale bars = 100 μ m.

(D) Nevus melanocytes express p15, whereas non-nevus melanocytes (white arrows) are p15-negative. Scale bar = 25 μ m.

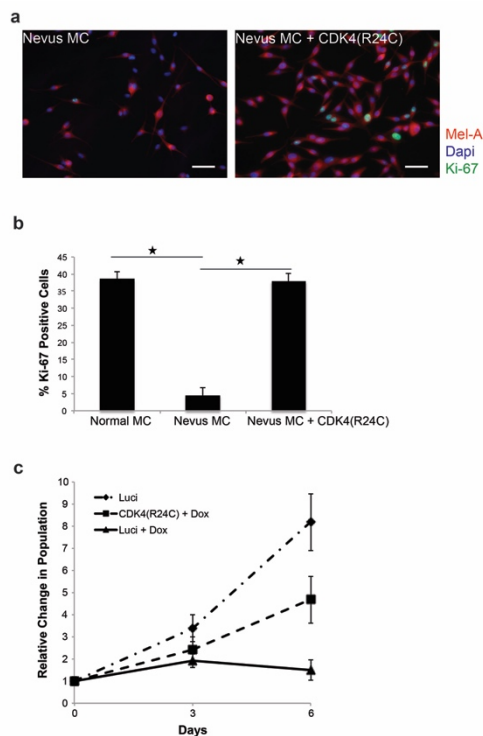


Figure 2.3: Active CDK4 reverses BRAFV600E-mediated melanocyte growth arrest.

(A) Ki-67 expression (green) of nevus MC (left) and nevus MCs transduced with CDK4(R24C) (right) on chamber slides. Sections were counterstained with Mel-A (red) and DAPI (blue).

(B) Percent Ki-67 positive cells in normal MCs, nevus MCs, and nevus MCs expressing CDK4(R24C). n = 3 biological replicates per experiment. *P<0.05. Scale bars, 10 μ m.

(C) Relative proliferation of diBRAF(V600E) MCs transduced with either a luciferase control (Luci) or activated CDK4 (CDK4(R24C)), and treated with or without 0.25 μ g/mL doxycycline. Values reflect the average \pm SEM of n = 3 biological replicates.

p15 Induction by BRAF is Both Sufficient and Necessary for Melanocyte Growth Arrest

To test whether expression of BRAF(V600E) is sufficient on its own to upregulate p15 and p16, we compared their expression in doxycycline treated diBRAF(V600E)-MCs, nevus-MCs, and normal MCs. Whereas normal MCs expressed very little p15 or p16, doxycycline treated diBRAF-MCs and nevus-MCs both expressed p15 and p16 at high levels in primary culture and *in vivo*. (Fig. 2.3A-D). Extended culture of primary nevus-MCs *in vitro* showed that elevated levels of p15 and p16 were maintained along with the growth-arrested phenotype. Importantly, p15 induction and the associated growth arrest are both dependent on the level of BRAF(V600E) expression. Levels of p15 initially increase proportionally with increasing BRAF(V600E) protein. However, at the highest doxycycline-induced BRAF levels, or with high-level BRAF-expression driven by a conventional lentivirus utilizing a constitutive PGK promoter, p15 protein induction is attenuated, and melanocytes continue to proliferate (Fig. 2.4A). This highlights the need to consider BRAF protein levels when using model systems, and led us to rely on the native nevus cells for functional *in vivo* experiments. To determine whether p15 is sufficient to cause MC growth arrest without simultaneous induction of other growth regulators including p16, we transduced primary melanocytes with p15 or p16. Melanocytes expressing p15 halted proliferation, while MCs expressing p16 continued to divide, albeit more slowly than controls (Fig. 2.4B). Through virus titering and quantitative PCR, we demonstrated that these proliferation differences did not result from relatively lower levels of p16 gene expression. The relative proliferation effects correlated well with p-Rb protein, with p-Rb levels lowest in the p15 expressing melanocytes. Although p15 and p16 share structural homology through their ankyrin repeat domains, there are significant regions of divergent sequence, particularly in the N-terminus, that may serve to make p15 a more efficient CDK inhibitor (reflected by lower p-RB).

Additionally, previous work using a series of cell lines and chimeric p15/p16 domain swap constructs established that sequences unique to the p15 N-terminus confer p15 with the ability to influence cell cycle beyond Rb, and that p16 does not possess this activity (Aytac et al., 1999). While the specific interacting proteins and pathways mediating this additional p15 activity are not yet established, they are likely functionally important in nevus melanocytes. To test whether BRAF(V600E)-induced growth arrest requires p15 or p16, we transduced diBRAF(V600E) cells with shRNAs targeting p15 (p15i) or p16 (p16i) (Fig. 2.4C and 2.4D). Without doxycycline, diBRAF(V600E) cells harboring p15i or p16i proliferated normally as expected. With doxycycline, proliferation of diBRAF(V600E) cells expressing control or p16i slowed dramatically, while p15i cells continued to proliferate. Together, these data indicate that p15 is both necessary and sufficient for BRAF(V600E)-mediated growth arrest. To ensure that the observed proliferation phenotype of the p15 knockdown was due to loss of p15 and not an off-target effect of the shRNA, we restored p15 expression in diBRAF(V600E) melanocytes expressing the p15 shRNA, and demonstrated that cells again growth arrested as expected. As an additional control, we also validated the phenotype using a CRISPR-Cas9 approach targeting the CDKN2B locus. As with shRNAs targeting p15 mRNA, CDKN2B ablation by CRISPR-Cas9 prevented BRAF(V600E)-induced growth arrest. As CDKN2A and CDKN2B are frequently simultaneously deleted in melanoma, we next investigated whether simultaneous loss of p15 and p14/16 activity had an additive effect on overcoming BRAF(V600E) growth arrest. We utilized the melanoma-associated dnp53 mutant (R248W) to recapitulate the functional effects of p14 loss. Accordingly, we compared the relative proliferation of diBRAF(V600E) melanocytes expressing shRNAs targeting p15, to matched cells with the p16 shRNA and dnp53, or the combination of p15 and p16 shRNAs and dnp53. In the absence of BRAF(V600E) expression, all cell populations proliferated normally, indicating that there were no off-target effects that compromised general cell cycle regulation. As seen previously, melanocytes expressing BRAF(V600E) growth-arrested, while BRAF(V600E) cells with p15 knockdown proliferated, albeit more slowly than normal controls lacking

BRAF(V600E). BRAFV600E-expressing cells with p16 knockdown and dnp53 expression failed to proliferate. However, cells with the combination of BRAF(V600E), p15/p16 knockdown, and dnp53 proliferated faster than the cells with p15 knockdown alone. Therefore, the combinatorial loss of p15, p14 (through dnp53) and p16 activity promoted proliferation in the face of BRAF(V600E) to a greater extent than the loss of the individual elements. These results are consistent with our data showing that while each of the proteins encoded by the CDKN2A/CDKN2B locus are important in melanomagenesis, p15 is an especially important mediator of the BRAF growth arrest.

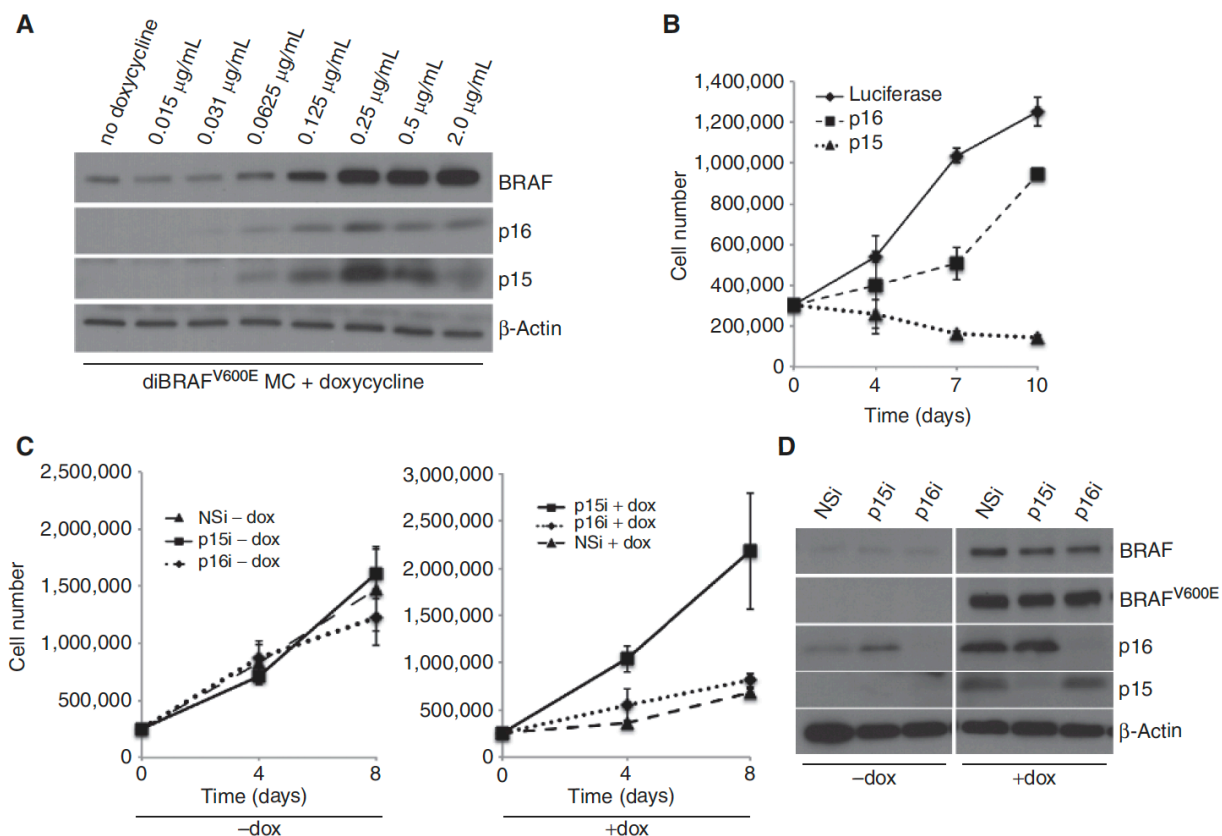


Figure 2.4: p15 is Necessary and Sufficient to Arrest Melanocyte Proliferation.

(A) Western blot analysis of BRAF, p15, and p16 expression in diBRAF(V600E) melanocytes in response to increasing levels of doxycycline. β -Actin was used as a loading control.

(B) Proliferation of normal human melanocytes engineered to express p15 or p16.

(C) Proliferation of diBRAF(V600E) melanocytes with non-silencing control (NSi), p15 (p15i) or p16 (p16i) shRNA knockdown, without (left) or with (right) 0.25 μ g/mL doxycycline. Data are shown as average \pm SEM for B and C. n = 3 biological replicates for each group.

(D) Western blot analysis of BRAF, BRAF(V600E), p15, and p16 in diBRAF(V600E) cells with non-silencing control (NSi), p15 (p15i), and p16 (p16i) shRNA knockdowns. β -Actin was used as a loading control. Western blot results and growth curves were representative of three biological replicates composed of distinct melanocyte populations.

p15 is Diminished in Melanoma

To discover whether p15 helps restrain the oncogenic activity of BRAF(V600E) *in vivo*, we examined informative clinical cases of matched nevi with adjacent melanomas (Fig. 2.5A). p15 protein was diminished in the malignant melanomas compared to adjacent nevi (Fig. 2.5B and 2.5C). We also examined a series of 12 additional randomly selected malignant melanomas and 15 benign nevi, along with 5 nevus-melanoma cases and found that the majority of nevi strongly expressed both p15 and p16, while the majority of melanomas showed very low to undetectable p15 and p16. This pattern of coordinate regulation of p15 and p16 is consistent with the latest Cancer Genome Atlas analysis of 278 melanomas in which 93% of melanomas with homozygous deletion of CDKN2A (p16) also harbor homozygous deletions of CDKN2B (p15) (Cerami et al., 2012); (Gao et al., 2013)). Simultaneous loss of these two cell cycle inhibitors likely reflects the close proximity of the adjacent *CDKN2A/CDKN2B* loci on chromosome 9p21.3. Importantly, the TCGA series includes a tumor in which *CDKN2B* is lost while *p16* remains intact, a genetic event that has also been described in other series (Glendening et al., 1995). Consistent with these previous reports, we also identified a clinical case in our sample group in which a p16 positive melanoma developed in the epidermis overlying a benign nevus. While the nevus melanocytes robustly expressed both p15 and p16, the melanoma retained only p16, and lacked p15 expression. Together these findings highlight the functional importance of p15 loss in human melanoma, and suggest that p15 expression may serve as a clinically useful tool to help distinguish between benign and malignant melanocytic neoplasias that are otherwise histologically ambiguous.

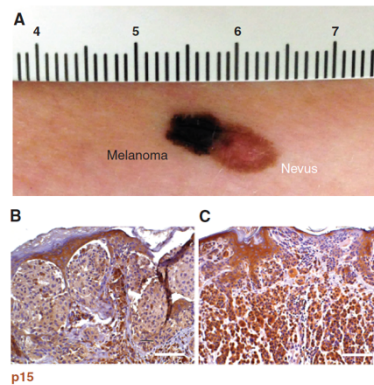


Figure 2.5: BRAF-Induced p15 is Decreased in Melanoma.

(A) Representative clinical image from $n = 5$ cases in which melanoma developed in continuity with a pre-existing nevus.

(B) p15 expression is markedly diminished in the malignant proliferative nests of the melanoma portion of (A) compared to (C) the benign nevus portion. Scale bars, 100 μ m.

BRAF(V600E) Activates p15 Expression Through TGF β Signaling

In other cell contexts TGF β /SMAD activity induces p15 expression (Hannon et al. 1994 ; Seoane 2001). We questioned whether BRAF(V600E) induced TGF β expression in human melanocytes and found that BRAF(V600E) increased both TGF β mRNA and protein secretion in nevus and diBRAF(V600E) melanocytes. (Fig. 2.6A and 2.6B). To determine whether TGF β was sufficient to recapitulate the anti-proliferative effects of BRAF(V600E), we added TGF β to primary MC cultures. As expected, this induced p15 and arrested growth (Fig. 2.6C). p15 induction resulting from either exogenous TGF β or BRAF(V600E) is dependent on the TGF β receptor, as the TGF β receptor inhibitor SB-431542 blocked p15 induction in both cases (Fig. 2.6D). These data are consistent with human nevus tissue, which displays robust SMAD activation (Lo et al. 2008). The specific transcription complexes downstream of BRAF responsible for directly activating TGF β transcription are not definitively established, but are likely to include EGR-1. EGR-1 has been shown to bind TGF β promoter regulatory domains in other human cells (Llu et al., 1996) (Baron et al.), and EGR-1 is a firmly established ERK 1/2 target (Ben-Chetrit et al., 2013). Consistent with these prior studies, EGR-1 was upregulated in BRAF(V600E) nevus

melanocytes. Also consistent with this ERK-dependent p15 induction, inhibition of ERK signaling by the MEK inhibitor U0126 blocked BRAF-driven p15 induction.

We next sought to determine whether inhibiting BRAF(V600E) itself would restore proliferation in melanocytes harboring constitutively active BRAF. We treated both our engineered doxycycline inducible diBRAF(V600E), and primary nevus derived V600E melanocytes with the selective BRAF(V600E) small molecule inhibitor PLX4720. As expected, PLX4720 treatment, when delivered with doxycycline to diBRAFV600E cells, prevented both p15 induction and the corresponding growth arrest. In contrast, when the inhibitor was delivered to diBRAF cells in which growth arrest had been previously established by antecedent doxycycline administration, cells remained growth arrested, and p15 levels remained higher than in normal cells. This suggests that under in vitro culture conditions, BRAF activity and the corresponding p15 induction are necessary for establishing the growth arrest, but that additional events may also serve to reinforce and maintain it. Though unexpected, the finding of persistent growth arrest despite BRAF(V600E) inhibition is consistent with clinical observations, in which vemurafenib-treated patients do not typically display obvious morphological changes in preexisting benign nevi. Also consistent with this, is our observation that PLX4720 does not reverse growth arrest in primary melanocytes isolated directly from nevus specimens. Additionally, we found that melanocytes expressing inducible BRAF(V600E) that underwent growth arrest after 3 days of doxycycline administration, and were subsequently cultured in media lacking doxycycline, remained growth arrested. This reinforces the idea that melanocytes may employ additional BRAF-independent mechanisms that maintain the growth-arrested state, once established.

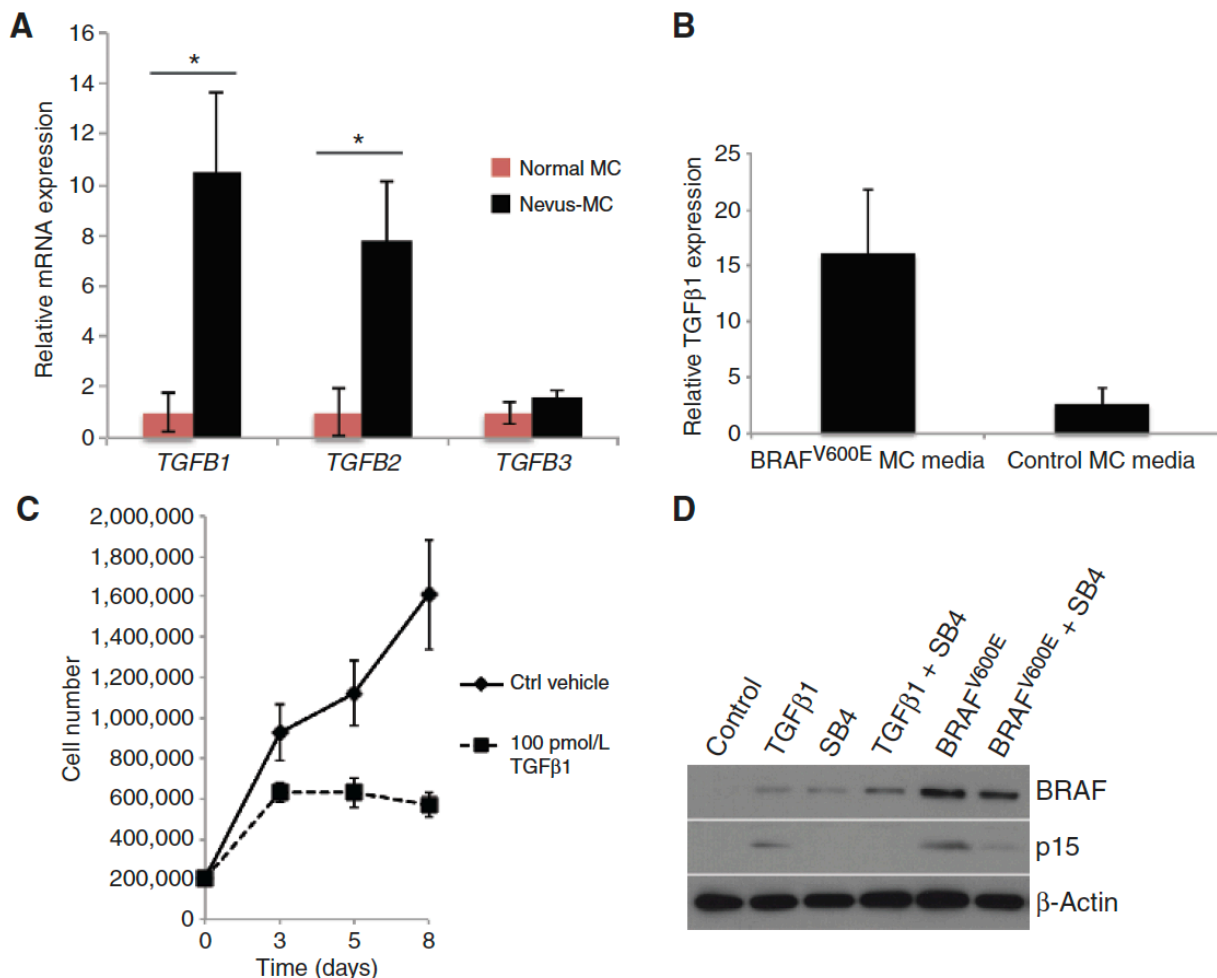


Figure 2: TGFβ Secretion Induces p15 Expression and Drives Melanocyte Growth Arrest.

(A) Relative transcription of TGFβ-1, TGFβ-2, and TGFβ-3 in nevus MCs and normal MCs determined by TaqMan qPCR. $n = 3$ biological replicates for normal MC and $n = 4$ biological replicates for nevus MC. $*P < 0.05$.

(B) TGFβ levels in culture media from diBRAF(V600E) or normal melanocytes. Data are shown as average \pm SEM, $n = 3$ biological replicates for diBRAF(V600E) MCs and normal MCs.

(C) Proliferation of luciferase-transduced melanocytes with or without 100pM exogenous TGFβ. Data are shown as average \pm SEM. $n = 3$ biological replicates for each group.

(D) 100pM TGFβ or BRAF(V600E) driven p15 induction is inhibited by 50μM SB431542 TGFβ receptor blockade in human melanocytes.

p15 Loss Reverses Nevus-MC Growth Arrest In Vivo and Promotes Progression to Melanoma

Finally, to determine whether p15 loss promotes progression from benign nevus to melanoma, we transduced nevus-MCs with shRNA targeting p15 (p15i), or control shRNA (NSi), dnp53, and hTERT and seeded them with normal human keratinocytes on native human dermis. Xenografts were harvested at 60 and 100 days. At 60 days post grafting, nevus-MCs harboring anti-p15 shRNAs proliferated to form nests of melanocytes at the dermal-epidermal junction. Conversely, nevus-MCs harboring the control hairpin engrafted, but were present only as single cells at regular intervals along the basement membrane of the tissue, and did not proliferate into melanocytic nests (Fig. 2.7). At 100 days post grafting, nevus-MCs harboring control shRNAs maintained their arrested state, while those with p15 knockdown proliferated into large nests, and displayed hallmark features of melanoma *in situ* including large histologically atypical melanocytes with high mitotic index and Pagetoid cells migrating upward through epidermis (Fig. 2.7). To determine whether loss of p16 was also sufficient to reverse the BRAF(V600E) induced growth arrest of nevus-MCs *in vivo*, we repeated the experiment with nevus-MCs harboring shRNAs targeting p16. Consistent with our *in vitro* data, we found that p16 knock down nevus-MCs proliferated in the xenograft setting, but did so less robustly than melanocytes lacking p15. Loss of p16 led to modest increases in melanocyte density that was intermediate between the controls and that of the p15 knockdown tissues.

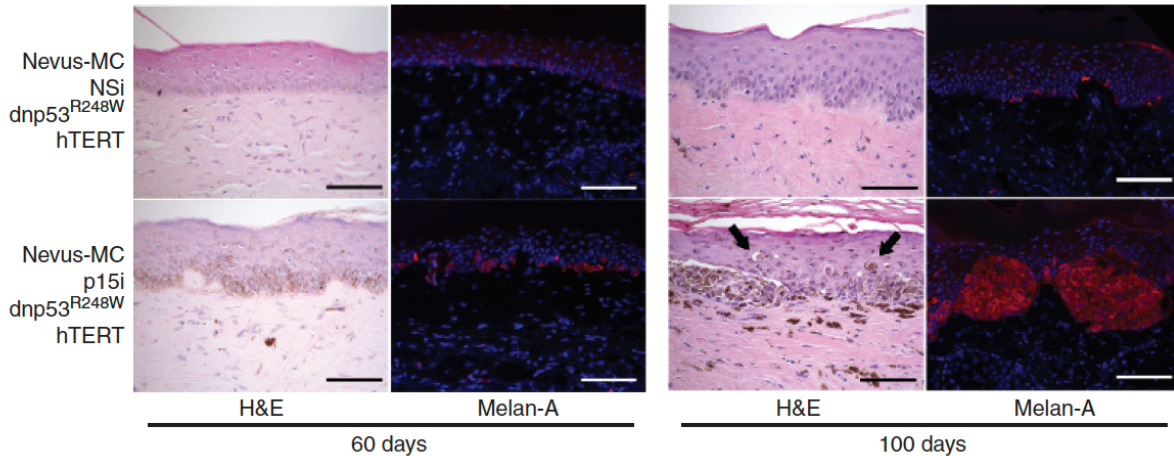


Figure 2.7: p15 Loss Reverses Nevus-MC Growth Arrest and Promotes Progression to Melanoma *in vivo*.

Hematoxylin and eosin staining with Mel-A immunofluorescence of Nevus MC expressing control shRNA (NSi), dnp53(R248W), and hTert (Row 1), and Nevus MC expressing shRNA against p15 (p15i), dnp53(R248W), and hTert (Row 2). Tissue from human skin xenografts was harvested at either 60 days (left) or 100 days (right) and is representative of n=3 biological replicates. Arrows indicate upward epidermal Pagetoid scattering of neoplastic melanocytes. Scale bars = 100µm.

This work demonstrated the importance of p15^{INK4B} in mediating cell cycle arrest in human melanocytic nevi. Consistent with the observations of Michaloglou et al, these data further suggested that while p16^{INK4A} is induced by BRAF^{V600E}, it appears to play a less potent role than p15^{INK4B} in establishing growth arrest in melanocytes both *in vitro* and *in vivo*. If p16^{INK4A} upregulation did not potently inhibit cell proliferation in human melanocytes, we questioned what its role in melanoma progression might be. To better elucidate the role of CDKN2A gene products in the progression from melanocytic nevus to melanoma we sought to directly test the effects of CDKN2A loss in human melanocytes and established melanoma cell lines.

Part 3: Role of CDKN2A in growth arrest and additional roles in invasion and metastasis.

(Reproduced from Zeng et al. Cancer Cell 2018)

Targeted engineering of primary human melanocytes

To explore the consequence of *CDKN2A* loss in a model that retains both the cell type and genome representative of the early stages of melanoma progression, we harnessed CRISPR-Cas9-mediated homology directed-repair (HDR) to edit the endogenous genetic loci of primary human melanocytes. In human melanomas, focal deletions and point mutations in *CDKN2A* most commonly affect exon 2 (Sviderskaya et al., 2003). We therefore designed a strategy to engineer a focal replacement of *CDKN2A* exon 2 with a CMV-promoter driven EGFP (Fig. 8A). Candidate sgRNAs for targeting exon 2 were designed and introduced in combination with Cas9 protein into normal human melanocytes (NHMs) using an optimized electroporation protocol. The Cas9 cut the expected genome sequence with high efficiency and without notable effects on the top predicted off-target sites. We used a double nickase (dCas9) cutting strategy to further reduce off-target cutting (Chen et al., 2013) (Ran et al., 2013). We introduced plasmids expressing each sgRNA and dCas9 in combination with a double-stranded template for HDR containing 2 kb homology arms. Three weeks after transfection 8–17% of NHMs remained EGFP-positive, whereas control cells that received only the HDR template were EGFP-negative (Fig. 8B). EGFP-expressing NHMs were isolated via flow cytometric cell sorting (FACS) and compared to sibling NHMs with an intact *CDKN2A* locus (Fig. 8C). Polyclonal EGFP-expressing NHMs exhibited the correct genotype for successful knock-in and the corresponding loss of p16^{INK4A} and p14^{ARF} expression, whereas expression of p15^{INK4B} from the *CDKN2B* locus was retained (Fig. 8D–8E). To further validate the specificity of our editing, we expanded three single cell clones and performed targeted genome sequencing of over 500 cancer genes. In each clone, there was only one fully-clonal genetic alteration, a bi-allelic *CDKN2A* deletion (Fig. 8F). Other alterations were present in only small fractions of the clonal populations, implicating *CDKN2A* editing as likely the

only genetic change induced by the engineering event. These data demonstrate that our optimized strategy for engineering locus-specific changes in NHMs is both tractable and precise.

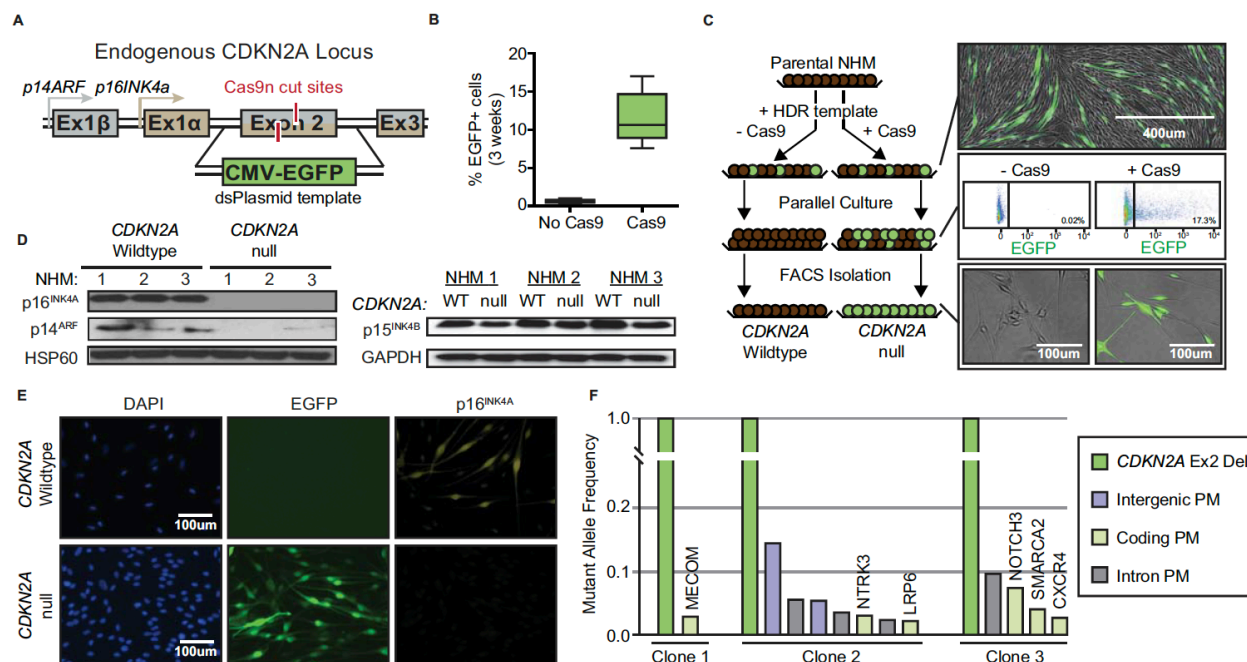


Figure 2.8: Engineering of *CDKN2A* null melanocytes.

(A) Strategy for introducing focal knock-in of CMV-EGFP to replace exon 2 of *CDKN2A*.

(B) Percentage of EGFP-positive NHMs three weeks after editing the *CDKN2A* locus. Data represent mean, 25th and 75th percentiles, minimum and maximum values of eight CRISPR reactions on three preparations of NHMs.

(C) Strategy for isolating *CDKN2A* null NHMs for comparison to wild-type siblings cells. Directly after transfection, both Cas9- and Cas9+ conditions contain EGFP+ cells (top). Over time, Cas9- cells become uniformly EGFP-, and the remaining EGFP+ cells in the Cas9+ population are isolated (middle). Isolated cells are stably EGFP+ and compared to matched EGFP- cells (bottom).

(D) Western blot detection of both *CDKN2A* protein products (p16INK4A and p14ARF, left) and *CDKN2B* protein product (p15INK4B, right) in isolated EGFP+ and EGFP- NHM populations

(E) Immunofluorescent visualization of p16INK4A expression in EGFP+ and matched EGFP- NHMs.

(F) Targeted sequencing of three clonal EGFP+ populations to monitor for off-target Cas9 cutting. Graphed are the mutant allele frequencies of deletions (Del) and point mutations (PM) in intergenic, coding and intronic regions. NHM1-3 refers to independent primary melanocyte derivations and engineering events.

p16^{INK4A} suppresses melanocyte motility and invasion

We next sought to characterize the oncogenic contributions of *CDKN2A* loss in primary NHMs. *CDKN2A* deletions were engineered into low-passage neonatal NHMs, as above, and compared to *CDKN2A* wild-type sibling cells. To compare cell behavior in the two sorted populations, we utilized digital holographic cytometry, which permits simultaneous quantification of cell division, death, senescence, and motility of adherent cells over long-term culture (Fig. 9A) (Hejna et al., 2017). Compared to wild-type sibling cells, *CDKN2A* null NHMs proliferated more rapidly and exhibited increased longevity in culture, consistent with previous observations (Obata et al., 1997 (Obata et al.) (Sviderskaya et al., 2003) (Sviderskaya, 2002). However, despite increased longevity, *CDKN2A* null NHMs were not immortalized and possessed reduced telomere length before undergoing growth-arrest after 60–70 doublings. Growth-arrest could be rapidly induced through transduction of BRAF^{V600E} cDNA as previously reported (Haferkamp et al., 2009); (Kumar et al., 2014) (Lu et al., 2016) (Michaloglou et al., 2005). Interestingly, the percentages of cells that underwent BRAF^{V600E}-induced growth-arrest were comparable in both *CDKN2A* null and wild-type cells suggesting BRAF^{V600E} overexpression can induce growth arrest in a *CDKN2A* independent manner.

In addition to the expected effect of *CDKN2A* loss on cell proliferation, another interesting phenotype emerged from our digital holographic analysis. *CDKN2A* null NHMs were significantly more motile compared to wild-type sibling cells (Fig. 9B). To account for movement associated with cell division, actively dividing cells were excluded from the analysis, and the increased motility remained significant (Fig. 9C). Corroborating these observations, *CDKN2A* null NHMs also exhibited enhanced migration in live-imaged scratch assays (Fig. 9D–9E) and enhanced invasion across high-density basement membrane extracts in transwell assays (Fig. 9F). The increased motility of *CDKN2A* null NHMs was independent of the expression level, intracellular location or identity of the fluorescent protein used in the engineering. To verify the phenotype was the consequence of loss of a *CDKN2A* gene product, we transduced *CDKN2A* null NHMs with either

p14^{ARF} or p16^{INK4A} cDNA. Expression of p16^{INK4A} reverted the motility phenotype, whereas expression of p14^{ARF} did not (Fig. 9G). These data demonstrate that the p16^{INK4A} product encoded by the *CDKN2A* locus inhibits cellular motility in primary NHMs.

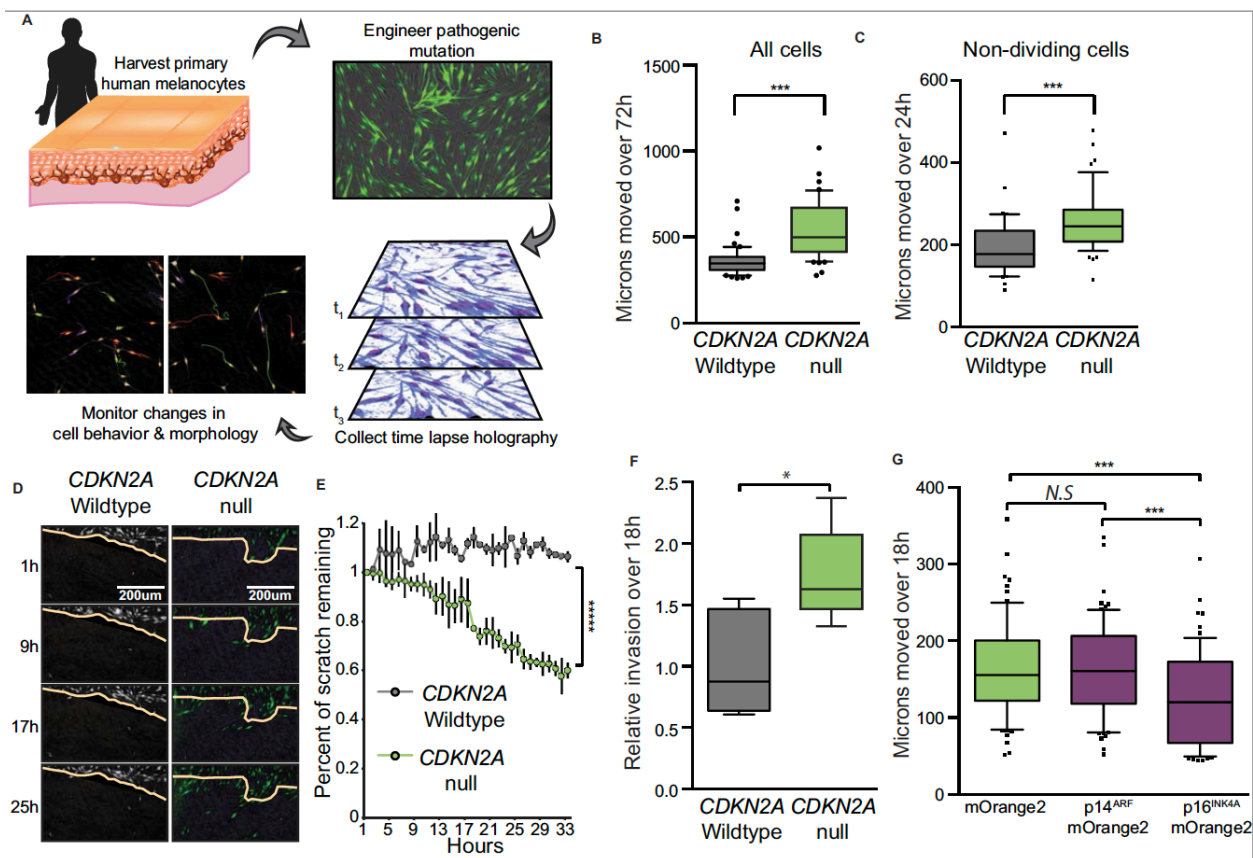


Figure 2.9: CDKN2A loss promotes melanocyte motility and invasion

(A) Schematic of experimental set-up. For each experiment, NHMs are derived from donated tissue and engineered for CDKN2A loss as in Figure 1. After isolation, CDKN2A null and wild-type sibling cells are monitored via digital holographic cytometry for 72 hr. The rate of cell division, motility, morphology, growth arrest and detachment are quantified. Representative holographic phase shift images (bottom left) show colored comet tails tracking cells.

(B) Single cell motility analysis of CDKN2A null NHMs compared to wild-type siblings. Box and whisker plot represents mean, 10th, 25th, 75th and 90th percentiles of at least fifty cells each from three CRISPR reactions of three preparations of NHMs.

(C) Quantification as in (B) but excluding cells that divided during the 72 hr time period surrounding 24 hr of analysis.

(D and E) Time-lapsed holographic phase shift images (D) and quantification (E) of NHMs migrating into scratched region. Yellow line indicates scratch limit at first time point. Error bars represent standard deviation of the mean of three CRISPR reactions of three preparations of NHMs.

(F) Quantification of transwell invasion assays where CDKN2A null NHMs and wild-type siblings were required to migrate through high-density basement membrane extract. Box and whisker plots represent mean, 25th and 75th percentiles, minimum and maximum values of five CRISPR reactions of three preparations of NHMs.

(G) Single cell motility analysis of CDKN2A null NHMs transduced with and sorted for the indicated vectors. Box and whisker plot represents mean, 10th, 25th, 75th and 90th percentiles of at least fifty cells each from three transductions.

Asterisks indicate p value of * <0.05 to ***** <0.000005 from unpaired t-test. N.S. indicates no significant difference.

p16^{INK4A} regulates motility independent of driver mutation

To determine whether *CDKN2A* loss alters melanocyte motility in the presence of melanoma driver mutations, we first engineered wild-type or *CDKN2A* null NHMs to harbor the *BRAF*^{V600E} point mutation. We transfected ribonucleoprotein (RNP) complexes containing Cas9 and sgRNA targeting exon 15 of the *BRAF* locus (Fig. 2.10A). We designed a single-stranded (ss)DNA HDR template to introduce the point mutation encoding V600E along with three silent mutations that suppress subsequent re-binding of the sgRNA (Fig. 2.10A). To detect mutant *BRAF*, we developed a digital droplet quantitative (dd-q)PCR assay with 100 percent specificity for the V600E allele and sensitivity down to 0.1 percent mutant allele frequency (MAF). Three weeks after co-transfection of the RNP with the HDR template into NHMs, 5–9% of the *BRAF* sequences in the culture were mutant. The MAF of the engineered NHMs increased rapidly in standard culture conditions over two months. The resulting populations were ~80% heterozygous for *BRAF*^{V600E}, expressed the *BRAF*^{V600E} protein, and demonstrated the concomitant increase in MAPK signaling.

After engineering the *BRAF*^{V600E} mutation into *CDKN2A* null and wild-type melanocytes (Fig. 2.10B), we observed that *CDKN2A* loss induced motility independent of either *BRAF* status or treatment with vemurafenib (Fig. 2.10C). To further investigate the pervasiveness of p16^{INK4A}-regulated motility, we obtained ten human melanoma lines representing different driver mutations and *CDKN2A* states (Fig. 2.10D). *CDKN2A* null or silenced lines were more motile than lines with p16^{INK4A} expression. Similar to the engineered NHMs, the enhanced motilities of lines that did not express p16^{INK4A} were reverted upon ectopic expression of p16^{INK4A} (Fig. 2.10E). Concordantly, motility was increased in all *CDKN2A*-expressing lines upon targeted p16^{INK4A} knockdown. In contrast, the manipulation of p16^{INK4A} did not consistently alter proliferation across each line (Fig. 2.10F). These data demonstrate that regulation of cellular motility by p16^{INK4A} occurs independent of the driver mutation and is not constitutively tied to cellular proliferation.

The acquisition of invasive behavior is a critical bottleneck to the series of events that occur during metastatic dissemination of melanoma. Previous reports have connected *CDKN2A* loss with metastatic dissemination in mouse model systems, but the mechanism has been attributed to indirect effects of p16^{INK4A} on cell cycle regulation or p14^{ARF} on p53-mediated apoptosis (Ackermann et al., 2005) (Aguirre, 2003) (Krimpenfort et al., 2001) (Pavey et al., 2002)). Since our data connect loss of *CDKN2A* (specifically p16^{INK4A}) with the acquisition of invasive behavior, we chose two lines from our panel to investigate whether p16^{INK4A} loss could directly affect the outcome of an *in vivo* assay for metastatic dissemination, independent of its inhibitory role on proliferation.

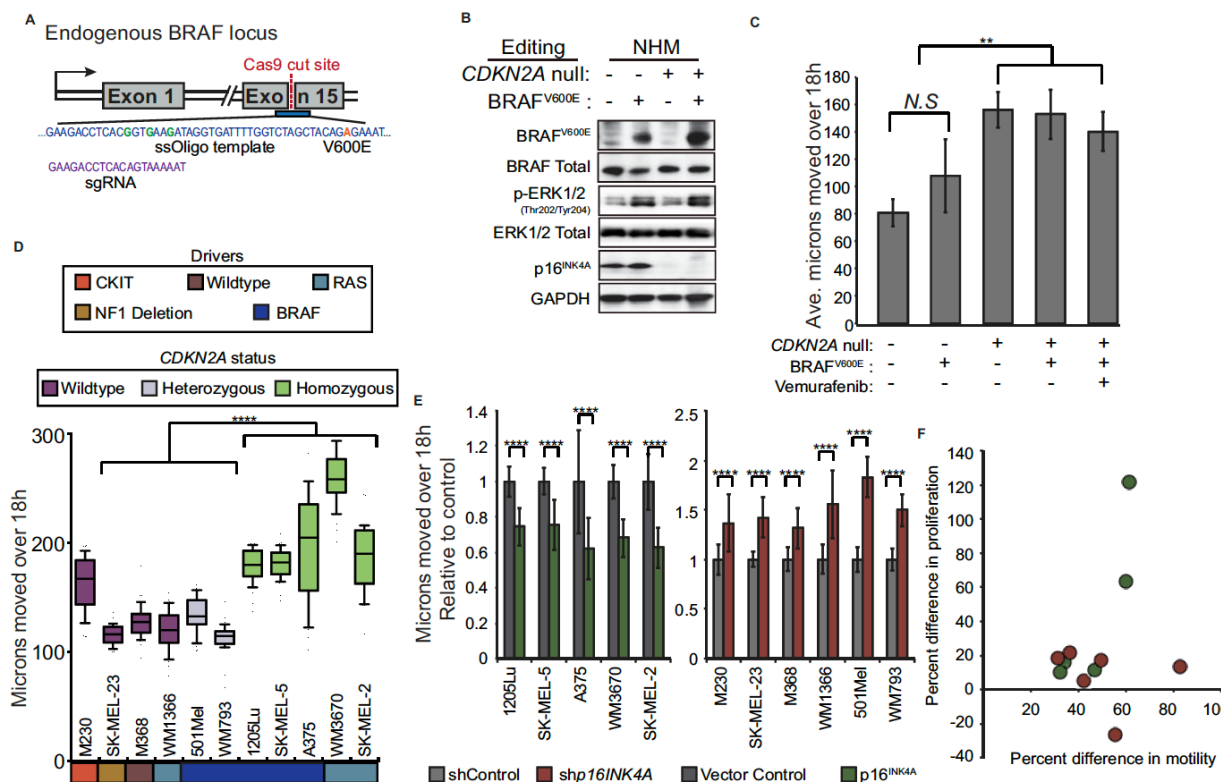


Figure 2.10: p16INK4A regulates motility independent of driver mutation

(A) Strategy for introducing BRAFV600E point mutation. Center of HDR template is shown (blue) with point mutations causing intended codon change (orange) or silent mutations disrupting sgRNA binding (green) highlighted. sgRNA sequence shown in purple.

(B) Western blot detection of BRAFV600E and p16INK4A expression and ERK phosphorylation in engineered NHMs.

(C) Population motility analysis of NHMs engineered with BRAFV600E and/or CDKN2A deletion. Error bars represent standard deviation of the mean of three experiments.

(D) Comparison of motility in ten melanoma lines with different genetic backgrounds. Lines were classified by activating driver mutation (BRAF, NRAS, CKIT or Wild-type) and CDKN2A status. CDKN2A status was designated as either wildtype and expressed (Wild-type), mono-allelic disruption and expressed (Heterozygous), bi-allelic disruption (Homozygous), or wild-type and silenced (Silenced). Box and whisker plot represents mean, 10th, 25th, 75th and 90th percentiles of forty cells per line.

(E) Effect of EF1a-driven p16INK4A expression on motility in CDKN2A null or silenced melanoma lines (left). Effect of shRNA-mediated p16INK4A knockdown on motility in p16INK4A expressing melanoma lines (right). Error bars represent standard deviation of the mean of forty cells per condition.

(F) Comparison of the effect of p16INK4A loss on proliferation and motility in ten melanoma lines. Red dots represent comparison of shRNA-mediated p16INK4A knock-down normalized to vector controls in p16INK4A expressing melanoma lines. Green dots represent comparison of vector controls normalized to EF1a-driven p16INK4A expression in CDKN2A null or silenced lines. No significant correlation between proliferation and motility was observed.

Asterisks indicate p value of ** <0.005 to **** <0.00005 from unpaired t-test. N.S. indicates no significant difference.

p16^{INK4A} loss induces metastasis in WM793 melanoma line

The WM793 melanoma line was derived from a *BRAF*^{V600E} – mutant early stage primary melanoma and is immortalized, but does not metastasize when injected subcutaneously into immune-compromised mice (Herlyn et al., 1985). In contrast, its derivative line, 1205Lu, disseminates to the lung (Juhász et al., 1993). To investigate genetic differences between the non-metastatic WM793 cell line and its metastatic derivative line 1205Lu, we performed targeted sequencing and copy number analysis. Known pathogenic alterations were shared between both cell lines, confirming their common ancestry, but each also harbored private point mutations and copy number alterations, most of which were not considered drivers (Fig. 2.11A–2.11C). However, the metastatic 1205Lu cell line harbored a bi-allelic deletion and associated loss of p16^{INK4A} expression, while the WM793 cell line retained a copy of the *CDKN2A* locus and expression of p16^{INK4A} (Fig. 2.11B).

To assess the effect of p16^{INK4A} expression on metastatic potential, derivative lines of 1205Lu and WM793 that respectively added back and knocked down p16^{INK4A} were developed. Derivative lines were injected subcutaneously into the flanks of immune-compromised mice, and lungs were harvested for analysis after 5 weeks (Fig. 2.11D). Metastasis formation was abolished in the p16^{INK4A}-expressing 1205Lu line, and conversely, WM793 cells acquired the ability to metastasize to the lung upon p16^{INK4A} knockdown (Fig. 2.11E–2.11H). Despite the increase in metastatic potential upon p16^{INK4A} knockdown, the growth rate of the primary tumor at the animals' flank remained low, and we observed no correlation between *in vitro* or *in vivo* proliferation rates and metastasis (Fig. 2.11I). These data demonstrate that metastatic potential can be gained through spontaneous or targeted loss of p16^{INK4A} via a mechanism that is uncoupled from its regulation of proliferation.

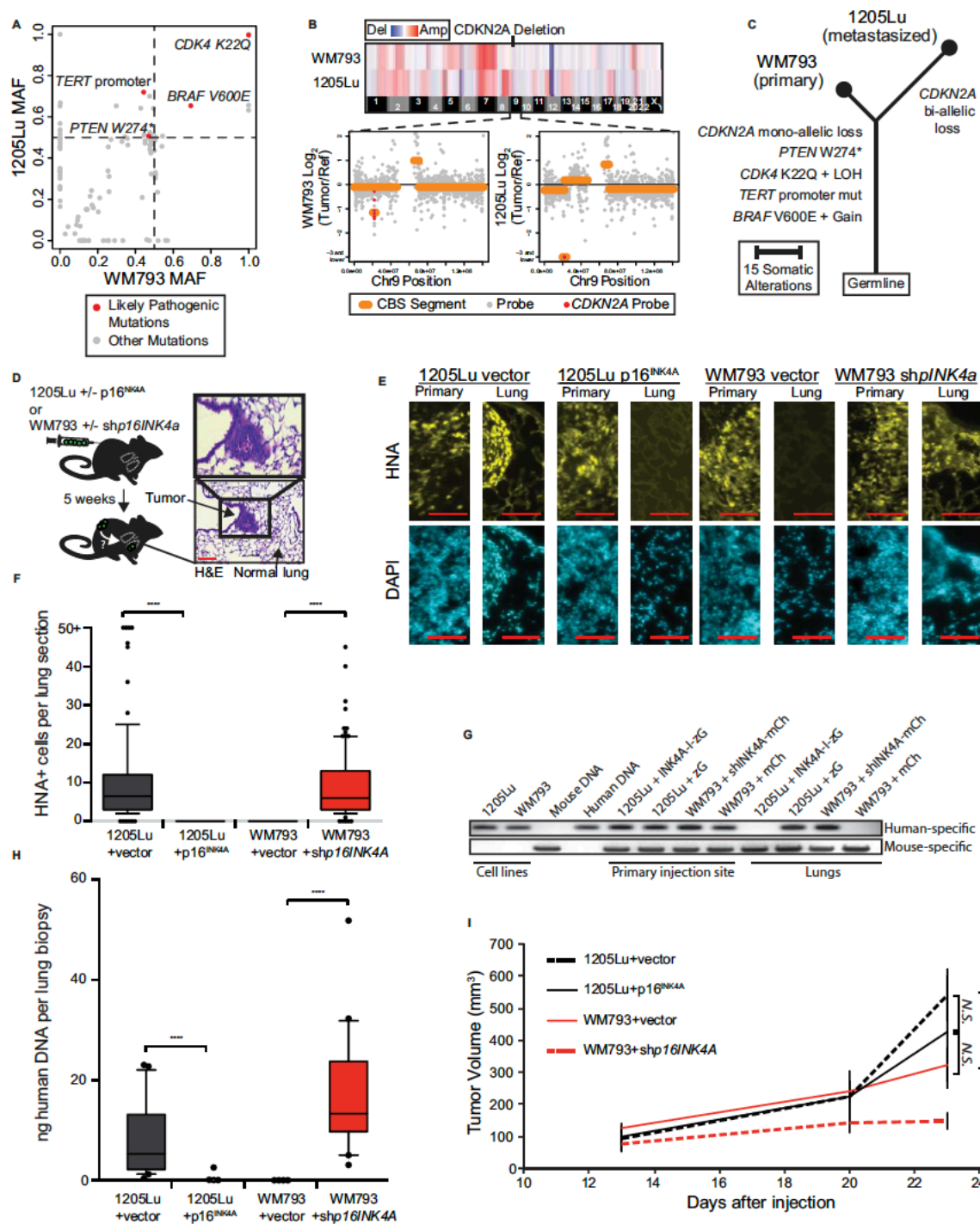


Figure 2.11: p16INK4A loss induces metastasis in WM793 melanoma line.

(A) A 500 gene panel, comprised of established cancer genes, was used to sequence the WM793 and 1205Lu cell lines. Point mutations are stratified by their mutant allele frequencies (MAFs) in each cell line as shown. Likely pathogenic mutations are highlighted in red. Data points along the diagonal represent mutations shared between the cell lines, and data points along either axis represent private mutations.

(B) Copy number variation between WM793 and 1205Lu cell lines inferred from sequencing depth (top). A focal heterozygous (bottom left, WM793) and homozygous (bottom right, 1205Lu) deletion affecting CDKN2A is highlighted in red.

(C) Phylogenetic tree representation of the genetic relationship between the primary WM793 and the derivative metastatic 1205Lu cell lines.

(D) Schematic of experimental setup for metastasis assay. WM793 cells transduced with either pSICOR-mCherry or pSICOR-shp16INK4A-mCherry or 1205Lu cells transduced with either pHIV-zsGreen or pHIV-p16INK4A-IRES-zsGreen were sorted for fluorescent protein expression and injected subcutaneously into NSG mice (n=5 per condition). Primary tumor volume was monitored and lung metastasis was analyzed after five weeks. Representative H&E stained lung section shows metastasized lesion (right). Red scale bars = 100 μ m.

(E) Representative lung sections with immunofluorescent stain for human nuclear antigen (HNA). Red scale bars = 100 μ m.

(F) Quantification of IF images from (E), showing the number of HNA positive cells in the lung for each condition (each group represents 100 quantified sections over 5 mice). Box and whisker plots represent mean, 10th, 25th, 75th & 90th percentiles.

(G) PCR amplification of genomic DNA from mouse lungs was performed using human (top) or mouse (bottom) specific primers to detect micro-metastases. All lobes were tested and a representative experiment is shown.

(H) Quantification of human specific DNA in murine lung across experiments. Values are absolute concentration of human DNA per sample measured via quantitative PCR. Data represent biopsies from 20 lung lobes over 5 mice per condition. Horizontal bars represent mean.

(I) Volume of primary tumors for all mice. Error bars represent standard deviation of the mean. Asterisks indicate p value of ** <0.005 and **** <0.00005 from unpaired t-test. N.S. indicates no significant difference.

Ultimately, we proposed that loss of p16^{INK4A} promoted melanocyte motility and invasion and conferred metastatic capability through activation of the *POU3F2* gene that encodes BRN2. Although the regulation of BRN2 is complex, we found that in human melanocytes BRN2 expression is inhibited by p16^{INK4A} - RB interactions and that loss of p16^{INK4A} in the progression to invasive melanoma leads to restoration of BRN2 expression.

Part 4: Potential regulation beyond the Cyclin Dependent Kinase inhibitors

The research presented in this section helps to clarify the roles of the CDKis p16^{INK4A} and p15^{INK4B} in the formation of melanocytic nevi and progression to melanoma. Despite the initial focus on p16 in arresting cell proliferation, we show that p16's neighboring gene p15 is intimately involved in establishing and maintaining growth arrest in melanocytes. p16 upregulation downstream of BRAF^{V600E} signaling likely contributes to the growth arrest of nevus melanocytes, however, bi-allelic deletion of p16 clearly plays an important role in enhancing the motility and invasive capacity of melanoma cells. Although it might be tempting to "close the file" on nevus growth arrest by attributing it to increased p15 and p16 expression, to do so would ignore the vast cascade of intracellular changes introduced by BRAF^{V600E} signaling. As suggested by previous research, upregulation of p15 and p16 are two of the many downstream of constitutive BRAF activation. DNA damage induced by hyper replication, depletion of intracellular nucleotide pools, and reorganization of chromatin may also play significant roles in establishing or maintaining growth arrest. Additionally, my research into *CDKN2B* demonstrated an upregulation of many CDKi family members, each of which would benefit from a more thorough investigation into their roles in cell cycle regulation. Going forward, it would be helpful to assess each of these events in a melanocyte specific cellular context, ideally leveraging the molecular tools afforded by the CRISPR revolution, in order to gain greater insight into the formation of melanocytic nevi.

Chapter 3: microRNAs Restrain Proliferation in BRAFV600E Melanocytic Nevi

(Reproduced from McNeal et al. 2020).

Part 1: microRNAs regulate a nevus-specific transcriptome.

Cutaneous melanoma is a potentially fatal skin cancer arising from the pigment-producing melanocytes of the basal layer of the human epidermis (Bastian, 2014). Despite the development of targeted therapies, such as small molecule inhibitors and immunotherapy, mortality rates of advanced melanoma remain stubbornly high (Siegel et al., 2017). If detected in its earliest stages, however, melanoma can often be cured through surgical excision (Vitiello et al., 2018).

Acquired activating V600E mutations in the BRAF proto-oncogene drive approximately 50% of all cutaneous melanomas (Pollock et al., 2003) (Garnett and Marais, 2004). Yet, when a melanocyte acquires a BRAF^{V600E} mutation, the cell does not immediately transform to cancer. Instead, it undergoes rapid clonal proliferation followed by growth arrest resulting in a stable pigmented skin macule known as a benign nevus or mole (Robinson et al., 1998) (Yeh et al., 2013). Despite the continued expression of BRAF^{V600E}, the majority of nevi remain innocuous for the lifespan of the individual, suggesting that nevus cells have robust intrinsic defenses against hyperproliferation.

Aberrant MAPKinase signaling downstream of BRAF^{V600E} produces a cascade of intracellular changes, each of which may contribute to the establishment and/or maintenance of growth arrest. BRAF^{V600E} expression has been shown to induce negative feed-back loops that ultimately dampen MAPKinase signaling (Uribe et al., 2006). DNA hyper-replication from oncogenic activation can simultaneously deplete cellular nucleotide pools and trigger DNA damage response pathways (Aird et al., 2013) (Di Micco et al., 2006). Epigenetic remodeling of chromatin observed in nevi can silence key transcriptional targets stymying proliferation (Stolz et al., 1991). Increased gene expression of cyclin dependent kinase 4/6 (CDK4/6) inhibitors, such

as p16^{INK4A} and p15^{INK4B}, is also associated with benign nevi (Michaloglou et al., 2005) (McNeal et al., 2015) (Zeng et al., 2018).

Although each of these factors likely contributes to the growth arrest phenotype of stable melanocytic nevi, the mechanisms that drive the bi-phasic process of nevogenesis – temporary proliferation prior to growth arrest - remain elusive. DNA sequencing of human nevi revealed that proliferating BRAF^{V600E} melanocytes have no additional genetic changes that distinguish them from growth-arrested nevus melanocytes (Shain et al., 2015), suggesting that transcriptional regulation is crucial for establishing the bi-phasic phenotype and ultimately restraining hyperproliferation. Interestingly, the growth restraint itself is non-permanent. Outside the context of transformation, nevus melanocytes can re-enter the cell cycle following exposure to specific stimuli, as seen in cases of recurrent nevi (King et al., 2009) or widespread nevus eruption (Burian and Jemec, 2019). Further, it remains unclear how the known mechanisms governing nevus growth arrest are overcome during melanoma initiation. For example, while p16^{INK4A} is expressed in the majority of nevi, >80% of melanoma *in situ* outgrowths from nevi and 40% of advanced melanomas retain its expression (Zeng et al., 2018) (Funk et al., 1998) (Keller-Melchior et al., 1998) (Reed et al.) (Talve et al.) (Wang et al., 1996). Insight into the mechanisms that distinguish BRAF^{V600E}-driven melanocyte expansion, growth arrest, and escape could reveal new approaches for detection, prevention, and therapeutic intervention in melanoma.

A unifying characteristic of BRAF^{V600E}-induced growth arrest pathways is the remodeling of the melanocyte transcriptome, which must remain durable to prevent nevus transformation to melanoma. microRNAs are small non-coding RNAs that regulate networks of genes and confer robustness to transcriptional programs (Ebert and Sharp, 2012). Aberrant microRNA expression has been reported in numerous human cancers, including melanoma, where they have been shown to play both oncogenic and tumor suppressive roles (Georgantas et al., 2014) (Nemlich et al., 2013) (Kanemaru et al., 2011) (Forloni et al., 2014). microRNAs regulate biological processes through complementary binding to the 3' untranslated region (3' UTR) of mRNA networks, and

therefore can serve as useful probes for unraveling complex transcriptional programs (Melton et al., 2010) (Judson et al., 2013) (Pencheva et al., 2012) (Levy et al., 2010). Seminal studies of gene networks targeted by miRNAs specific to aggressive melanoma revealed mechanisms required for metastatic dissemination (Pencheva et al., 2012). Here, we have taken a similar approach to unravel the mechanisms driving neovogenesis and melanoma initiation. Using clinical specimens of human nevi with adjacent melanoma, and primary human melanocytes derived from both normal skin and nevi, we identified elevated MIR211-5p and MIR328-3p expression as part of a nevus-specific transcriptome. Expression of both microRNAs mediates BRAF^{V600E} - induced growth arrest by regulating networks of dozens of genes. Both microRNAs converge to inhibit aurora kinase B (AURKB) translation, which is required to induce growth arrest in BRAF^{V600E} melanocytes and melanoma cells. In turn, we demonstrate that MIR211-5p and MIR328-3p regulation of AURKB plays a crucial role in human nevus formation and that their loss permits progression to melanoma.

Part 2: Role of MIR211-5p and MIR328-3p in Human Melanocytes and Nevus Formation.

Identification of nevus-enriched microRNAs

We sought to characterize a miRNA program specifically expressed in nevi, as compared to healthy melanocytes or melanoma arising from nevi (Fig. 3.1A). To first identify miRNAs down-regulated during transformation, we analyzed small RNA-sequencing from a previously established cohort of nevus with adjacent melanoma. Melanocytic nevus and melanoma portions of each case were isolated and subjected to targeted exon, mRNA, and small RNA sequencing (Shain et al., 2018) (Torres et al., 2020) (Fig. 3.1B). For each case, the nevus component was phylogenetically confirmed as a precursor to the adjacent melanoma (Shain et al., 2018). All lesions shared the BRAF^{V600E} driver mutation. We performed differential expression analysis using the DESeq2 *R* package (Love et al., 2014) to determine which microRNAs consistently

presented altered expression in the melanomas as compared to the precursor nevi. The analysis revealed a cohort of microRNAs exhibiting elevated expression in the nevus tissue, but down-regulated in the adjacent melanoma tissue, including MIR125b-5p, MIR100-5p, MIR328-3p, MIR211-3p, MIR125a-5p, and MIR211-5p (each p-value adjusted for multiple test correction of <0.05) (Fig. 3.1C). These observations are consistent with previous studies that have identified MIR125b-5p, MIR100-5p, and MIR211-5p as enriched in nevus tissue as compared with adjacent melanoma (Holst et al., 2011) (Damsky et al., 2015) (Levy et al., 2010). Likewise, our study confirmed previous reports identifying MIR21-5p as a melanoma-enriched microRNA downregulated in adjacent nevi (Wandler et al., 2017).

To probe for nevus-specific expression, as compared to normal human melanocytes, we next isolated melanocytes from fresh biopsies of long-standing nevi with no history of morphological change ($n = 6$) or healthy human skin with no visible melanocytic neoplasia ($n = 8$) (Fig. 3.1D-E). Sanger sequencing confirmed that melanocytes from healthy skin had two wildtype BRAF alleles while nevus melanocytes were heterozygous for the mutant BRAF^{V600E} allele (T1799A) (Fig. 3.1F). We then performed small-RNA sequencing on these samples. Differential expression analysis identified MIR125B-5p, MIR100-5p, MIR328-3p and MIR211-5p as increased in BRAF^{V600E} nevus melanocytes vs. BRAF^{WT} ($p < 0.05$) (Fig. 3.1G). Taken together, these results suggest these miRNAs form part of a nevus-specific transcriptome that increase in expression with the establishment of the nevus state then decrease upon transition to melanoma.

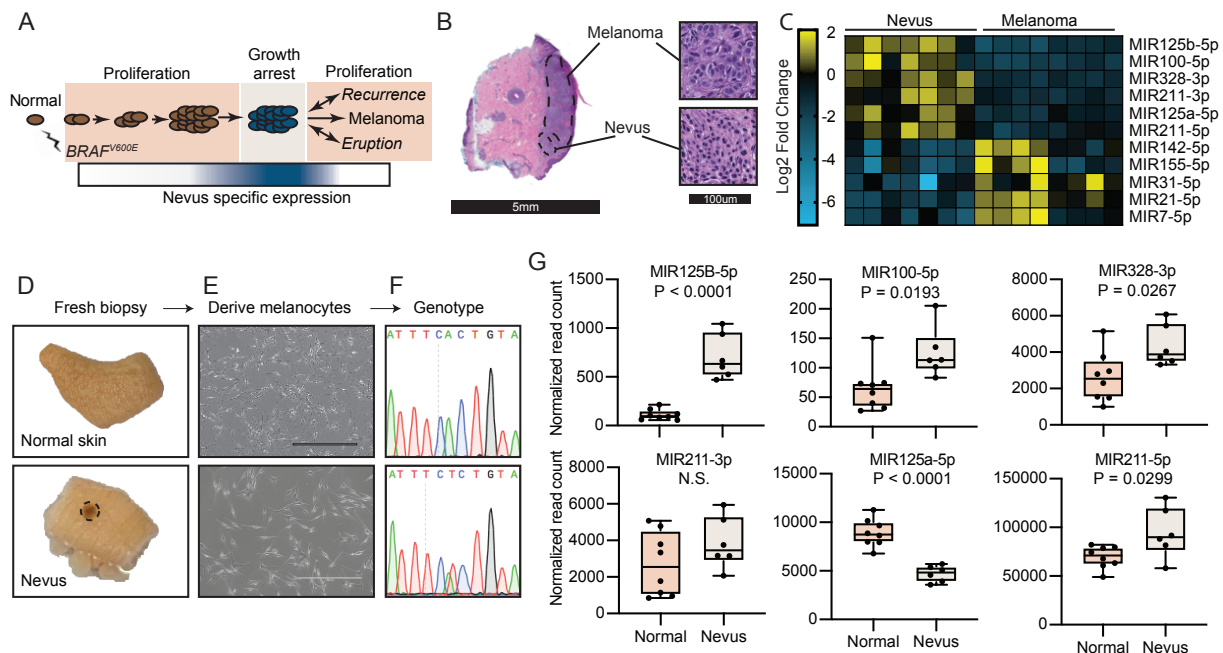


Figure 3.1: Identification of nevus- enriched microRNAs.

(A) Schematic highlighting plastic nature of BRAF^{V600E} nevus associated growth arrest and putative nevus specific transcriptional program.

(B) H&E of representative nevus to melanoma transition case with higher magnification insets of nevus and melanoma portions.

(C) Heatmap of top nevus and melanoma-enriched microRNAs from small-RNA sequencing of transition cases (n = 7 matched biological replicates of nevi and melanoma) (adj. p<0.05).

(D) Images of biopsies x10 representative photomicrographs.

(E) Human foreskin-derived melanocytes (top) and human nevus-derived melanocytes (bottom) x10 representative photomicrographs.

(F) Matched sanger sequencing chromatograms.

(G) Box-Whisker plots of nevus-enriched microRNAs expression in BRAFWT human melanocytes (peach, n= 8 biological replicates) and BRAFV600E human nevus melanocytes (tan, n = 6 biological replicates). P-values calculated by unpaired T Test.

MIR211-5p and MIR328-3p induce growth arrest in human melanocytes.

To better characterize the effects of nevus-specific miRNAs on human melanocyte proliferation, we nucleofected primary human melanocytes with RNA mimics corresponding to the mature sequences of MIR125B-5p, MIR100-5p, MIR328-3p and MIR211-5p, as well as non-targeting control mimics, and assayed proliferation over 7 days. Nucleofection of MIR211-5p or MIR328-3p each led to diminished melanocyte proliferation in comparison to the non-targeting control (* = $p < 0.05$) (Fig. 3.2A). To validate specificity and potency of each mimic, we generated dual fluorescence reporters of MIR211-5p and MIR328-3p function (Fig. 3.2B). When co-transfected with the targeting microRNA mimics and analyzed via flow cytometry, we observed a uniform inhibition of reporter expression, consistent with subtle translational inhibition expected from microRNA expression (Fig. 3.2C).

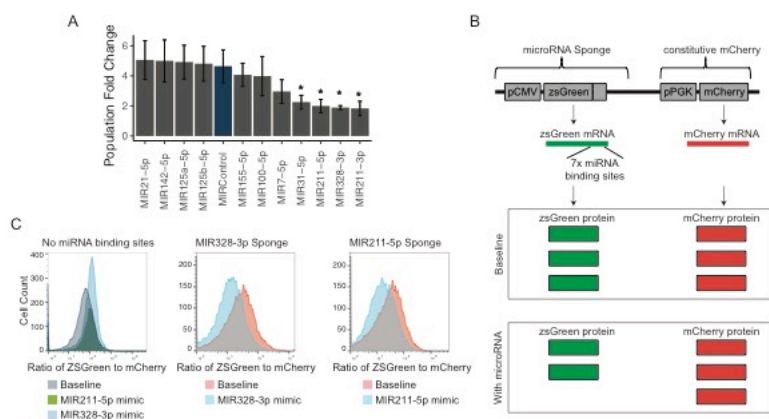


Figure 3.2: Screening and validation of MIR211-5p and MIR328-3p mimics

(A) Mean and standard deviation for population fold change of melanocytes nucleofected with nevus or melanoma-enriched microRNA mimics compared to non-targeting control (MIRControl) ($n = 3$ biological replicates) (p values calculated by unpaired TTest

* = $p < 0.05$).

(B) Schematic of microRNA sponge constructs, which serve as both reporters and inhibitors of microRNA function. A zsGreen cDNA expressing a 3' UTR with 7 tandem microRNA binding sites is expressed from the CMV promoter, whereas an mCherry that is not under microRNA regulation is expressed from the PGK promoter. After transduction, mCherry positive cells are expected to express the microRNA inhibitor and the ratio of zsGreen to mCherry provides a read-out of functional microRNA expression.

(C) FACS analysis depicting the zsGreen to mCherry ratio of melanocytes transduced with control, MIR328-3p, or MIR211-5p sponges, then nucleofected with MIR328-3p or MIR211-5p mimics. Physiological functional expression of the microRNAs is predicted to cause a subtle left-shift in the distribution, as observed.

To determine whether the proliferation defect was due to growth restriction or increased cell death, we monitored the effects of MIR211-5p and MIR328-3p on normal melanocyte behavior using digital holographic cytometry (DHC). DHC is a form of quantitative phase imaging (QPI) that permits long-term live imaging and assessment of cell division and death with single cell resolution (Hejna et al., 2017). We conducted DHC of nucleofected melanocytes over the course of 72 hours beginning at day 4 post-nucleofection. MIR211-5p and MIR328-3p overexpression induced a dramatic decrease in melanocyte proliferation in comparison to the non-targeting microRNA control (Fig. 3.3A). Single-cell analysis revealed only 32.9% and 25.1% of MIR211-5p or MIR328-3p expressing melanocytes divided between day 4 and 5 post-nucleofection, as compared to 85.9% of control cells (Fig. 3.3B). Growth arrested cells retained the appearance of healthy melanocytes, and the DHC analysis yielded no evidence of cell death. Growth arrest continued for 6-7 days (Fig. 3.3C-D). EdU uptake decreased with increasing concentration of MIR211-5p and MIR328-3p mimic 4 days post-nucleofection, indicating the rate of DNA replication was compromised in human melanocytes following MIR211-5p or MIR328-3p nucleofection (Fig. 3.3E). Corroborating these observations, cell cycle profiling demonstrated a consistent increase in the number of cells accumulating in S or G2/M phase of the cell cycle between days 3 and 7 following microRNA overexpression (Fig. 3.3F and 14G). In contrast, co-staining with propidium iodide and annexin V antibody 4 days post-nucleofection revealed no significant differences in the percentage of apoptotic melanocytes (Fig. 3.3H). Taken together, we conclude that over-expression of MIR211-5p and MIR328-3p in human melanocytes induces a proliferative arrest in the S/G2/M phases of cell cycle.

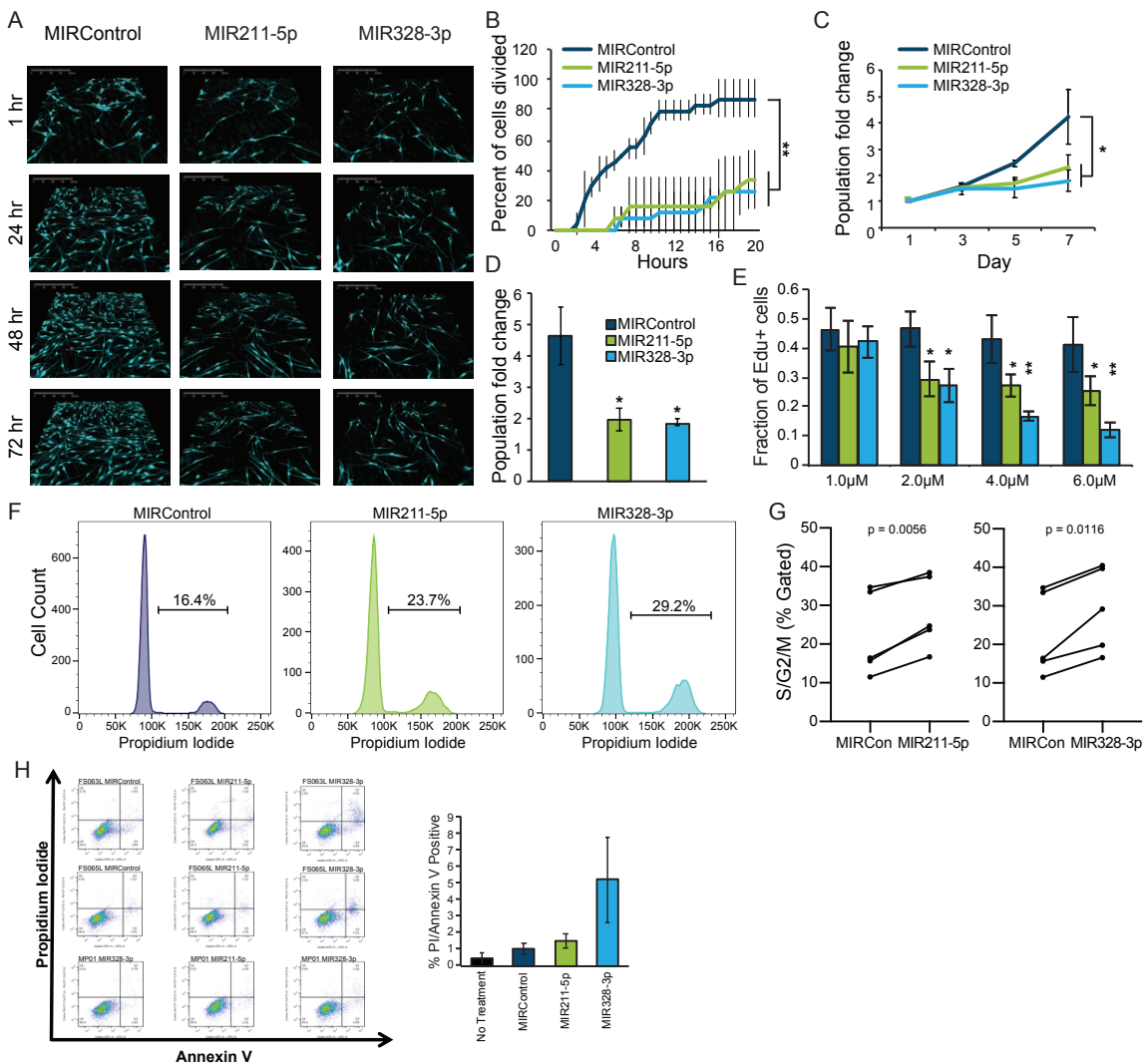


Figure 3.3: MIR211-5p and MIR328-3p induce growth arrest in human melanocytes.

(A) Representative images from live digital holographic imaging at indicated times post nucleofection of indicated microRNA mimics.

(B) Percent of melanocytes divided between days 4 and 5 post microRNA nucleofection for MIR211-5p (green), MIR328-3p (light blue) vs. MIRControl (dark blue). Digital holographic cytometry.

Line (C) and bar (D) plots of means and standard deviations of population fold change over 7 days of MIR211-5p and MIR328-3p nucleofected melanocytes vs. non-targeting MIRControl.

(E) Percent EdU positive cells after 4 days after nucleofection with 1, 2, 4, and 6 μ M miRNA mimic. (MIR211-5p (green), MIR328-3p (light blue) vs. MIRControl (dark blue), n=3 replicates).

(* = $p < 0.05$, ** = $p < 0.01$, unpaired T test)

(F) Representative histograms of propidium iodide staining as measured by flow cytometry. Percentages reflect percent cells in S or G2/M phases of cell cycle.

(G) Percent cells in S or G2/M phases of cell cycle 7 days post- nucleofection with MIRControl, MIR211-5p, or MIR328-3p.

(H) Dot plots for Annexin V/PI stain. Barplot of % Annexin V/PI positive cells. (n = 3 biological replicates).

Endogenous MIR328-3p and MIR211-5p contribute to BRAF^{V600E}-induced growth arrest

Our microRNA profiling of normal and nevus melanocytes and adjacent melanoma showed that MIR211-5p and MIR328-3p were enriched specifically in nevi. Ectopic expression of BRAF^{V600E} has been previously shown to induce growth arrest in human melanocytes (Michaloglou et al., 2005). As ectopic expression of MIR211-5p and MIR328-3p also induce growth arrest, we reasoned that endogenous expression of these microRNAs might contribute to BRAF^{V600E}-induced growth arrest. To test whether inhibition of endogenous MIR211-5p and MIR328-3p expression is sufficient to rescue BRAF^{V600E}-induced growth arrest, we leveraged a doxycycline inducible BRAF^{V600E} system (di-BRAF^{V600E}) (McNeal et al., 2015). We generated low passage human melanocytes expressing di-BRAF^{V600E} and exposed cells to doxycycline. Western blot analysis showed that the transduced melanocyte population expressed increasing levels of BRAF^{V600E} and ERK 1/2 phosphorylation when exposed to increasing concentrations of doxycycline (Fig. 3.4A). As expected, the induction of BRAF^{V600E} decreased proliferation in melanocytes from three separate donors (Fig. 3.4B). Cell cycle analysis revealed a dose-responsive increase in the S/G2/M phase arrest, similar to the miRNA overexpression (Fig. 3.4C). We were initially surprised by this result, as BRAF-driven G1 phase arrest has been reported, but closer inspection of these previously published data revealed an unappreciated S/G2/M phase arrest, as well (Zhu et al., 1998).

To determine whether MIR211-5p or MIR328-3p were necessary effectors of BRAF^{V600E}-induced growth arrest in human melanocytes, we inhibited MIR211-5p and MIR328-3p in BRAF^{V600E} melanocytes using two approaches. First, we nucleofected di-BRAF^{V600E} melanocytes with LNA microRNA inhibitors and assayed for Edu incorporation after 4 days. In the presence of a non-targeting control inhibitor, induction of BRAF^{V600E} decreased Edu uptake by 7% ($p < 0.01$). In contrast, in the presence of inhibitors targeting MIR211-5p or MIR328-3p, there was no significant decrease in mean Edu uptake in melanocytes regardless of BRAF^{V600E} expression (Fig. 3.4D). In parallel, we generated di-BRAF^{V600E} melanocyte lines that constitutively expressed

a microRNA sponge containing seven MIR211-5p or MIR328-3p binding sites and mCherry under control of independent promoters (Fig. 3.4E). We then conducted a competition assay between mCherry positive (sponge-expressing) and mCherry negative melanocytes. After five days of exposure to doxycycline, the mCherry population of cells expressing control sponge remained at constant, whereas the mCherry population of cells expressing sponges to MIR211-5p or MIR328-3p increased by 44.3% and 21.0%, respectively. Taken together, these results suggest that MIR211-5p and MIR328-3p independently contribute to BRAF^{V600E}-mediated growth arrest in human melanocytes.

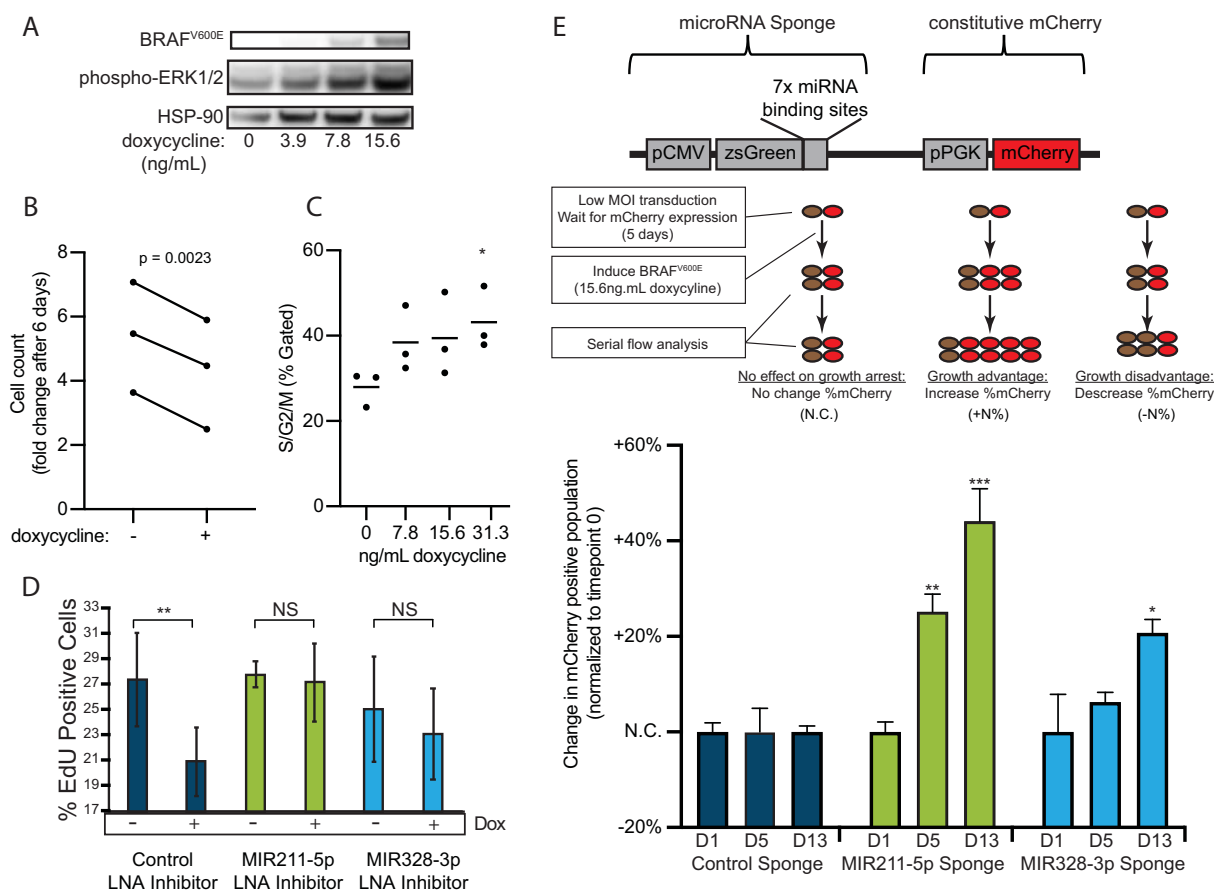


Figure 3.4: BRAF^{V600E} induced growth arrest requires MIR211-5p and MIR328-3p.

(A) Western Blot analysis of BRAF^{V600E}, phospho-ERK1/2 in diBRAF^{V600E} melanocytes in response to increasing concentration of doxycycline. HSP90 was used as a loading control.

- (B)** Population fold change for di-BRAFV600E MCs treated with 62.6 ng/mL doxycycline (paired T Test, n=3 biological replicates).
- (C)** Percent cells in S or G2/M phases of cell cycle after 7 days exposure to indicated concentrations of doxycycline. (* = $p < 0.05$, paired T Test)
- (D)** Mean and standard deviation of percent EdU positive diBRAFV600E melanocytes 7 days post-nucleofection with MIRControl, MIR211-5p, or MIR328-3p and with (+) or without (-) exposure to doxycycline. (** = $p < 0.01$, unpaired T test) (n = 6 biological replicates).
- (E)** Schematic of expected (top) and actual (bottom) results (mean and standard deviation) for competitive growth assay comparing diBRAFV600E melanocytes grown 13 days with exposure to doxycycline with or without mCherry tagged microRNA sponges. (* = $p < 0.05$, ** = $p < 0.005$, *** = $p < 0.0005$, unpaired T Test, n=3 replicates)

Part 3: Role of AURKB and GPR3 in Progression from Nevus to Melanoma

AURKB and GPR3 inhibition contributes to BRAF^{V600E}-induced growth arrest

Previous studies demonstrated that comprehensive characterization of microRNA targets can elucidate novel mechanisms in development and cancer progression. Having identified MIR211-5p and MIR328-3p as upregulated in human BRAF^{V600E} nevus melanocytes and contributors to BRAF^{V600E}-induced growth arrest, we next investigated the genetic networks regulated by MIR211-5p and MIR328-3p that converge to restrain melanocyte proliferation. We nucleofected normal human melanocytes with MIR211-5p, MIR328-3p, or non-targeting microRNA control mimics. Four days post nucleofection, we harvested total RNA from each sample and performed high-throughput mRNA sequencing. Computationally predicted targets of MIR211-5p and MIR328-3p were enriched among the genes down-regulated by each mimic respectively (Fig. 3.5A and 3.5B). . The majority of these targets exhibited 2-fold or less expression reduction, consistent with the established models of microRNA targeting on transcript levels.

To determine whether any of the downregulated transcriptional targets of the MIR211-5p or MIR328-3p contribute directly to the growth arrest microRNA phenotype, we performed a small interfering RNA (siRNA) screen against each target in normal human melanocytes. We tested a total of 131 down-regulated predicted targets of MIR211-5p and MIR328-3p. Of the

siRNAs tested, 86 inhibited predicted targets of MIR211-5p, 23 inhibited predicted targets of MIR328-3p, and 6 inhibited predicted targets of both microRNAs (Supplementary Table S1). The effect of each siRNA pool on EdU incorporation was compared to that of six controls: no mimic, a non-targeting siRNA control (Scramble 1), 2 non-targeting microRNA controls (Scramble 2 and Scramble 3), and MIR211-5p and MIR328-3p mimics. Knockdown of 62 of the 131 predicted target genes resulted in EdU uptake significantly less than that of the siControl ($p < 0.05$), though few induced changes as significant as the microRNA mimics themselves ((Fig. 3.5C). . These observations are consistent with previous reports that knockdown of individual genes in a microRNA target network can only partially phenocopy overexpression of a microRNA (Judson et al., 2013).

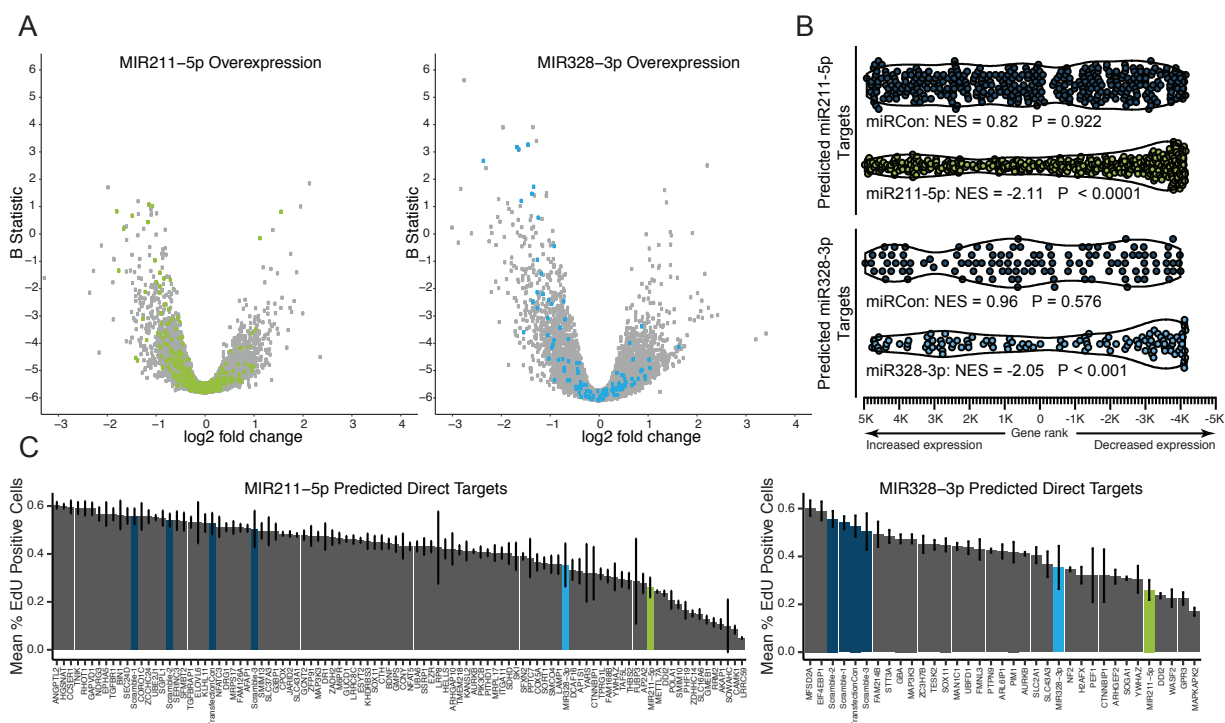


Figure 3.5: Identification of MIR211-5p and MIR328-3p mRNA targets.

(A) Volcano plots of mRNA sequencing from $n = 4$ biological replicates of melanocytes nucleofected with MIR211-5p (left) or MIR328-3p (right) vs. MIRControl. (MIR211-5p predicted targets = green, MIR328-3p predicted targets = light blue).

(B) GSEA analysis of MIR211-5p and MIR328-3p target mRNAs.

(C) Mean and standard deviation from $n = 3$ replicates of percent EdU positive melanocytes harboring knockdown of predicted MIR211-5p (left) or MIR328-3p (right) targets. Dark blue bars represent no mimic (nucleofection) control and three scrambled controls. Green bar represents MIR211-5p and light blue bar represents MIR328-3p.

To further narrow the scope of our study, we focused on genes that were down-regulated by both MIR211-5p and MIR328-3p and whereby knockdown significantly impaired EdU incorporation. We reasoned such genes represent potential network nodes where the MIR211-5p and MIR328-3p target networks converge. We identified AURKB and G-protein coupled receptor 3 (GPR3) as genes with significantly decreased expression upon expression of either microRNA (Fig. 3.6A). AURKB is predicted to be targeted by both MIR211-5p and MIR328-3p, whereas GPR3 is a predicted target of MIR328-3p only (Fig. 3.6B). To investigate whether AURKB or GPR3 inhibition is required for the microRNA-induced growth arrest phenotype, we generated lentiviral expression constructs for each coding sequence, which lacked the predicted microRNA binding sites (Fig. 3.6C and 3.6D). Human melanocytes stably expressing each gene were nucleofected with MIR211-5p, MIR328-3p, or a non-targeting control. We assayed proliferation over 7 days and found that overexpression of AURKB rescued and GPR3 partially rescued the MIR211-5p induced growth defect (Fig. 3.6E). Likewise, AURKB overexpression partially rescued the MIR328-3p induced growth arrest, whereas GPR3 overexpression did not ameliorate the phenotype.

To determine whether AURKB or GPR3 expression could rescue the BRAF^{V600E}-induced growth arrest in human melanocytes, we overexpressed either AURKB, GPR3, or zsGreen transgenes in human melanocytes previously transduced with the di-BRAF^{V600E} transgene. In the absence of doxycycline- induced BRAF^{V600E} expression, AURKB increased melanocyte proliferation (Fig. 3.6F). When BRAF^{V600E} was expressed, AURKB rescued proliferation. In contrast, GPR3 expression decreased melanocyte proliferation, however, when BRAF^{V600E} was expressed, GPR3-expressing cells did not further decrease proliferation (Fig. 3.6F). To validate

the finding that AURKB could rescue BRAF^{V600E}-induced growth arrest *in vitro*, we asked whether AURKB was sufficient to restore proliferation to growth arrested human nevi. We transduced non-proliferating nevus melanocytes from three independent donors with lentivirus harboring AURKB and mCherry at low MOI. QPI for 90 hours post-infection demonstrated that nevus melanocytes that expressed mCherry (and therefore AURKB) significantly increased proliferation in comparison to mCherry negative nevus melanocytes (Fig. 3.6G). These results further suggest that inhibition of AURKB by MIR211-5p and MIR328-3p is essential for the BRAF^{V600E}-induced growth arrest in human melanocytes.

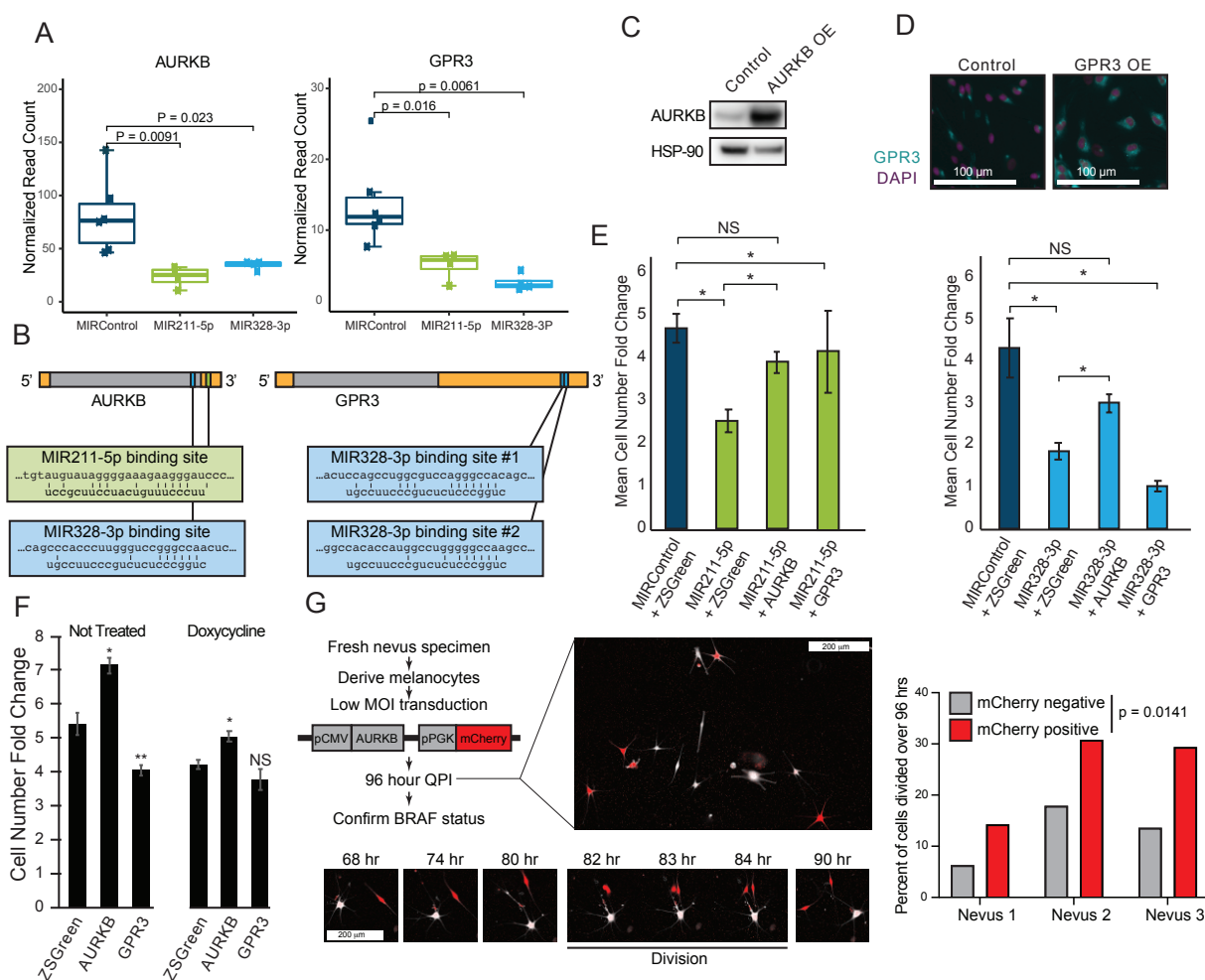


Figure 3.6: AURKB and GPR3 inhibition contribute to BRAF^{V600E}-induced growth arrest. (A) Normalized read counts for AURKB or GPR3 in melanocytes nucleofected with MIRControl (dark blue), MIR211-5p (green), or MIR328-3p (light blue). P-values calculated by Wilcoxon test (n = 4 biological replicates for each condition).

- (B)** Schematics showing potential binding sites of MIR211-5p and MIR328-3p in the 3' UTRs of AURKB (left) and GPR3 (right).
- (C)** Western Blot of AURKB expression in human melanocytes with or without lentiviral AURKB overexpression. HSP90 is the loading control.
- (D)** Representative photomicrographs (20X) of immunofluorescence for GPR3 (green) or (Hoechst) (purple) in human melanocytes with GPR3 lentiviral overexpression (GPR3 OE) or without (Control) over-expression.
- (E)** Cell number fold change mean and standard deviation for melanocytes overexpressing zsGreen control, AURKB, or GPR3 and nucleofected with MIR211-5p (left) and MIR328-3p (right). P values calculated by type 2 unpaired T Test. (*= $p < 0.05$) (n = 6 biological replicates).
- (F)** Cell number fold change mean and standard deviation for melanocytes transduced with doxycycline inducible BRAFV600E and either ZSGreen control, AURKB, or GPR3, and then treated with (+) or without (-) dox. (p values calculated by unpaired T-Test and compare to ZSGreen (+) or ZSGreen (-) dox respectively *= $p < 0.05$) (n = 6 biological replicates).
- (G)** Experimental design (top left) and representative images capturing dividing nevus melanocyte (bottom left) and quantification (right) of digital holography of human nevus cells infected with low titer AURKB/mCherry lentivirus. (n = 3 biological replicates) (p value calculated by paired T-Test).

Increased AURKB and GPR3 expression are associated with progression to melanoma

Taken together, our results demonstrate that BRAF^{V600E} nevus melanocytes express increased levels of MIR211-5p and MIR328-3p, and that these microRNAs contribute to growth arrest through inhibition of AURKB and GPR3. If true, we would expect that the expression of these genes would be elevated in melanoma as compared to nevi. Transcriptional profiling of nevi (n = 11) and adjacent melanoma (n = 12) from human FFPE tissue revealed that AURKB and GPR3 transcripts are significantly upregulated in melanoma in comparison to nevi – an inverse expression pattern of MIR211-5p and MIR328-3p (Fig. 3.7A). Immunohistochemistry (IHC) of human nevus (n = 11) and melanoma (n = 11) sections further demonstrated that AURKB and GPR3 expression is upregulated in melanomas relative to nevi (Fig. 3.7B). If upregulation of either gene were also essential for melanoma growth, we would further expect that inhibition would revert BRAF^{V600E} melanoma cells to a growth-arrested state. Two BRAF^{V600E} human melanoma cultures – one established line (501MEL) and one derived from a low passage patient-derived xenograft tumor (HCIMel019) – were treated with the selective AURKB inhibitor, Barasertib (Helfrich et al., 2016). Both cultures were highly sensitive to the compound, consistent

with a previous report (Fig. 3.7C) (Porcelli et al., 2015). Live DHC imaging revealed no evidence of cell death, but rather growth arrest coupled to significantly increased cell volume, consistent with known functions of AURKB (Fig. 3.7D-E).

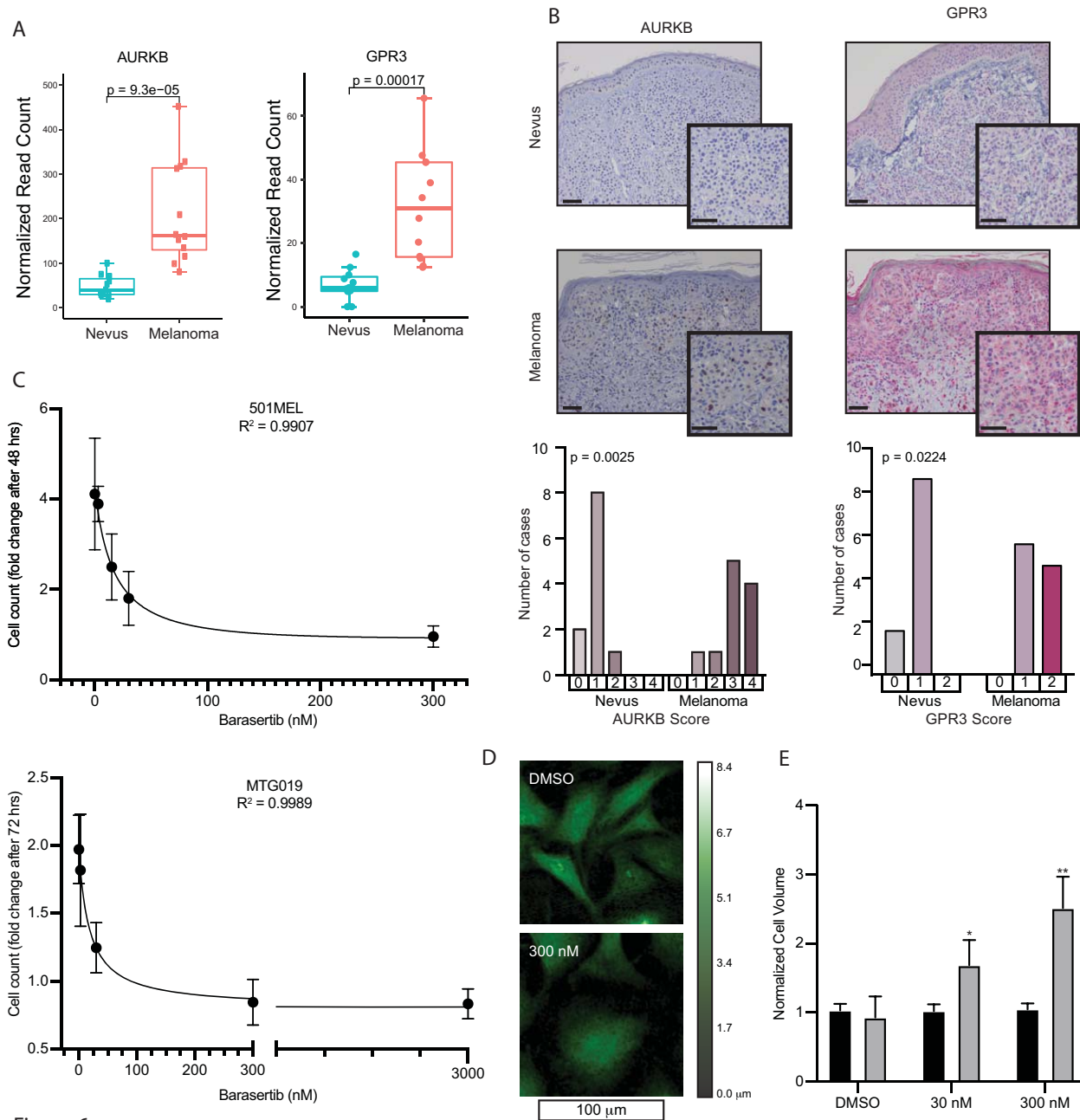


Figure 3.7: AURKB expression promotes melanoma growth.

(A) Normalized read counts for AURKB (left) and GPR3 (right) expression in matched nevi and adjacent melanoma (n = 11 nevi and 12 matched melanomas) (p values calculated by Wilcoxon test).

(B) Representative images (top) and quantification (bottom) of immunohistochemical staining for AURKB (brown chromagen) and GPR3 (red chromagen) expression in FFPE samples of nevi and melanoma. (n = 11 each group).

(C) Dose response curves for established human melanoma cell line (501MEL) and primary human melanoma culture (HCIMel019) treated with AURKB inhibitor, barasertib.

(D) Representative digital holographic images of HCIMel019 treated with DMSO control or 300 nM barasertib.

(E) Quantification of cell volume 48 hours after treatment with indicated concentrations of barasertib (n=3 replicates, * = p <0.05, ** = p<0.01, unpaired T test).

Part 4: Discussion of the role of microRNAs in nevus formation and progression to melanoma.

A long-standing question in the field of melanoma biology asks: how are nevi formed? A single mutation – BRAF^{V600E} – drives temporary proliferation followed by subsequent growth arrest, but the mechanisms that underlie this bi-phasic phenotype remain opaque. Equally perplexing is the conditional nature of growth arrest induction, wherein incompletely excised nevi can regrow to their former dimensions (King et al., 2009), or established nevi can erupt in response to external stimuli (Burian and Jemec, 2019). The mechanisms that permit these events are as ambiguous as nevocogenesis itself and require that the growth-arrest phenotype be both recurrently plastic and durable. Such reversible characteristics are more likely to be associated with environmental or transcriptional changes, rather than genetic. Here we identified two microRNAs that are elevated specifically in growth-arrested nevi and are both necessary and sufficient for BRAF^{V600E}-induced growth arrest *in vitro*. The microRNAs are downregulated, and their target expression increases in melanoma arising from nevi. Previous studies using melanoma cell lines representative of the advanced disease have identified MIR211-5p as either

a tumor suppressor or an oncomir, dependent on context (Vitiello et al., 2017) (Bell et al., 2014) (Levy et al., 2010) (Díaz-Martínez et al., 2018) (Golan et al., 2019) (Sahoo et al., 2019) (Mazar et al., 2016) (Mazar et al., 2010). Our data demonstrate that in the context of primary human melanocytes with little to no mutational burden, the transcriptional activation of MIR211-5p and MIR328-3p are at least partially responsible for nevus-associated growth arrest and that melanoma initiation from nevi requires their subsequent suppression.

Our data provide evidence that increased expression of MIR211-5p and MIR328-3p represent intracellular events that complement previously reported transcriptional changes required to establish and maintain growth arrest in nevus melanocytes. In particular, the genes p16^{INK4A} and p15^{INK4B} are potently upregulated in response to BRAF^{V600E} signaling and thought to contribute to nevus-associated growth arrest (Michaloglou et al., 2005) (McNeal et al., 2015) (Zeng et al., 2018). Like MIR211-5p and MIR328-3p, expression of both genes can induce melanocyte growth arrest *in vitro* and are frequently lost during transformation to melanoma. However, in contrast to inhibition of MIR211-5p and MIR328-3p, inhibition or genetic ablation of the CDKN2A locus does not rescue BRAF^{V600E} induced growth arrest (Halaban et al., 1998) (Michaloglou et al., 2005) (Haferkamp et al., 2009) (McNeal et al., 2015) (Zeng et al., 2018). Similarly, deletion of the locus does not prevent neovogenesis in mouse models (Dhomen et al., 2009) (Damsky et al., 2015). Another important distinction is the phase of the cell cycle regulated by each gene. p16^{INK4A} and p15^{INK4B} each inhibit CDK4/6-Cyclin D phosphorylation of RB, leading to a G0/G1-S phase cell cycle arrest (Zhang et al., 1999) (Hannon and Beach, 1994). Conversely, MIR211-5p and MIR328-3p block cell cycle progression through S and G2/M phases. Taken together, these observations suggest that microRNA-mediated inhibition of cytokinesis and CDKi-inhibition of cell cycle entry represent two complimentary mechanisms that each contribute to the initiation and the maintenance of growth arrest. Restriction across multiple stages of the cell cycle would enhance the durability of growth arrest in melanocytic nevi, further explaining why so few nevi transform to malignant disease over the lifespan of the individual. The upregulation of

multiple cell cycle checkpoints downstream of BRAF^{V600E} may also help explain the difficulties in determining a single phase of the cell cycle in which nevus cells are growth-arrested. Indeed, the extent of p16^{INK4A} expression varies across nevus specimens, ranging from no expression, to mosaic or uniform expression (Smith et al., 2016).

We identified expression of MIR211-5p and MIR328-3p as a cell-intrinsic mechanism that restrains nevus cell proliferation without the need for further genetic alterations. However, an open question remains regarding the upstream mechanism regulating these microRNAs. We favor a “two-factor” model, whereby increased expression requires both BRAF^{V600E} and activation of a second signaling pathway. In this model, melanocytes that have acquired BRAF^{V600E} would proliferate rapidly until the second pathway, and consequently MIR211-5p and MIR328-3p, is activated. MIR211-5p has previously been reported to be transcriptionally regulated by both MITF (Levy et al., 2010), and UV exposure (Su et al., 2020). Future studies determining how these microRNAs are regulated in BRAF^{V600E} nevus cells might identify useful therapeutic targets for nevus reduction or melanoma prevention.

Regardless of the cause of their expression, analysis of the mechanism of microRNA action, which is pleiotropic and characterized by the simultaneous regulation of networks of target genes, has proven a valuable system for probing the mechanisms of cellular transitions (Melton et al., 2010) (Pencheva et al., 2012) (Judson et al., 2013). In this study, we demonstrate that MIR211-5p and MIR328-3p converge on AURKB mRNA, the depletion of which is necessary to establish both the microRNA-induced growth arrest and BRAF^{V600E}-induced growth arrest in human melanocytes. While AURKB is clearly essential to MIR211-5p and MIR328-3p-mediated proliferation arrest, we recognize that AURKB likely represents one of many MIR211-5p and MIR328-3p targets that contribute to BRAF^{V600E}-induced growth arrest in melanocytic nevi. Indeed, data from our siRNA experiment suggest that depletion of multiple targets each phenocopy growth arrest in melanocytes. Previous studies have identified KCNMA1, TGFBR1, TGFBR2, IGF2R, NFAT5, NUA1, and EDEM1 as MIR211-5p targets in advanced melanoma

lines (Mazar et al., 2010) (Levy et al., 2010) (Bell et al., 2014) (Golan et al., 2019) (Vitiello et al., 2017). Although we consider the growth suppressive effects of the microRNAs to be the summation of target gene network regulation, it is notable that ectopic AURKB expression on its own was capable of restoring proliferation in previously growth-arrested patient-derived nevus cultures, suggesting this gene is a critical downstream signaling node of these microRNAs in this context. These observations corroborate a previous report that AURKB inhibition is an effective therapy in pre-clinical mouse melanoma models (Porcelli et al., 2015), and support further development of AURKB inhibitors as a potential adjuvant or therapeutic candidate.

Chapter 4: Primary Cilia in Melanocytic Nevi and Melanoma

Part 1: Biomarkers to distinguish nevi from melanoma.

Thus far this work has focused on defining the intracellular changes induced by BRAF^{V600E} signaling that establish and enforce growth arrest in nevus melanocytes. Understanding the cellular mechanisms that contribute to growth arrest is essential to treating melanoma in two ways. First, knowledge of the factors leading to, and maintaining, growth arrest allows researchers to exploit potential vulnerabilities in nevus cells and early-stage melanomas to keep them from progressing to more damaging disease. Second, and perhaps more immediately, this knowledge enables physicians to better classify nevi and melanoma so as to more effectively treat their patients. Consistently distinguishing between nevi and melanoma, especially in early-stage lesions, presents a difficult challenge for dermatologists and dermatopathologists. Current techniques involve biopsying lesions, staining with a series of melanocyte and melanoma markers and then assessing whether the lesion might pose an immediate threat to the patient. While these practices can often distinguish common nevi from later stage melanoma, it remains difficult to reliably separate atypical or dysplastic nevi (nevi with irregular borders) from early stage melanoma. Recently, DNA sequencing and copy number variant (CNV) calling have helped resolve difficult cases, however, these approaches are costly to the patient and often less accessible to the physician as well as requiring expert interpretation. Therefore, it is paramount that we develop superior biomarkers to distinguish nevi from melanoma *in situ*.

Two potential classes of biomarker under active development are microRNAs and the primary cilia organelle. In 2019, Torres et al. published work suggesting that the ratios of expression of specific microRNAs could be used to accurately predict whether a lesion was a nevus or melanoma. The study collected RNA from formalin fixed samples of human nevi and adjacent melanoma and determined microRNA expression for each case. The authors then used

machine learning algorithms to establish patterns of microRNA expression that best represented each type of lesion. Ultimately, they found that their classification system achieved a sensitivity of 81% and a specificity of 88% on an independent cohort of classified lesions. Remarkably, these improved sensitivity and specificity marks were independent of tumor cell content within the sample, or the patient's age - two previously confounding factors in microRNA expression analyses (Torres et al., 2020). microRNAs therefore present a promising diagnostic tool for the classification of nevi and melanoma.

Distinguishing atypical and dysplastic nevi from melanoma *in situ* is particularly problematic, as both lesions possess similar histological features in the epidermis. The ability to biopsy and section and stain these lesions can provide helpful evidence to suggest whether the lesion is currently or may progress to malignancy. However, even with ability to view the cellular composition of each lesion under the microscope, it can still be difficult to determine the difference between the two. Current techniques often rely on identifying proliferative markers such as HMB-45, GP100 (Prieto and Shea, 2011), and S100 family proteins (Nonaka et al., 2008) (Petersson et al., 2009). Interpreting the staining results can be confounded, however, as each section represents a single time-point without providing information about the lesion's evolution. Are cells that stain positive for proliferation markers actively proliferating? Or do these markers represent a period of proliferation that is currently under durable growth arrest? To resolve these complications it is therefore crucial to establish markers that provide a more binary diagnosis of malignant vs. benign.

Part 2: Primary Cilia Biology

Primary cilia are an organelle composed largely of microtubules. These hair-like structures project from a single centrosomal centriole known as the basal body. The centriole provides the intracellular base and anchors the primary cilia within the cell membrane. The extracellular component is known as the axoneme and is composed of a ring of 9 microtubule doublets. Although surrounded by the cell membrane, the cilium contains receptor and effector molecules that transduce signals from the extracellular environment into the cell (Choudhury et al., 2020).

Despite similar sounding names, primary cilia are distinct from motile cilia in both structure and function. Motile cilia, which can be found on eukaryotic flagella, or on respiratory epithelia cells have a similar microtubule structure, but contain an additional two microtubule singlets and have dynein arms attached to the outer microtubules. Unlike motile cilia, primary cilia have no known role in cellular movement (Mitchison and Valente, 2017).

Role of primary cilia in cell signaling

Given their antenna-like structure and association with signaling molecules, primary cilia are thought to transduce extracellular signals to the nucleus. The signaling role of primary cilia has been best defined by their ability to propagate signals in the hedgehog signaling pathway. Hedgehog ligands bind to the transmembrane receptors patched 1 (PTCH1) and patched 2 (PTCH2), which are found on the membrane of the primary cilia. Smoothened (SMO) accumulates at the primary cilium and activates gli family zinc finger 2 (Gli2), which in turn regulates gli family zinc finger 1 (Gli1). Gli1 amplifies hedgehog transcriptional activity. When inactive, suppressor of fused homolog (SUFU) binds to GLI family proteins and represses transcriptional activity (Bangs and Anderson 2017) (Bangs and Anderson, 2017).

Role of primary cilia in Basal Cell Carcinoma

Basal cell carcinoma (BCC) represents the disease state in which the role of primary cilia is best understood. BCC arises in proliferative keratinocytes in the lowest layer of the epidermis. In normal physiology, these keratinocytes divide, migrate upwards, and differentiate forming additional layers of the epidermis. UV induced mutations in hedgehog signaling pathway proteins drive BCC increasing basal keratinocyte proliferation and inhibiting differentiation. Bi-allelic loss-of-function mutations have been identified in PTCH1 and PTCH2, as well as in the hedgehog pathway inhibitor, SUFU. Similarly, mono-allelic activating mutations have been identified in SMO. Constitutive activation or loss of inhibition of downstream signaling via SMO result in uncontrolled proliferation that lead to keratinocyte lesions in the epidermis. Fortunately, BCC is not invasive and can often be treated with surgical resection. In more advanced cases where a larger area of skin is impacted, vismodegib and sonidegib, which antagonize SMO, are extremely effective. Although BCC represents a disease state with selection for primary cilia expression, primary cilia tend to be lost in cancers arising in other cell types. Loss of primary cilia has similarly been reported in a variety of cancers including pancreatic cancer, renal cell carcinoma, breast cancer, cholangiocarcinoma, as well as in melanoma (Choudhury et al. 2020) (Choudhury et al., 2020).

Part 3: Primary Cilia Expression in Nevi and Melanoma.

In 2011, Kim and colleagues stained paraffin embedded tissue sections of human nevi and melanomas in various stages of progression. They found that melanoma *in situ*, invasive melanoma, and metastatic melanoma were all characterized by loss of primary cilia. Interestingly, nevi retain primary cilia expression, suggesting that expression of this organelle may serve as an effective marker to differentiate cases of benign growth-arrested nevi from melanoma. Because primary cilia are naturally disassembled and resorbed during the interphase of cell division, the authors asked whether the lack of cilia in melanoma was simply due to the increase in proliferative rate of malignant cells. By co-staining for Ki-67, a cell cycle protein that is expressed in all stages of the cell cycle except for G0 (van Dierendonck et al., 1989), they showed that many Ki-67 negative cells also lacked primary cilia. This finding suggested that primary cilia expression was selected against independently of the proliferative state of melanoma cells (Kim et al. 2011) (Kim et al., 2011).

In 2016, Lang and colleagues confirmed this finding and expanded the role of primary cilia staining in the histopathological classification of melanocytic lesions. They specifically asked whether primary cilia expression could differentiate histologically ambiguous atypical dysplastic nevi from melanoma. To do this, they stained formalin fixed tissue sections of human melanocytic lesions for acetylated alpha tubulin, which marks the modified tubulins of the ciliary axoneme. Gamma tubulin was used to stain the centrosome, indicating the presence and absence of the elongated primary cilia. In addition, the authors co-stained sections with SOX10 to identify nevus or melanoma cells of melanocytic origin. Primary cilia were counted as individual sets of gamma-tubulin stained centrosomes with an elongated alpha tubulin stained structure. A primary cilium index was then generated for each lesion by dividing the number of SOX10 positive cells with primary cilia by the number of total SOX10 positive cells in the tissue section. They found that, while primary cilia staining can be mosaic in atypical dysplastic nevi, the gradient of primary cilia expression decreases as the severity of dysplasia in the nevi increases (Lang et al. 2016) (Lang

et al., 2016). This finding strongly suggests that primary cilia expression changes with progression from benign melanocytic lesion to melanoma and that it can serve as a useful biomarker for differentiating melanocytic lesions with atypical or complex histology.

Part 4. Transcriptional profiling of primary cilia-associated genes in nevi and melanoma.

To better understand the mechanisms underlying primary cilia loss in progression to melanoma, we investigated the transcriptional profile of primary cilia-associated genes in nevi and melanoma. We hypothesized that loss of the primary cilium organelle should be preceded or accompanied by transcriptional changes in genes encoding primary cilia proteins. Specifically, we thought that genes encoding structural proteins of primary cilia would be downregulated during progression to melanoma. To test this hypothesis, we analyzed transcriptomic data from 20 FFPE cases of human nevi with adjacent melanoma. This cohort comprised 17 nevi, 20 melanomas, and 5 intermediate lesions with complex histology that pathologists could not decisively call nevus or melanoma. We next obtained an annotated list of 318 genes thought to be associated with primary cilia from the Reiter Lab UCSF, which specializes in primary cilia biology. This gene list derived from an analysis of primary cilia literature and encompassed genes thought to contribute to primary cilia structure, signaling molecules that co-localize with primary cilia, as well as genes that are thought to negative regulate primary cilia expression.

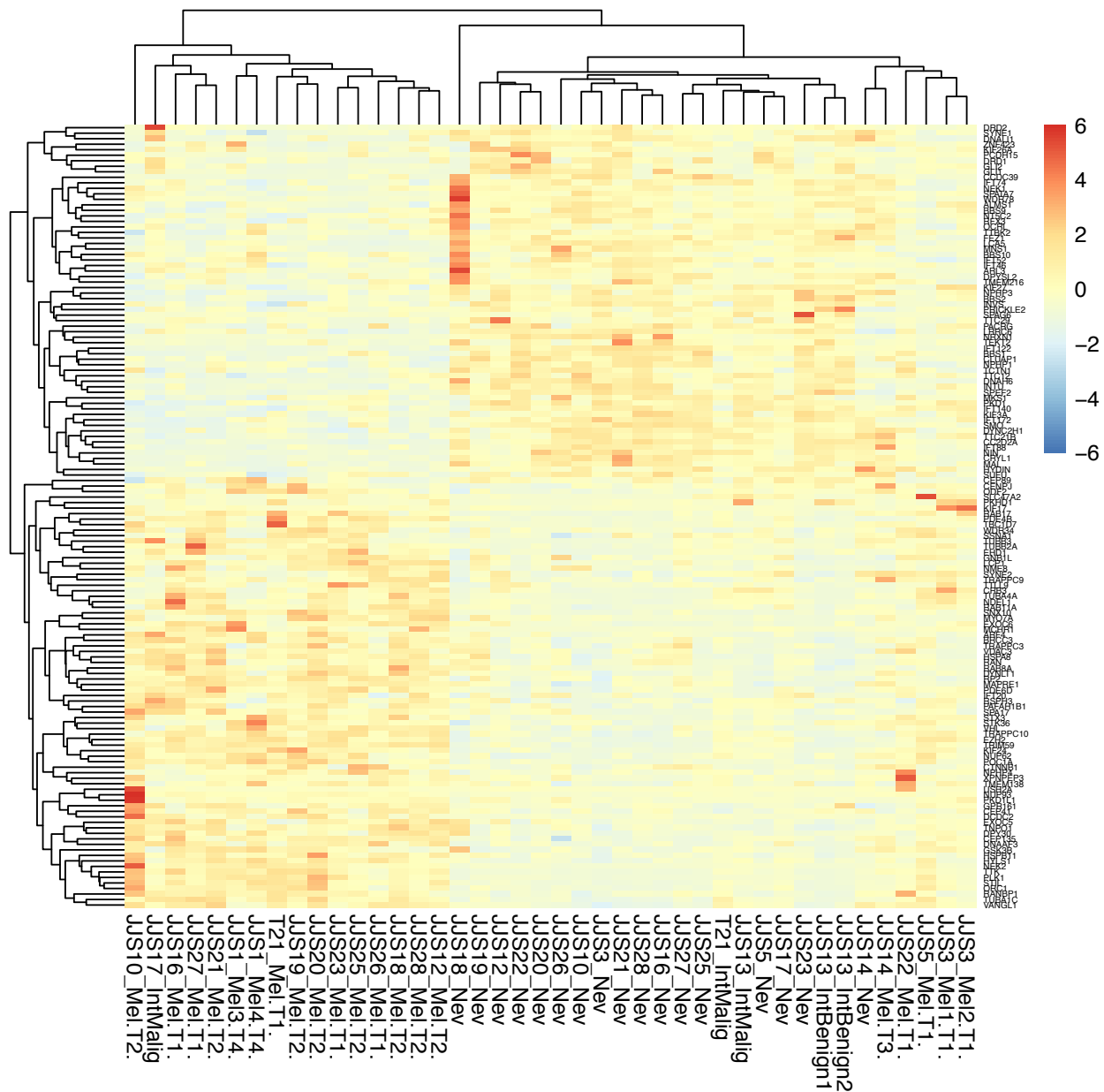


Figure 4.1: Differentially expressed primary cilia-associated gene expression in nevi and melanoma.

Heatmap of differentially expressed primary cilia-associated gene expression in matched adjacent nevi (n = 17), melanoma (n = 20), and intermediate lesions (n = 5).

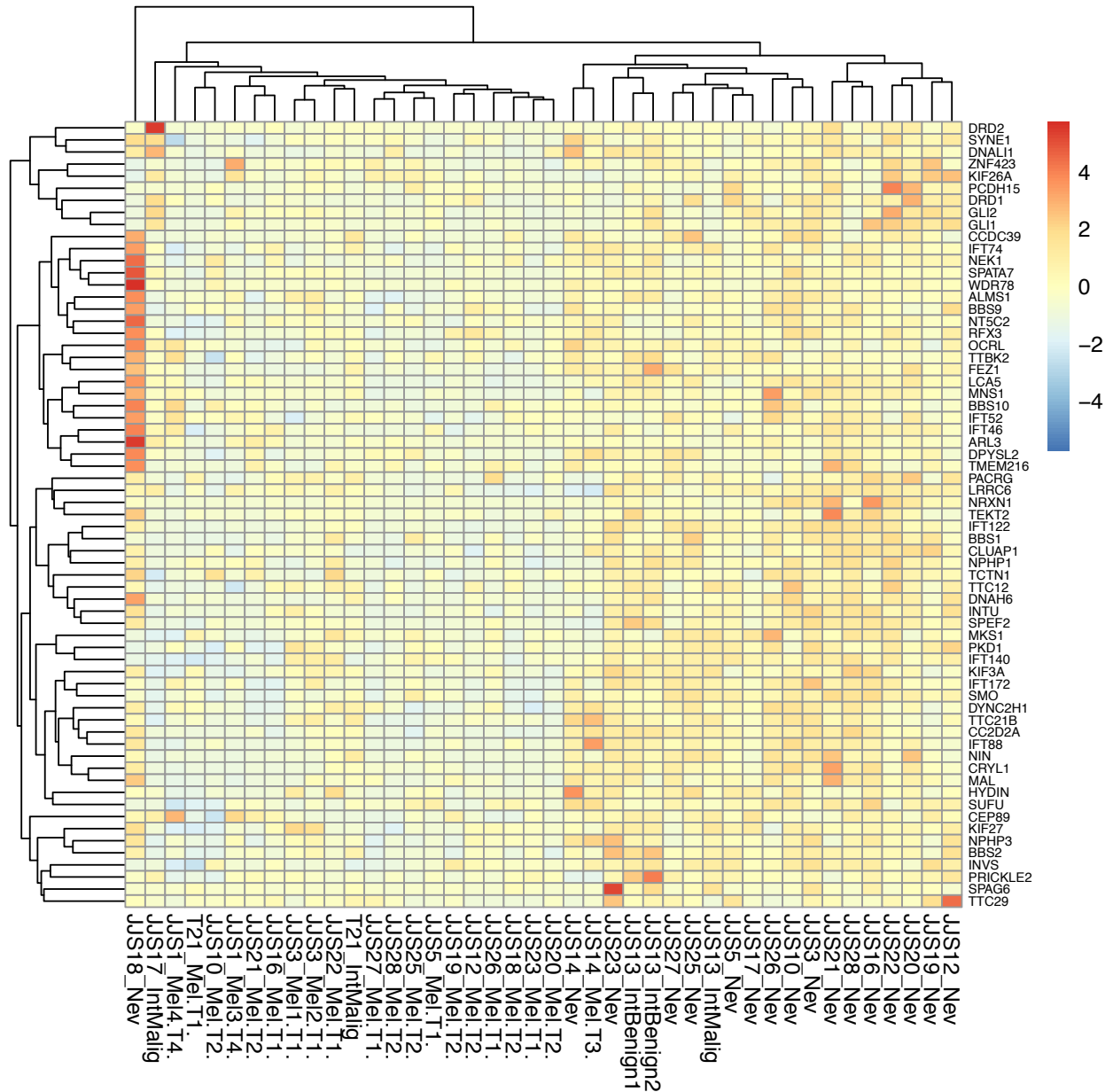


Figure 4.2: Nevus-enriched primary cilia gene expression distinguishes nevi from melanoma.

Heatmap nevus-enriched primary cilia-associated gene expression in matched adjacent nevi (n = 17), melanoma (n = 20), and intermediate lesions (n = 5).

I performed differential expression analysis on the module of primary cilia-associated genes to determine which of the genes were differentially expressed between nevi and adjacent melanomas. Using DESeq2, I determined that 142 of the 318 cilia genes were differentially

expressed between the nevus and melanoma samples. I then performed hierarchical clustering using the hclust algorithm as part of the pheatmap R package and plotted the expression of the differentially expressed genes as a heatmap (Figure 4.1). Clustering the transcriptomic profiles of primary cilia-associated genes by sample revealed a set of genes enriched in the nevi and downregulated in adjacent melanoma, as well as a set of genes enriched in the melanomas and downregulated in the adjacent nevi. The dendrograms show that the majority of the melanoma samples cluster together and that the majority of nevus samples cluster more closely together than they do with the majority of melanomas. Surprisingly, there is a set of 5 melanomas that cluster in their own node, more closely to the nevi than to the other melanomas. Furthermore, 4 of the 5 intermediate lesions (T21_IntMalig, JJS13_IntMalig, JJS13_IntBenign1, and JJS13_IntBenign2) clustered more closely with the nevi than the melanoma, while one (T21_IntMalig) clustered more closely with the melanomas.

To determine if the clustering could be further refined, I performed hierarchical clustering using the subset of genes that were shown to be differentially expressed and upregulated in nevi in comparison to adjacent melanoma (Figure 4.2). I found that this gene set improved the clustering and that the five melanomas that previously clustered more closely with the nevi now clustered more closely with the other melanomas. It should be noted that this re-cluster caused nevus samples JJS18_Nev to become an outlier given that its general gene expression was greater than that of the other samples. However, the pattern of expression is more similar to that of the nevi than the melanomas. Notably, the intermediate lesion T21_Intmalig now clusters more closely with the melanomas, while the JJS13_IntMalig and JJS13_IntBenign samples continue to cluster more closely with the nevi. Re-assessment of the JJS13 samples shows that the majority of cells in each of the samples still express primary cilia and therefore it is not surprising that the cluster more closely with cilia positive nevi. Finally, the JJS14_Nev and JJS14_Mel cases continue to cluster more closely with the nevi, although clearly as their own subset. Further assessment of these lesions need to be performed to determine why that might be the case.

Of the primary cilia-associated genes enriched in nevi, we expected to find genes associated with primary cilia construction. Several genes that contribute to primary cilia structure were indeed upregulated in nevi including intraflagellar transport 88 (IFT88), kinesin-like protein 3A (KIF3A), and centrosomal protein 89 (CEP89). In 1993, scientists discovered that loss of IFT88 in *chlamydomonas* leads to loss of flagella. Similarly, mice lacking IFT88 homolog Tg737 have deformed primary cilia in their kidneys and have polycystic kidney disease (Pazour et al. 2000) (Pazour et al., 2000). KIF3A has been shown to be necessary for extending microtubules that comprise primary cilia, (Arnaiz et al. 2009 (Arnaiz et al., 2009), Avidor-Reiss et al. 2004 (Avidor-Reiss et al.), Liu et al. 2007, (Liu et al., 2007) Pazour et al. 2005 (Pazour et al., 2005), Wigge et al. 1998) (Wigge et al., 1998). CEP89 is a centrosomal protein whose loss has similarly been associated with loss of primary cilia (Andersen et al. 2003) (Andersen et al., 2003), Nogales-Cadenas et al. 2009) (Nogales-Cadenas et al., 2009). Additionally, SYNE1, a gene that is also essential for primary cilia is shown to be upregulated in nevi (Liu et al., 2007) (Stubbs et al., 2008).

Besides genes associated with primary cilia structural elements, hedgehog pathway signaling molecules that typically associate with primary cilia are upregulated in nevi. These include SMO, which localizes to the cilia membrane when sonic hedgehog (SHH) is bound to the receptor PTCH1. Similarly, GLI2, which localizes together with other hedgehog proteins in the cilium tip (Blacque et al., 2005) is also upregulated. In addition, GLI1, which is not found in the cilium, but interacts with GLI2 and amplifies hedgehog pathway signaling is also upregulated. Interestingly, SUFU, which suppresses hedgehog signaling is likewise enriched in nevi in comparison to melanoma. This is likely due to the localization of SUFU together with the GLI transcription factors to the ciliary tip (Laurençon et al., 2007), an event that cannot occur in the absence of primary cilia expression typically observed in melanoma.

Taken together, the enrichment of genes associated with primary cilia structure and genes that encode signaling molecules that localize to the cilium in nevi but not in melanoma suggests that there are transcriptional changes that underlie the loss of primary cilia during progression to

melanoma. Indeed, with few exceptions, the expression of primary cilia genes enriched in nevi in comparison to adjacent melanoma effectively clusters the nevus and melanoma samples of this cohort. An expanded cohort is required to validate whether this method of clustering is generally applicable to nevi and melanoma. Furthermore, this work suggests that the visible loss of primary cilia, as assessed by cilia protein staining, can be attributed to change in transcriptional program within melanoma cells that actively suppresses primary cilia expression.

Chapter 5: Discussion

Cell-intrinsic factors contribute to the growth-arrested state of melanocytic nevi.

Taken together, the research compiled in this dissertation demonstrates that many cell-intrinsic factors contribute to establishing and maintaining the growth-arrested state of melanocytic nevi.

Cyclin dependent kinase inhibitors contribute to nevus growth arrest and their loss permits progression to melanoma.

We have shown that BRAF^{V600E} signaling directly induces transcriptomic changes in human melanocytes, including the upregulation of cyclin dependent kinase inhibitors including p15^{INK4B} and p16^{INK4A}. Although p15^{INK4B} and p16^{INK4A} play variable roles in nevus development, the upregulation of these inhibitors blocks cell cycle progression and their subsequent genetic loss provides a route to the malignant transformation of nevi. Furthermore, loss of p16^{INK4A} proves necessary for inducing invasive and metastatic behaviors in melanoma cells.

microRNAs establish and maintain the transcriptome of growth-arrested nevi.

We further demonstrate that microRNAs contribute to establishing and maintaining the growth arrest state of nevi. Specifically, MIR211-5p and MIR328-3p regulate networks of target genes in melanocytes that converge on AURKB and ultimately inhibit cell cycle progression. The subsequent downregulation of MIR211-5p and MIR328-3p relieves that repression and provides additional transcriptomic remodeling that permits malignant transformation.

Primary Cilia formation supports the nevus state.

Our research also suggests that formation of the primary cilia organelle through the transcription of primary cilia-related genes contributes to growth-arrest in nevi. Immunohistochemistry clearly shows that melanoma cells express primary cilia at far lower levels

than nevi. By examining transcriptomic data from matched human nevus and adjacent melanoma samples, we observe distinct transcriptional signatures for nevi and melanoma with regard to cilia-related genes.

Future directions:

While this work highlights several cell-intrinsic factors that contribute to the formation and maintenance of human BRAF^{V600E}-induced melanocytic nevi, the full complexity of nevi remains elusive. Fully dissecting the cell-intrinsic changes induced by mutant BRAF^{V600E} expression in human melanocytes, and determining the convergence points of these changes, appears fundamental to understanding growth-arrest in nevi. Further research examining the plasticity of the nevus transcriptome that nevus eruption and nevus recurrence, while maintaining the durability of long-term growth arrest should be prioritized. Moreover, determining which factors critical to nevus formation are necessary to restrain melanocytic nevi from transforming to melanoma will provide therapeutic opportunities to improve our treatment of this disease.

Materials and Methods

Methods for McNeal et al. 2015:

Isolation of Melanocytes from Human Nevi

Benign human melanocytic nevi were excised from patient donors seen in the Dermatology clinic at the Hospital of the University of Pennsylvania according to an IRB approved protocol. A portion of each specimen was processed for routine histological examination to confirm the clinical diagnosis of benign nevus. The tissue samples were microdissected to isolate nevus from surrounding normal tissue. Nevus tissue was then mechanically separated into fine pieces, and enzymatically dissociated in a mixture of dispase and collagenase for 2 hours. The resulting supernatant was spun at 218g for 5 minutes to pellet the extracted cells, which were subsequently resuspended in melanocyte Medium 254 (Invitrogen). The cells were plated onto 6-cm collagen-coated tissue culture plates (BD Falcon). Melanocytes were further isolated from contaminating fibroblasts by selective trypsinization and 4 day exposure to 100 µg/mL G418.

Melanocyte Culture

Primary melanocytes were extracted from fresh discarded surgical human foreskin specimens as described previously (28) with some modifications detailed as follows. After overnight incubation in Dispase, the epidermis was separated from the dermis and treated with trypsin for 10 minutes. Cells were pelleted and plated on selective MC Medium 254 (Invitrogen) with Human Melanocyte Growth Supplement, and 1% penicillin and streptomycin. TGFb-1 was purchased from R&D Systems and used at a concentration of 100 pM. Doxycycline (hyclate) hydrochloride was purchased from Sigma, dissolved in sterile, deionized water, and used at a concentration of 0.25µg/mL. SB-431542 was purchased from EMD Millipore, dissolved in DMSO, and used at a concentration of 50µM.

Immunoblot Analyses and Antibodies

Adherent cells were washed once with DPBS and lysed with 1% NP-40 buffer (150 mM NaCl, 50 mM Tris, pH 7.5, 1 mM EDTA, and 1% NP-40) containing 1X protease inhibitors (Roche) and 1X phosphatase inhibitors (Roche). Lysates were quantified (Bradford assay), normalized, reduced, denatured (95 °C) and resolved by SDS gel electrophoresis on 4-15% Tris/Glycine gels (Bio-Rad). Resolved protein was transferred to PVDF membranes (Millipore) using a Semi-Dry Transfer Cell (Bio-Rad), blocked in 5% dry milk in TBS-T and probed with primary antibodies recognizing BRAF (Abcam, ab33899, 1:500), BRAF-V600E (Spring Bioscience, VE1, 1:500), p15 (Abcam, ab 53034, 1:500), p16 (BD Pharmingen, #551153, 1:500), and β -Actin (Cell Signaling Technology, #3700, 1:4000). After incubation with the appropriate secondary antibody, proteins were detected using either Luminata Crescendo Western HRP Substrate (Millipore) or ECL Western Blotting Analysis System (GE Healthcare).

Immunohistochemistry

Formalin fixed paraffin embedded (FFPE) human skin tissue sections from patients with benign nevus and melanoma, or human xenograft tissues were screened for p15 protein expression using peroxidase/DAB (diaminobenzidine)-complex method (EXPOSE biotin free detection kit, Abcam, Cambridge, MA). Tissue sections were deparaffinized and rehydrated. To retrieve the antigens, tissue sections were microwaved in 10mM Citrate buffer pH 6.0. To quench endogenous peroxidase, tissues were incubated in 3% H₂O₂. Tissues were then incubated with primary antibody to p15 (1:200; Abcam, Cambridge, MA) for three hours at room temperature. The secondary antibody, goat anti-rabbit HRP conjugated, was supplied with the kit and incubated 18 min at room temperature. Following multiple washes in TBS, the antigen-antibody complex was visualized with 3.3% DAB-solution. The tissues were counterstained with hematoxylin, dehydrated and a coverslip was applied.

Quantification of Immunohistochemistry Staining

Tissue sections from human nevi, melanomas, and melanomas arising in continuity with existing nevi were stained for p15 or p16 expression using methods described in the previous immunohistochemistry section. 10X photomicrograph images of representative tissue sections were taken using the Zeiss microscope. Tiff files of the images were saved and transferred to Adobe Photoshop where pixels corresponding to p15 or p16 IHC staining were selected using the color selection tool. Images corresponding to the single specific color were then analyzed using FIJI (Image J) to determine the number of pixels in each sample. The number of pixels representing the total staining, including the DAPI counterstain, was also obtained so that the levels of p15 and p16 expression could be normalized to the total amount of label in each section. Final ratios of p15 and p16 expression were calculated by dividing the number of p15 or p16 pixels by the total pixels in each section.

Generation of Lentiviral Vectors

The following lentiviral plasmids were used to express the corresponding human genes: diBRAF, p15, p16, CDK4(R24C), dominant-negative p53(R248W), hTERT, and luciferase. The human BRAF (V600E) gene was inserted immediately after the TetO operator in a modified version of the doxycycline-inducible lentiviral pTRIPZ vector (Thermo Scientific), in which the shRNA hairpin sequences were deleted. Human p15 (Addgene 16454), CDK4(R24C), p53(R248W), and hTERT (28) were cloned into the pRRL lentivector (40). Human p16 was expressed using Addgene plasmid #22263 (Eric Campeau). shRNAs were expressed from pLKO.1 and are available through OpenBiosystems. The nucleotide sequences of the specific hairpin sequences used are available upon request.

Quantitative RT/PCR

mRNA was extracted from melanocytes according to the RNeasy Mini Kit protocol (Qiagen), and reverse transcribed to cDNA using the High Capacity RNA-to cDNA kit (Applied

Biosystems). Quantitative PCR of the resulting cDNA was carried out using Power SYBR Green Master Mix (Applied Biosystems) and gene-specific primers, in triplicate, on a ViiA 7 Real-Time PCR System (Life Technologies). The following primers were used for detection; CDK2 forward: 5'-CAG GAT GTG ACC AAG CCA GT-3'; CDK2 reverse: 5'-GGC TGG CCA AGA CTA GAA GG-3'; CDK4 forward: 5'- GTG CAG TCG GTG GTA CCT GA-3'; CDK4 reverse: 5'- AAG GCA AAG ATT GCC CTC TCA-3'; CDK6 forward: 5' – ACA GAG CAC CCG AAG TCT TG – 3'; CDK6 reverse: 5'-CTG GGA GTC CAA TCA CGT CC-3'; p14ARF forward: 5'- ACG GGT CGG GTG AGA GTG -3'; p14ARF reverse: 5'- GTG GCC CTC GTG CTG ATG -3'; p15 forward: 5'- CAC CCC CAC CCA CCT AAT TC-3'; p15 reverse: 5'-TGA GTG TCG AGG GCC AGA TA-3'; p16 forward: 5'-GCC CAA CGC ACC GAA TAG-3'; p16 reverse: 5'- ACG GGT CGG GTG AGA GTG -3'; p18 forward: 5'- GTG GGG CAT CGG AAC CAT AA-3'; p18 reverse: 5'- AAA GTA GAG GCA ACG TGG GG-3'; p21 forward: 5'- GAT GTA GAG CGG GCC TTT GA-3'; p18 reverse: 5'- AAA GTA GAG GCA ACG TGG GG -3'. Relative expression was determined using the 2- $[\Delta\Delta Ct]$ method followed by normalization to the wild-type melanocyte transcript levels.

Growth Curves

Cells were seeded into 6-well plates at a density of 2.0×10^5 or 2.5×10^5 cells per well. At regular intervals, cells were trypsinized, resuspended, and manually counted on Kova Glasstic Slide 10 (Hycor). Cells were subsequently spun down and re-seeded into 6-well plates at equal densities.

Sanger Sequencing

mRNA was isolated from nevus melanocytes using the RNeasy kit and reverse transcribed to cDNA. Sanger sequencing was conducted by the University of Pennsylvania DNA Sequencing facility. Samples submitted contained 60 ng DNA, and 3.2 pmoles each of forward and reverse primers in a volume of 9 μ L. The sequencing primers used were ordered from Integrated DNA

Technologies and are as follows; BRAF forward: 5'- GCA CGA CAG ACT GCA CAG GG -3'; BRAF reverse: 5'- AGC GGG CCA GCA GCT CAA TAG -3'.

Preparation of 3-D Organotypic Skin Cultures

Organotypic skin grafts containing MCs were established using modifications to previously detailed methods (10, 28). The Keratinocyte Growth Media (KGM) used for keratinocyte-only skin grafts was replaced with Melanocyte Xenograft Seeding Media (MXSM). MXSM is a 1:1 mixture of KGM and Keratinocyte Media 50/50 (Gibco) containing 2% FBS, 1.2 mM calcium chloride, 100 nM Et-3 (endothelin 3), 10 ng/mL rhSCF (recombinant human stem cell factor), and 4.5 ng/mL r-basic FGF (recombinant basic fibroblast growth factor). 1.5×10^5 melanocytes and 5.0×10^5 keratinocytes were suspended in 80 μ L MXSM, seeded onto the dermis, and incubated at 37 °C for 4 days at the air-liquid interface.

Mouse Xenografting

Organotypic skin tissues were grafted onto 5-7 week old female ICR Scid mice (Taconic) according to an IACUC-approved protocol at the University of Pennsylvania. Mice were anesthetized in an isoflurane chamber. Murine skin was removed from the upper dorsal region of the mouse. Reconstituted human skin was reduced to a uniform 11 x 11 mm square and grafted onto the back of the mouse with individual interrupted 6-0 nylon sutures. Mice were dressed with Bactroban ointment, Adaptic, Telfa pad and Coban wrap. Dressings were removed 2 weeks after grafting.

Viral Transfection and Transduction

Viral transductions were performed as described previously (10, 27, 28). HEK293T cells were cultured to 40% confluency and incubated in DMEM supplemented with 5% FBS and 1% antibiotic and antimycotic in 6-well plates. For each well, 1.22 μ g lentiviral vector was mixed with viral packaging plasmids pCMV Δ R8.91 (0.915 μ g) and pUC-MDG (0.305 μ g). This plasmid solution

and 7.2 μ l of Fugene 6 Transfection Reagent (Promega) were added to 96 μ l of supplement-free DMEM. The resulting mixture was incubated at room temperature for 15 minutes and then added into the HEK293T culture media. At 16 hours post-transfection, 10 mM sodium butyrate was added onto the cells. At 24 hours, the culture media was replaced and the cells were incubated at 32°C. At 45 hours, viral supernatant was collected by filtering the media through a .45 μ m syringe filter (Argos). Melanocytes seeded at 2.5×10^6 cells per well were incubated in viral supernatant in the presence of 5 μ g mL⁻¹ polybrene and centrifuged at 300 x g for 60 minutes at room temperature. After incubating the transduced melanocytes for 15 minutes at 37°C, viral supernatant was removed and replaced with growth media.

CRISPR-Cas9 Cloning and Transduction

Guide RNAs were designed using software tools developed by the Zhang Lab and provided on the website <http://www.genome-engineering.org/> (Hsu et al., 2013). Guide RNAs were subsequently cloned into lentiCRISPRv2 (Addgene # 52961) according to the accompanying protocol (Sanjana et al., 2014 and Sanjana et al., 2014). Guide RNA sequences are as follows: lentiCRISPR GFP 5' GAA GTT CGA GGG CGA CAC CC 3'; lentiCRISPR p15.2 5' CCC GAA ACG GTT GAC TCC GT 3'. LentiCRSIPR transductions in human melanocytes were conducted as previously described for the other lentiviral constructs used in this study.

Statistics

Mean values were compared using an unpaired Student's two-tailed T-Test.

Zeng et al. 2018 Methods

Analysis of clinical specimens and sequence

Histopathologic Assessment

Clinical specimens were collected and analyzed in compliance with the UCSF Human Research Protection Program (11-07951). Two cohorts of transitional lesions were analyzed in this study. A transitional lesion is a lesion with two or more histopathologically distinct areas – for example, in Figure S5A, we show three transitional lesions - one with a portion of benign nevus and a portion of invasive melanoma; one with a portion of MIS and a portion of melanoma; and one with a portion of MIS and a portion of nevus. By analyzing transitional lesions we could perform inter- and intra- tumoral comparisons in order to identify the stage at which *CDKN2A* loss occurred both within individual tumors and across many tumors.

The first cohort of transitional lesions comprised 82 cases for which we performed DNA sequencing to determine the timing of *CDKN2A* somatic alterations during melanoma progression. This cohort spanned a broad spectrum of histopathologically distinct areas, including 31 nevus areas, 18 melanoma in situ areas, 23 thin invasive melanoma areas (stage T1), and 32 thick invasive melanoma areas (stage T2+). In a subset of 20 of these transitional lesions with sufficient material to isolate both DNA and RNA, we also performed RNA-sequencing to identify the relationship between *CDKN2A* loss and *p16INK4A* or *BRN2* expression.

The second cohort of transitional lesions was comprised of 23 cases for which we utilized Melan-A, BRN2, Ki67 and p16^{INK4A} immunostaining in order to confirm the timing of p16^{INK4A} loss at the protein level and its relationship to other BRN2 and Ki67. This cohort had a more focused spectrum of histopathologic areas, encompassing nevi associated with melanoma in situ or melanoma in situ associated with invasive melanoma.

Cases from both cohorts were retrieved from the UCSF Dermatopathology archive as formalin-fixed paraffin-embedded tissue blocks. Sequencing was performed by the UCSF Clinical Cancer

Genomics Laboratory and protein staining by the UCSF Dermatopathology and Oral Pathology Service.

Histopathologically distinct areas associated with each transitional lesion were independently evaluated by a panel of 3-8 dermatopathologists for staging and/or immunostaining interpretation. Transitional lesions include nevus, melanoma in situ, invasive thin melanoma (T1 melanoma) and invasive thick melanoma (T2 melanoma or higher). For genomic analysis, distinct areas were manually microdissected with a scalpel and dissection scope from a series of 10-20um unstained sections following the guidance of a pathologist.

Genomic Analysis

Genomic DNA was sequenced as previously described (Shain et. al. NEJM 2015 ⁴). Briefly, 25-250ng of genomic DNA was prepared for sequencing using KAPA Biosystems Illumina compatible library preparation kit (KAPA Hyper Prep Kit, Cat# KK8504). Target enrichment was performed using a custom gene panel of approximately 500 genes (SeqCap EZdeveloper library 24 reactions, Ref #: 06471706001, gmi.ucsf.edu/testing/). 100bp paired-end sequencing was performed on an Illumina HiSeq 2500 instrument. For clinical samples, *CDKN2A* gene status was analyzed in this study. Read alignment, mutational analysis, and copy number analysis was performed as previously described^{4,57}. Thirty-seven transitional lesions were previously sequenced and reanalyzed here ⁴.

For comparison of WM793 and 1205Lu cell lines, after sequencing as described above, their genomic landscapes were compared, as previously described ⁴, to delineate the shared (trunk) and private (branch) mutations in each cell line (see Figure 4C). There was no source of normal tissue associated with these cell lines, and therefore somatic point mutations were inferred by subtracting known SNPs (1K Genome Project) from variants. It is likely that a small number of private, germline SNPs are present in the trunk of the phylogenetic tree, however, this did not hinder the goal of this analysis, which was to identify differences between the two cell lines.

Transcriptomic analysis

Matched RNA-sequencing was performed on a subset of 20 transitional lesions. For this subset of cases, every other unstained section was microdissected and used instead for RNA isolation (Ambion 1975). 100ng of total RNA was prepared for sequencing using KAPA stranded RNA-Seq Library Preparation Kit (KR0934). This kit uses random priming for cDNA synthesis, and thus target enrichment was performed using xGen Lockdown Reagents (Cat# 1072281) and Nimblegen Capture Baits (Roche, customized), thereby depleting ribosomal RNA prior to sequencing. 100bp paired-end sequencing was performed on an Illumina HiSeq 2500 instrument. *P16INK4A* and *BRN2* gene status were analyzed in this study. Sequencing reads were aligned using STAR⁵⁸ and transcript abundance was estimated using RSEM⁵⁹.

For melanocytes, RNA sequencing was performed on 3 sets of wild-type and CDKN2Aex2::CMV-EGFP melanocytes preparations. Library construction was performed using TruSeq Stranded mRNA LT (Illumina) followed by single end 75-bp sequencing on the NextSeq 500 (Illumina). QC was performed using FastQC followed by trimming using Trimmomatic⁶⁰. Sequencing reads were aligned using Tophat with differential analysis performed using CuffDiff⁶¹.

Cell culture and analysis

Melanoma lines

The WM793 and 1205Lu melanoma lines were gifted by the Herlyn lab (Herlyn et al Cancer Research 1985)⁴¹, and grown in DMEM H-16 supplemented with 10% FBS (Corning, 35-010-CV), 0.1mg/mL Pen-Strep, and 0.002mg/mL L-Glutamine at 37°C with 5% CO₂.

Primary melanocytes

Foreskins were provided by Dr. Thea Mauro in accordance with UCSF Human Research Protection Program protocol. After PBS washing, the skin was cut into 1cmx1cm squares and cleared of fat prior to incubation with Dispase for 24hours at 4°C with the epidermis side facing

upwards. After washing, the epidermis was isolated, sectioned into small pieces, and trypsinized at 37°C for 5 minutes. After quenching and low-speed centrifugation, cell pellets were plated in NHM media (Medium 254 (ThermoFisher M254500) supplemented with HMGS (ThermoFisher S0025) and Pen-Strep) and incubated at 37°C overnight. Fresh media containing G418 (1ug/ml) was added 24 hours later until a pure NHM population was observed. Once established in culture, NHMs were verified as pigmented, possessing melanocyte morphology, and expressing Sox10 and Melan-A as follows: cells were washed with PBST (PBS with 0.05% TritonX), blocked with PBST with 3%BSA and 0.01%Donkey serum for an hour, incubated with primary antibody (Table S2) in blocking buffer overnight at 4°C, washed, incubated with secondary antibody (anti-rabbit-Cy5, anti-mouse 488 and anti-goat 594 (Life Technologies)) for 2 hours, washed with DAPI-containing PBST, and imaged. After verification, NHMs were maintained in NHM media. Medium was refreshed twice a week and cells were passaged upon reaching 80% confluence with 0.05% Trypsin quenched 1ml 0.5mg/ml serpin trypsin inhibitor (Life technologies 17075029).

Lentivirus transduction

293T cells were co-transfected with 3rd generation lentivirus packaging vectors and expression construct (pSico-mcherry, pSico-shINK4A-mCherry, pHIV-EF1a-IRES-ZsGreen, pHIV-EF1a-IRES-INK4A-ZsGreen or pHIV-EF1a-IRES-ARF-ZsGreen) using jetPRIME transfection reagent (Polyplus 114-15). Virus was harvested 72 hours post transfection, filtered through 0.45um filter and 10ug/ml of Polybrene (SIGMA H9268) was added prior to plating. Media was switched to standard culture media either 24 hours (cell lines) or 6 hours (NHM) post infection. 72 hours post infection the cells were trypsinized, washed in PBS, filtered and sorted for mCherry, mOrange2 or ZsGreen positive cells.

Transfection

NHMs were transfected using the Neon Electroporation system (ThermoFisher), as described in the manufacture's protocol. Briefly, NHMs were trypsinized, washed, and resuspended in R buffer

at a final concentration of 2.0×10^7 cells/mL. Cells were mixed with either 150pmol siRNA, 1ug expression or reporter plasmid or CRISPR/Cas9-HDR reagents (see NHM engineering) and electroporated with two 20ms 1500V pulses in a 10uL Neon transfection tip (ThermoFisher MPK1096), then plated into 500uL pre-warmed media in a 24-well tissue culture treated plate. Cell lines were transfected using either jetPRIME transfection reagent (Polyplus 114-15) for plasmid or Lipofectamine RNAiMax (ThermoFisher 13778150) for siRNA. The concentration of siRNA, plasmid and transfection reagent followed the manufacture's protocol.

Flow cytometric analysis

Primary melanocytes, 1205Lu and WM796 melanoma cells were either CRISPR engineered to be EGFP positive, or transduced to be mCherry, mOrange2 or ZsGreen positive. Fluorescent protein expressing cells were sorted out for pure populations. The cells were trypsinized, centrifuged and resuspended in PBS, following which they were analyzed and sorted on the FACS Aria III (BD biosciences) on the FITC channel (ZsGreen⁺ and EGFP⁺ cells) or PE channel (mOrange2⁺ and mCherry⁺ cells). Further analysis and quantification was performed using FlowJo (Treestar)

Holographic imaging and microscopy

Holographic imaging was conducted as previously described³⁴. Briefly, imaging was conducted with a HoloMonitor M4 imaging cytometer with high precision automated stage (Phase Holographic Imaging, Lund, Sweden) installed in a standard tissue culture incubator. Cells were plated in 6-well standard tissue culture plates, plated at 10,000 – 100,000 cells per well depending on cell type and experiment and covered with a Hololid (PHI). For motility analyses, holograms were generated every hour for indicated time and analyzed using the Hstudio software package (PHI). For growth arrest analyses, cells were classified based upon quantitative optical metrics as previously described³⁴, where cells were defined as growth arrested if they stopped dividing while adopting a morphology indistinguishable from NHMs treated with CDK4/6 inhibitor⁶².

Fluorescent images were captured with an EVOS FL inverted microscope (ThermoFisher), colored images were captured with a Lieca Dmi1 light microscope, and high quality scans of clinical specimens were scanned with a ScanScope XT scanner (Aperio).

Invasion analyses

In vitro invasion assays were conducted using transwell cassettes coated with high-density basement membrane extract as described in manufacture's protocol (Trevigen, 3483-096-K)

NHM engineering

Introduction of BRAF^{V600E} point mutation

crRNA (Table S3, IDT) and tracrRNA (IDT 1072533) were resuspended in nuclease-free IDTE buffer (IDT 11-01-02-02) and combined for a final concentration of 100 μ M each and assembled into sgRNA via heating at 95°C for 5min then cooled to room temperature. Cas9:sgRNA RNPs were formed by combining 120pmol sgRNA and 100pmol recombinant Cas9 protein (qb3 Berkeley), heating at 37°C for 5min then cooling to room temperature. 120pmol of crRNA:tracrRNA complexes was mixed with 100pmol BRAF ssOligo HDR template (Table S3), then electroporated into low-passage NHMs (passage 2-5 after isolation) as described above. sgRNA and ssOligo HDR template, without recombinant Cas9, were transfected for no Cas9 controls. After electroporation, NHMs were plated directly into media containing 5 μ M L755507 for enhancement of HDR recombination⁶³. After 3 days, genomic DNA was harvested for indel analysis via the TIDE approach⁶⁴.

Introduction of CDKN2A knock-in

Low-passage NHMs (passage 2-5 after isolation) were electroporated as described above with 800ng each of pHDR-CDKN2A-Ex2-CMV-EGFP, pEN35-CDKN2A-Ex2-L and pEN35-CDKN2A-Ex2-R and plated directly into media containing 5 μ M L755507 for enhancement of HDR recombination⁶³. pHDR-CDKN2A-Ex2-CMV-EGFP without pEN35 plasmids were transfected as

no Cas9 controls. Transfected NHMs were maintained and expanded in normal conditions until fluorescent signal was no longer observed in no Cas9 controls (~ 3weeks). EGFP positive and EGFP negative cells were then sorted from the Cas9 and no Cas9 populations, respectively to generate CDKN2A::EGFP and wild-type sibling NHMs.

Mouse injection and metastasis assay

All protocols described in this and other sections regarding animal studies were approved by the UCSF Institutional Animal Care and Use Committee. Ethical endpoint for tumor transplantation experiments was reached when a tumor reached = 2.5 cm in any single dimension. Transduced WM793 and 1205Lu cells were sorted and subcutaneously injected (8×10^6 cells) into immunodeficient female mice (NOD.Cg-Prkdcscid Il2rgtm1Wjl/SzJ) aged 6~8 weeks by a technician blinded to the identity of the cells. Each week the mice were monitored for tumor size using a digital caliper and recorded with the guidance of the Helen Diller Comprehensive Cancer Center Preclinical Core (UCSF). 5 weeks post injection the lungs were perfused with 4%PFA, and mice were humanely sacrificed. A piece of each lobe was harvested for obtaining genomic DNA and the remaining lobes were incubated in sucrose overnight to be used for immunofluorescence and H&E staining.

Lung metastasis was determined by staining of human nuclei specific primary antibody (HNA Table S2). Primary tumor and lung were sectioned on a cryostat and incubated at room temperature for 20 minutes. The sections were washed with PBST, blocked with 3%BSA PBST, incubated with primary antibody 1:50 in blocking buffer overnight, washed 2 times with PBST, and incubated with secondary antibody anti-Cy5/488 (Life Technologies) for 2 hours. After washing, the slides were coated with 20ul of mounting media with DAPI (Life Technologies) and HNA positive cells were counted by an observer blinded to the identity of each sample.

Molecular Biology

Western blot analysis

Protein extracts were mixed with NuPAGE LDS Sample Buffer (ThermoFisher NP0007), NuPAGE Sample Reducing Agent (ThermoFisher NP0004) and heated for 10min at 70°C. Protein (10ug/lane) was resolved on NuPAGE Novex 4-12% or 16% Bis-Tris Protein Gels, 1.0 mm, 15-well (ThermoFisher NP0323BOX) and transferred using a Mini-Trans-Blot Cell Trans-Blot semi-Dry transfer cell (BioRad) onto 0.22Um PVDF membranes (ThermoFisher 88520). Membranes were blocked with Membrane Blocking Solution (ThermoFisher 000105) for 1 hour at room temperature (22°C). The membranes were then incubated overnight at 4°C with primary antibodies (Table S2). The membranes were washed with TBS and 0.1% Tween20 (TBST), incubated with horseradish peroxidase-conjugated secondary antibody (GE Healthcare NA934) 1:15000 for 1 hour at room temperature, washed four times with TBST, and visualized with Lumina Forte Western HRP substrate (Millipore WBLUF0500).

RT-qPCR

RNA from cell lines was isolated with TRI reagent according to the manufacturer's protocol (Sigma T9424). RT-qPCR was performed following the instructions for SensiFAST cDNA Synthesis Kit and SensiFAST SYBR No-ROX Kit (Bioline BIO-65053 & BIO-98020) with CFX96 Real-Time PCR Detection System (BioRad). Relative expression level was calculated using $2^{-\Delta\Delta CT}$ method. RPL90 was used as a housekeeping gene for normalization. The sequences of primers used for qPCR analysis are listed in Table S3.

Human genomic DNA qPCR

Genomic DNA was isolated using ISOLATE II Genomic DNA Kit (Bioline BIO-52067). Quantitative PCR was performed to detect human DNA in mouse lung using SensiFAST SYBR No-ROX Kit (Bioline BIO-98020) on the CFX96 Real-Time PCR Detection System(BioRad). Standard curves

using known concentrations of pure human genomic DNA were generated to calculate absolute value. The sequences of primers used for qPCR analysis are listed in Table S3.

Digital droplet qPCR

FAM- and HEX- tagged probes that specifically bound BRAF V600 and E600 alleles, respectively, were designed as non-binding sense strands to the ddOligo HDR template (Table S3). A PCR primer was designed to span the probe-binding region. Probes and primers were synthesized by Bio-Rad. PCR reactions were assembled using premixtures of each probe (5 μ M) and primer (18 μ M), 150ng genomic DNA, FAM and HEX probes and ddPCR Supermix (Bio-Rad) according to manufacturer's protocol. Droplet generation with a QX100 Droplet Generator was performed according to the manufacturer's instructions (Bio-Rad), and the reaction was transferred into a 96-well PCR plate for standard PCR on a C1000 Thermal Cycler (Bio-Rad). The thermal cycling program conducted was: step 1, 95 °C 10 min; step 2, 94 °C 30 s; step 3, 50 °C–58 °C or 60 °C gradient 1 min; repeat steps 2 and 3 39 times; step 4, 98 °C 10 min. After the PCR was completed, the droplets were analyzed using a QX100 Droplet Reader (Bio-Rad). BRAF^{V600E} mutation percentage was calculated based on the copy number of BRAF^{V600E} per ul (x) and the copy number of BRAF^{WT} per ul (y) with the formula: percentage of BRAF^{V600E} (%) = $X/(X+Y)*100$.

Telomere length assay

The telomere length measurement assay is adapted from the published original method by Cawthon (Cawthon et al Nucleic Acids Res 2002; Lin et al Journal of Immunological Methods 2010)^{65,66}. The telomere thermal cycling profile consists of:

Cycling for T(telomic) PCR: 96°C for 1 minute; denature at 96°C for 1 second, anneal/extend at 54°C for 60 seconds, with fluorescence data collection, 30 cycles.

Cycling for S (single copy gene) PCR: PCR: 96°C for 1 minute; denature at 95°C for 15 seconds, anneal at 58°C for 1 second, extend at 72°C for 20 seconds, 8 cycles; followed by denature at

96°C for 1 second, anneal at 58°C for 1 second, extend at 72°C for 20 seconds, hold at 83°C for 5 seconds with data collection, 35 cycles.

The primers for the telomere PCR are tel1b [5'-CGGTTT(GTTTGG)5GTT-3'], used at a final concentration of 100 nM, and tel2b [5'-GGCTTG(CCTTAC)5CCT-3'], used at a final concentration of 900 nM. The primers for the single-copy gene (human beta-globin) PCR are hbg1 [5'-GCTTCTGACACAACACTGTGTTCACTAGC-3'], used at a final concentration of 300 nM, and hbg2 [5'-CACCAACTTCATCCACGTTCCACC-3'], used at a final concentration of 700 nM. The final reaction mix contains 20 mM Tris-HCl, pH 8.4; 50 mM KCl; 200 μ M each dNTP; 1% DMSO; 0.4x Syber Green I; 22 ng E. coli DNA per reaction; 0.4 Units of Platinum Taq DNA polymerase (Invitrogen) per 11 microliter reaction; ~6 ng of genomic DNA. Tubes containing 26, 8.75, 2.9, 0.97, 0.324 and 0.108ng of a reference DNA (human genomic DNA from buffy coat, Roche 11691112001) are included in each PCR run so that the quantity of targeted templates in each research sample can be determined relative to the reference DNA sample by the standard curve method. The same reference DNA is used for all PCR runs.

To control for inter-assay variability, 8 control DNA samples are included in each run, and the T/S ratio is calculated. If the T/S ratio for duplicates varies by more than 7%, the sample is re-run. The average CV for this study was 1.6%.

Plasmid construction

The lentiviral expression construct pHIV-ZsGreen was a gift from Bryan Welm and Zena Werb (Addgene plasmid # 18121)⁶⁷. pHIV-mOrange2 was constructed by digesting pHIV-zsgreen with *Bau151* and inserting the mOrange2 coding sequence. pHIV-INK4A-zsGreen, pHIV-ARF-zsGreen, pHIV-ARF-mOrange2, pHIV-INK4A-mOrange2, and pHIV-BRAFV600E-mOrange2 were all generated by inserting the indicated coding sequence into the *EcoRI* and *XbaI* sites of the indicated parental pHIV constructs. pSicoR-Ef1a-mCh-Puro was a gift from Bruce Conklin (Addgene plasmid # 31845, Salomonis, et, al. PNAS 2010). pGL410-BRN2p (BRN2 promoter

luciferase reporter) was generated by placing 2kb of sequence upstream of the BRN2 transcriptional start site into the Bgl2 and Xho1 sites. pHDR-CDKN2A was generated by amplifying 2kb left and right arms from human genomic DNA and using Cold Fusion (System Bio) to combine with the CMV promoter, EGFP ORF, and an Amp/Ori cassette. For conducting double nickase CRISPR-Cas9, we used pEN35, generously provided by Elphege Nora. pEN35 was constructed by introducing the (F&E) modification into the sgRNA backbone of px335^{32,33}. All constructed vectors are available on Addgene.

Statistics

Unpaired T-tests were used for Gaussian distributions and Mann-Whitney tests for non-Gaussian distributions or for samples of unequal variance. Exact p-values were calculated as reported by Prism 6.

Data deposition

Sequencing data used in this study are in the process of being deposited to public databases and, in the meantime, are available upon request.

McNeal et al 2020 Methods

RNA sequencing from FFPE tissue and analysis

We previously established a cohort of melanoma specimens presenting with an intact adjacent benign nevus (Shain et al., 2018). All cases had been retrieved from the UCSF Dermatopathology archive as formalin-fixed paraffin-embedded (FFPE) tissue blocks. Histopathologically distinct areas were independently evaluated by a panel of 5-8 dermatopathologists for staging and genotyped (Shain et al., 2018). Distinct tumor areas were manually micro-dissected with a scalpel under a dissection scope from unstained tissue sections following the guidance of a pathologist in order to limit stromal cell contamination.

Target exon sequencing, phylogenetic analysis, and RNA and small RNA sequencing of each tumor area were previously described (Torres et al., 2020) (Shain et al., 2018) (phs001550.v2.p1). For this study, fifteen different areas (8 malignant and 7 benign) from seven cases were selected based upon BRAF status and confidence of diagnosis. After adaptor sequences were removed, small RNA-seq reads were aligned to a human reference (hg37) with Bowtie (Langmead et al., 2009) and then small RNA reference groups (miRBase21) were counted. Differential expression analysis was performed from feature counts using DESeq2 (Love et al., 2014) with p-values adjusted for multiple testing with the Benjamini-Hochberg method (p-adj). Previously published messenger RNA sequencing datasets from *Shain et al. 2018* (Shain et al., 2018) produced from these samples were re-analyzed here with DESeq2.

RNA sequencing from cultured normal and human nevus melanocytes

MicroRNA sequencing libraries were constructed with the TailorMix Small RNA Library Preparation Kit (SeqMatic, CA) from total RNA extracted from human melanocytes using TRIzol Reagent (Thermo Fisher Cat. # 15596-026) and purified of melanin with the RNeasy Power Clean Pro Cleanup Kit (Qiagen Cat. # 13997-50). Sequencing was performed on the Illumina HiSeq2500 platform at single-end 50bp. Processing, alignment, and analysis of the reads were conducted as described above.

For mRNA sequencing of melanocytes containing microRNA mimics, synthesized mature miRNAs (name and catalog number) were nucleofected into human melanocytes as described below. Four days post-nucleofection, total RNA was collected from biological quadruplicates with TRIzol Reagent (Thermo Fisher Cat. # 15596-026). 150bp paired end sequencing was then conducted on mRNA by GeneWiz. After adaptor sequences were removed, reads were aligned to a human reference (hg37) with Bowtie2 and HTSeq was used to count reads. Differential expression analysis was performed from normalized counts using EdgeR and

LimmaVoom (Law et al., 2014) with p-values adjusted for multiple testing by the Benjamini-Hochberg method (p-adj).

Cell Derivation and Culture

Benign human melanocytic nevi were excised with informed consent from patient donors at the University of California San Francisco Dermatology clinic (San Francisco, CA) according to an Institutional Review Board- approved protocol. Patient studies were conducted in accordance with the Declaration of Helsinki. The tissue samples were microdissected to isolate nevus from surrounding normal tissue. Nevus tissue was then mechanically separated into pieces and enzymatically dissociated in a 1:1:1 mixture of DMEM:Dispase:Collagenase (DMEM Thermo Fisher Cat # 10569044 : Dispase : Collagenase)for 1 hour at 37°C. Melanocytes were further isolated from epidermal keratinocytes and fibroblasts by selective trypsinization and 5- day exposure to 10µg/mL G418 (Geneticin). BRAF status of nevus-derived melanocytes was confirmed via sanger sequencing (Quintarabio) using the primer (BRAF forward: 5'- GCA CGA CAG ACT GCA CAG GG -3'; BRAF reverse: 5'- AGC GGG CCA GCA GCT CAA TAG -3'). BRAFWT (normal) human melanocytes were isolated from de-identified and IRB consented neonatal foreskins. Foreskin tissue was incubated overnight at 4°C in Dispase and epithelia were mechanically separated from the dermis the following morning using forceps. The epithelial tissue was minced and incubated in trypsin for 10min at 37°C. Trypsin was quenched with DMEM + 10% FBS + 1% antibiotic/antimycotic and tissue was centrifuged at 300xg for 5min at room temperature. The supernatant was aspirated and the cell/tissue pellet was resuspended in Melanocyte medium (ThermoFisher, M254500) supplemented with HMGS (ThermoFisher, S0025) and plated in low volume to promote cell adherence.

The 501Mel human melanoma line (Gift from Dr. Boris Bastian, CVCL_4633) were cultured in RPMI media with 10% Fetal Bovine Serum (FBS), 1% Penicillin-Streptomycin (Pen-Strep), 1% L-Glutamine (L-Glut), and 1% Non-Essential Amino Acid (NEAA) cell culture supplement.

The human melanoma cell line HCIMel019 was derived from patient-derived xenograft (PDX) tumors propagated in mice. An HCIMel019 (P2) subcutaneous tumor was resected from a mouse and minced in tissue digestion buffer consisting of 100 μ M HEPES (Gibco, 15630-080), 5% FBS (DENVILLE, FB5001-H), 20 μ g/ml gentamicin (Gibco, 15710-064), 1x insulin (Gibco, 51500-056), and 1mg/ml collagenase IV (Gibco, 17104-019) in DMEM (Gibco, 11965-092). The tumor slurry was digested overnight in 37°C with gently shaking. The cells were filtered through a 100 μ m pore size filter (Falcon, 352360) and red blood cells were removed with RBC lysis buffer consisting of 0.5M EDTA, 0.5M KHCO₃ (Sigma, 237205), and 5M NH₄CL (Sigma, A9434). The remaining cells washed with PBS and cultured in a humidified incubator at 37°C and 5% CO₂ in Mel2 media consisting of 80%MCDB153 (Sigma, M7403), 20% L15 (Gibco, 11415-064), 2% (DENVILLE, FB5001-H), 1.68mM CaCL (Sigma, C4901), 1x insulin (Gibco, 51500-056) 5ng/ml EGF 5ng/ml (Sigma Aldrich, E9644), 15 μ g/ml Bovine Pituitary Extract (Gibco 13028-014), and 1x Pen/strep (Gibco, 15070-063).

Mimic Nucleofection

Human melanocytes were trypsinized, quenched with DMEM + 10% FBS + 1% antibiotic/antimycotic and centrifuged at 300xg. The resulting cell pellet was resuspended in R Buffer at a concentration of 10,000 cells/ μ L and 10 μ L nucleofected with mature miRIDIAN microRNA mimics (Dharmacon) (hsa-MIR211-5p C-300566-03-0005, hsa-MIR328-3p C-300695-03-0005, MIRControl 1 CN-001000-01-05, MIRControl 2 CN-002000-01-05) with a final concentration of 4 μ M. microRNA LNA inhibitors (Qiagen) (anti-hsa-MIR211-5p YI04103166-ADC, anti-hsa-MIR328-3p YI04101608-ADC, anti-MIRControl 1 YI00199006-ADC, anti-MIRControl 2 YI00199007-ADC) were also nucleofected with a final concentration of 4 μ M

nucleofected using the NEON Transfection System and protocol (Thermo Fisher Cat. # MPK5000).

Generation of Lentiviral vectors

pTRIPZ-diBRA^{FV600E} was previously described (a gift from Todd Ridky) (McNeal et al. 2015). pLVX-AURKB and pLVX-GPR3 were generated by subcloning the respective human cDNA (from Addgene # 100142 and #66350) into the [MluI and BamHI sites] of the pLVX-Che-hi3 vector (a gift Sanford Simon) (Takacs et al. 2017). pLVX-anti-MIR211-5p, pLVX-anti-MIR328-3p, and pLVX-Che-zsGreen were generated by inserting zsGreen with or without a 3'UTR into the [MluI and XbaI sites] of the pLVX-Che-hi3 vector. The 3'UTRs contained 7 tandem microRNA binding sites to both report and inhibit microRNA function, as previously described (Judson et al. 2013). ZsGreen was subcloned from pHIV-zsGreen (a gift from Bryan Welm & Zena Werb (Addgene plasmid # 18121) (Bledau et al. 2007).

Lentiviral transduction

2.75×10^6 HEK293T cells were plated in 10cm tissue culture treated dishes and grown for approximately 24 hours in DMEM supplemented with 10% FBS and 1% antibiotic-antimycotic. For each 10cm plate, 3.3 μ g of pMLV-GagPol and 1.7 μ g of pVSV-G packaging plasmids were added to 500 μ L of jetPRIME buffer (Polyplus catalog # 712-60) and briefly vortexed to mix (Takacs et al 2017). 5 μ g of lentiviral vector and 20 μ L of jetPRIME transfection reagent were then added to the jetPRIME buffer and the mixture was briefly vortexed. The mixture was then incubated for 10min at room temperature and added to the HEK293T culture media. 48 hours post-transfection, viral supernatant was collected and filtered using 0.45 μ m syringe filters (Argos). Human melanocytes seeded at 1.0×10^5 – 2.0×10^5 cells/well density in 6-well plates were then incubated in viral supernatant in the presence of 10 μ g/mL polybrene and centrifuged at 300xg for 60 min at room temperature. Transduced melanocytes were incubated for 15min at 37°C after which the viral supernatant was removed and replaced with growth media.

Transduced cells were then either selected with puromycin (company, 1 µg/mL for 5 days) or sorted for mCherry expression using a BD FACSAria II. In some experiments, cells expressing pTRIPZ-diBRAFV600E were treated with doxycycline (company, number) at indicated concentrations.

Live Quantitative Phase Imaging

Digital holographic cytometry was performed using HoloMonitor M4 imaging cytometers (Phase Holographic Imaging, Lund, Sweden) and analyzed for cell proliferation, volume and death using HStudio (v2.6.3) as previously described in Hejna et al. 2017 (Hejna et al., 2017). For normal human melanocyte proliferation experiments, cells were seeded into 6-well culture plates (Sarstedt, 83.3920) at 100,000 cells per well and either live-imaged in a standard mammalian cell incubator or serially imaged at different days as indicated. For dose response curves, 60,000 501Mel cells or 150,000 HCIMel019 cells were plated per well. The next day, media was replaced with media containing indicated concentrations of barasertib (AurK-B inhibitor; AZD1152-HQPA | AZD2811) obtained from Selleckchem.com (Catalog No. A1147 – 5 mg) and cells were imaged for 48-72 hours. Live quantitative phase imaging coupled with fluorescent imaging was conducted using the Liveocyte platform (Phasefocus, Sheffield, UK).

EdU assays

Normal human melanocytes were nucleofected with microRNA mimics, LNA microRNA inhibitors, or infected with lentiviral vectors (as above) and seeded in 48-well plates at a density of 50,000 cells/well. 4 days post-seeding EdU was added to culture media at a final concentration of 10 µM. 24 hours after the addition of EdU, EdU media was removed and cells were stained for EdU incorporation and nuclei using the Click-iT EdU Imaging Kit (Thermo Fisher Cat. # C10337) and protocol. Images of EdU and nuclei staining were taken using the Evos FL microscope and quantified using FIJI.

microRNA qRT-PCR

Total RNA was extracted from melanocytes using TRIzol Reagent (Thermo Fisher Cat. # 15596-026) and purified of melanin with the RNeasy Power Clean Pro Cleanup Kit (Qiagen Cat. # 13997-50). RNA concentrations were established by NanoDrop. microRNAs were then converted to cDNA using TaqMan Advanced miRNA Assays (Thermo Fisher Cat. # A25576). Quantitative PCR was carried out in triplicate using the TaqMan Fast Advanced Master Mix (Thermo Fisher Cat. # 4444557) and TaqMan probes corresponding to each microRNA of interest on an Applied Biosystems 7900HT machine. MIR191-5p and MIR26a-5p were used as reference controls and the delta-delta CT method was used to approximate gene expression.

Western Blotting

Protein was collected using RIPA Buffer (Thermo Fisher Cat. # 89901) supplemented with HALT Protease Inhibitor (Thermo Fisher Cat. # 87786). Protein extracts were mixed with NuPAGE LDS Sample Buffer (ThermoFisher Cat. # NP0007), NuPAGE Sample Reducing Agent (ThermoFisher Cat. # NP0004) and heated for 10 min at 90 °C. Protein was resolved on NuPAGE Novex 4–12% Bis-Tris Protein Gels, 1.0 mm, 15-well (ThermoFisher Cat. # NP0323BOX) and transferred using a Mini-Trans-Blot Cell onto 0.22µm PVDF membranes (ThermoFisher Cat. # 88520). Membranes were blocked with Membrane Blocking Solution (ThermoFisher Cat. # 000105) for 20 min. at room temperature (22 °C). The membranes were then incubated overnight at 4 °C with primary antibodies at the following dilutions: anti-HSP90 (CST Cat. # 4874) 1:1000, anti-BRAFV600E (Spring Bioscience Corp Cat. # E19292) 1:1000, anti-phosphoERK1/2 (CST Cat. # 4970) 1:1000, anti-AURKB (Abcam ab2254) 1:1000. The membranes were then washed four times with PBS and 0.5% Tween20 (TBST) and incubated with horseradish peroxidase-conjugated secondary antibody 1:2000 for 30 min. at room temperature. The membranes were then washed four times with TBST and were visualized with Lumina Forte Western HRP substrate (Millipore Cat. # WBLUF0500).

Cell cycle and apoptosis profiling

Melanocytes were trypsinized with 0.05% Trypsin (Thermo Fisher Cat# 25300120) and quenched with DMEM + 10% FBS + 1% antibiotic/antimycotic. Cells were centrifuged at 1000 rpm for 5 min. The supernatant was aspirated, and cells were resuspended in ice cold 1X PBS with 3% BSA. Cells were centrifuged for additional 1 min and cells were resuspended in 500 μ L of ice cold 70% ethanol. Cells were then fixed for 1 hr at 4°C. After fixation, cells were centrifuged for 5 min at 1000rpm and washed 1X PBS with 3% BSA. Cells were resuspended in 200 μ L of 1X PBS with 0.5mg/mL propidium iodide (PI) (BioLegend Cat# 421301) and incubated in the dark at room temperature for 30 min. PI stained cells were analyzed with BD FACs Verse.

Annexin V/PI staining was performed by trypsinizing melanocytes as above. Cells were washed with PBS and resuspended with Annexin V binding buffer (BioLegend Cat# 422201) at a concentration of 1×10^6 cell/mL. 5 μ L of APC Annexin V antibody (BioLegend Cat# 640919) and 10 μ L of PI were added. Cells were gently vortexed and incubated 15min at room temperature in the dark. 400 μ L of Annexin V Binding Buffer was added and samples were analyzed on the BD FACs Verse.

Human nevus and melanoma tissue Immunohistochemistry

The clinical samples used in the study were procured with IRB approval from the archives of the UCSF Dermatopathology and Oral Pathology Service. All samples, 11 melanoma and 11 melanocytic nevi, had received prior pathological diagnosis by board-certified dermatopathologists (THM and UEL), were de-identified and re-verified histologically (UEL). Tissue was fixed in 10% neutral-buffered formalin, routinely processed, embedded in paraffin, and stained with hematoxylin and eosin. Formalin-fixed paraffin-embedded sections of 4 μ m thickness were stained with antibodies specific for AURKB (1:400 dilution, Abcam ab2254) and

GPR3 (1:125 dilution, Abnova H00002827-M01). Review of immunohistochemical stains was performed by UEL with semiquantitative grading for GPR3 (0=none; 1=patchy positive; 2=strong positive) and AURKB (0=none; 1=rare positive; 2=scattered positive; 3= frequent positive; 4=many positive).

References:

Ablain, J., Xu, M., Rothschild, H., Jordan, R.C., Mito, J.K., Daniels, B.H., Bell, C.F., Joseph, N.M., Wu, H., Bastian, B.C., et al. (2018). Human tumor genomics and zebrafish modeling identify *SPRED1* loss as a driver of mucosal melanoma. *Science* 362, 1055–1060.

Ackermann, J., Frutschi, M., Kaloulis, K., McKee, T., Trumpp, A., and Beermann, F. (2005). Metastasizing Melanoma Formation Caused by Expression of Activated N-Ras^{Q61K} on an INK4a-Deficient Background. *Cancer Res* 65, 4005–4011.

Agarwal, V., Bell, G.W., Nam, J.-W., and Bartel, D.P. (2015). Predicting effective microRNA target sites in mammalian mRNAs. *ELife* 4, e05005.

Aguirre, A.J. (2003). Activated Kras and Ink4a/Arf deficiency cooperate to produce metastatic pancreatic ductal adenocarcinoma. *Genes & Development* 17, 3112–3126.

Aird, K.M., Zhang, G., Li, H., Tu, Z., Bitler, B.G., Garipov, A., Wu, H., Wei, Z., Wagner, S.N., Herlyn, M., et al. (2013). Suppression of Nucleotide Metabolism Underlies the Establishment and Maintenance of Oncogene-Induced Senescence. *Cell Reports* 3, 1252–1265.

Akbani, R., Akdemir, K.C., Aksoy, B.A., Albert, M., Ally, A., Amin, S.B., Arachchi, H., Arora, A., Auman, J.T., Ayala, B., et al. (2015). Genomic Classification of Cutaneous Melanoma. *Cell* 161, 1681–1696.

Andersen, J.S., Wilkinson, C.J., Mayor, T., Mortensen, P., Nigg, E.A., and Mann, M. (2003). Proteomic characterization of the human centrosome by protein correlation profiling. *Nature* 426, 570–574.

Arnaiz, O., Malinowska, A., Klotz, C., Sperling, L., Dadlez, M., Koll, F., and Cohen, J. (2009). Cildb: a knowledgebase for centrosomes and cilia. *Database* 2009.

Avidor-Reiss, T., Maer, A.M., Koundakjian, E., Polyanovsky, A., Keil, T., Subramaniam, S., and Zuker, C.S. Decoding Cilia Function: Defining Specialized Genes Required for Compartmentalized Cilia Biogenesis. 13.

Aytac, U., Konishi, T., David, H., Mendoza, S., and Miller, C.W. (1999). Rb Independent Inhibition of Cell Growth by p15INK4B. *Biochemical and Biophysical Research Communications* 262, 534–538.

Baek, D., Villén, J., Shin, C., Camargo, F.D., Gygi, S.P., and Bartel, D.P. (2008). The impact of microRNAs on protein output. *Nature* 455, 64–71.

Bagga, S., Bracht, J., Hunter, S., Massirer, K., Holtz, J., Eachus, R., and Pasquinelli, A.E. (2005). Regulation by let-7 and lin-4 miRNAs Results in Target mRNA Degradation. *Cell* 122, 553–563.

Bandyopadhyay, D., Curry, J.L., Lin, Q., Richards, H.W., Chen, D., Hornsby, P.J., Timchenko, N.A., and Medrano, E.E. (2007). Dynamic BlackwellPublishingLtd assembly of chromatin complexes during cellular senescence: implications for the growth arrest of human melanocytic nevi. 15.

- Bangs, F., and Anderson, K.V. (2017). Primary Cilia and Mammalian Hedgehog Signaling. *Cold Spring Harb Perspect Biol* 9, a028175.
- Baron, V., Adamson, E., Calogero, A., Ragona, G., and Mercola, D. The transcription factor Egr1 is a direct regulator of multiple tumor suppressors including TGFb1, PTEN, p53, and fibronectin. *Cancer Gene Therapy* 10.
- Bartel, D.P. (2004). MicroRNAs: Genomics, Biogenesis, Mechanism, and Function. *Cell* 116, 281–297.
- Bastian, B.C. (2014). The Molecular Pathology of Melanoma: An Integrated Taxonomy of Melanocytic Neoplasia. *Annu. Rev. Pathol. Mech. Dis.* 9, 239–271.
- Bastian, B.C., LeBoit, P.E., and Pinkel, D. (2000). Mutations and Copy Number Increase of HRAS in Spitz Nevi with Distinctive Histopathological Features. *The American Journal of Pathology* 157, 967–972.
- Bejar, J. (2003). Mitf expression is sufficient to direct differentiation of medaka blastula derived stem cells to melanocytes. *Development* 130, 6545–6553.
- Bell, R.E., Khaled, M., Netanel, D., Schubert, S., Golan, T., Buxbaum, A., Janas, M.M., Postolsky, B., Goldberg, M.S., Shamir, R., et al. (2014). Transcription Factor/microRNA Axis Blocks Melanoma Invasion Program by miR-211 Targeting NUA1. *Journal of Investigative Dermatology* 134, 441–451.
- Ben-Chetrit, N., Tarcic, G., and Yarden, Y. (2013). ERK-ERF-EGR1, a novel switch underlying acquisition of a motile phenotype. *Cell Adhesion & Migration* 7, 33–37.

Bennett, D.C., and Lamoreux, M.L. (2003). The Color Loci of Mice - A Genetic Century. *Pigment Cell Res* 16, 333–344.

Berezikov, E. (2011). Evolution of microRNA diversity and regulation in animals. *Nat Rev Genet* 12, 846–860.

Blacque, O.E., Perens, E.A., Boroevich, K.A., Inglis, P.N., Li, C., Warner, A., Khattra, J., Holt, R.A., Ou, G., Mah, A.K., et al. (2005). Functional Genomics of the Cilium, a Sensory Organelle. *Current Biology* 15, 935–941.

Borgenvik, T.L., Karlsvik, T.M., Ray, S., Fawzy, M., and James, N. (2017). Blue nevus-like and blue nevus-associated melanoma: a comprehensive review of the literature: Blue nevus-like/blue nevus-associated melanoma. *ANZ J Surg* 87, 345–349.

Bouwhuis, M.G., Gast, A., Figl, A., Eggermont, A.M.M., Hemminki, K., Schadendorf, D., and Kumar, R. (2010). Polymorphisms in the CD28/CTLA4/ICOS genes: role in malignant melanoma susceptibility and prognosis? *Cancer Immunol Immunother* 59, 303–312.

Burian, E.A., and Jemec, G.B.E. (2019). Eruptive Melanocytic Nevi: A Review. *Am J Clin Dermatol* 20, 669–682.

Ceol, C.J., Houvras, Y., Jane-Valbuena, J., Bilodeau, S., Orlando, D.A., Battisti, V., Fritsch, L., Lin, W.M., Hollmann, T.J., Ferré, F., et al. (2011). The histone methyltransferase SETDB1 is recurrently amplified in melanoma and accelerates its onset. *Nature* 471, 513–517.

Cerami, E., Gao, J., Dogrusoz, U., Gross, B.E., Sumer, S.O., Aksoy, B.A., Jacobsen, A., Byrne, C.J., Heuer, M.L., Larsson, E., et al. (2012). The cBio Cancer Genomics Portal: An Open Platform for Exploring Multidimensional Cancer Genomics Data: Figure 1. *Cancer Discovery* 2, 401–404.

Chattopadhyay, C., Kim, D.W., Gombos, D.S., Oba, J., Qin, Y., Williams, M.D., Esmaeli, B., Grimm, E.A., Wargo, J.A., Woodman, S.E., et al. (2016). Uveal melanoma: From diagnosis to treatment and the science in between: Uveal Melanoma Review. *Cancer* 122, 2299–2312.

Chen, B., Gilbert, L.A., Cimini, B.A., Schnitzbauer, J., Zhang, W., Li, G.-W., Park, J., Blackburn, E.H., Weissman, J.S., Qi, L.S., et al. (2013). Dynamic Imaging of Genomic Loci in Living Human Cells by an Optimized CRISPR/Cas System. *Cell* 155, 1479–1491.

Chi, S.W., Zang, J.B., Mele, A., and Darnell, R.B. (2009). Argonaute HITS-CLIP decodes microRNA–mRNA interaction maps. *Nature* 460, 479–486.

Chou, W.C., Takeo, M., Rabbani, P., Hu, H., Lee, W., Chung, Y.R., Carucci, J., Overbeek, P., and Ito, M. (2013). Direct migration of follicular melanocyte stem cells to the epidermis after wounding or UVB irradiation is dependent on Mc1r signaling. *Nat Med* 19, 924–929.

Choudhury, A., Neumann, N.M., Raleigh, D.R., and Lang, U.E. (2020). Clinical Implications of Primary Cilia in Skin Cancer. *Dermatol Ther (Heidelb)*.

Cohen, C., Zavala-Pompa, A., Sequeira, J.H., Shoji, M., Sexton, D.G., Cotsonis, G., Cerimele, F., Govindarajan, B., Macaron, N., and Arbiser, J.L. (2002). Mitogen-activated Protein Kinase Activation Is an Early Event in Melanoma Progression. *Clinical Cancer Research* 8, 3728–3733.

Cortés-González, V., Zenteno, J.C., Guzmán-Sánchez, M., Giordano-Herrera, V., Guadarrama-Vallejo, D., Ruíz-Quintero, N., and Villanueva-Mendoza, C. (2016). Tietz/Waardenburg type 2A syndrome associated with posterior microphthalmos in two unrelated patients with novel *MITF* gene mutations. *Am. J. Med. Genet.* 170, 3294–3297.

Courtois-Cox, S., Genter Williams, S.M., Reczek, E.E., Johnson, B.W., McGillicuddy, L.T., Johannessen, C.M., Hollstein, P.E., MacCollin, M., and Cichowski, K. (2006). A negative feedback signaling network underlies oncogene-induced senescence. *Cancer Cell* 10, 459–472.

Damsky, W.E., and Bosenberg, M. (2017). Melanocytic nevi and melanoma: unraveling a complex relationship. *Oncogene* 36, 5771–5792.

Damsky, W., Micevic, G., Meeth, K., Muthusamy, V., Curley, D.P., Santhanakrishnan, M., Erdelyi, I., Platt, J.T., Huang, L., Theodosakis, N., et al. (2015). mTORC1 Activation Blocks BrafV600E-Induced Growth Arrest but Is Insufficient for Melanoma Formation. *Cancer Cell* 27, 41–56.

Darnell, R.B. (2010). HITS-CLIP: panoramic views of protein–RNA regulation in living cells. *WIREs RNA* 1, 266–286.

Dhillon, A.S., Hagan, S., Rath, O., and Kolch, W. (2007). MAP kinase signalling pathways in cancer. *Oncogene* 26, 3279–3290.

Dhomen, N., Reis-Filho, J.S., da Rocha Dias, S., Hayward, R., Savage, K., Delmas, V., Larue, L., Pritchard, C., and Marais, R. (2009). Oncogenic Braf Induces Melanocyte Senescence and Melanoma in Mice. *Cancer Cell* 15, 294–303.

Di Micco, R., Fumagalli, M., Cicalese, A., Piccinin, S., Gasparini, P., Luise, C., Schurra, C., Garre', M., Giovanni Nuciforo, P., Bensimon, A., et al. (2006). Oncogene-induced senescence is a DNA damage response triggered by DNA hyper-replication. *Nature* 444, 638–642.

Díaz-Martínez, M., Benito-Jardón, L., Alonso, L., Koetz-Ploch, L., Hernando, E., and Teixidó, J. (2018). miR-204-5p and miR-211-5p Contribute to BRAF Inhibitor Resistance in Melanoma. *Cancer Res* 78, 1017–1030.

van Dierendonck, J.H., Keijzer, R., van de Velde, C.J.H., and Cornelisse, C.J. (1989). Nuclear Distribution of the Ki-67 Antigen during the Cell Cycle: Comparison with Growth Fraction in Human Breast Cancer Cells. *Cancer Res* 49, 2999.

Dupin, E., Real, C., Glavieux-Pardanaud, C., Vaigot, P., and Le Douarin, N.M. (2003). Reversal of developmental restrictions in neural crest lineages: Transition from Schwann cells to glial-melanocytic precursors in vitro. *Proceedings of the National Academy of Sciences* 100, 5229–5233.

Ebert, M.S., and Sharp, P.A. (2012). Roles for MicroRNAs in Conferring Robustness to Biological Processes. *Cell* 149, 515–524.

Elbashir, S.M., Harborth, J., Lendeckel, W., Yalcin, A., Weber, K., and Tuschl, T. (2001). Duplexes of 21-nucleotide RNAs mediate RNA interference in cultured mammalian cells. *Nature* 411, 494–498.

Erickson, C.A., and Goins, T.L. Avian neural crest cells can migrate in the dorsolateral path only if they are specified as melanocytes. 10.

Fitzpatrick, T.B., and Szabo, G. (1959). Part III: General Considerations of Skin Pigmentation: The Melanocyte: Cytology and Cytochemistry¹¹From the Division of Dermatology, University of Oregon Medical School, Portland, Oregon and the Department of Anatomy, Emory University Medical School, Atlanta, Georgia. *Journal of Investigative Dermatology* 32, 197–206.

Fleischman, R.A., Saltman, D.L., Stastny, V., and Zneimer, S. (1991). Deletion of the c-kit protooncogene in the human developmental defect piebald trait. *Proceedings of the National Academy of Sciences* 88, 10885–10889.

Forloni, M., Dogra, S.K., Dong, Y., Conte, D., Ou, J., Zhu, L.J., Deng, A., Mahalingam, M., Green, M.R., and Wajapeyee, N. (2014). miR-146a promotes the initiation and progression of melanoma by activating Notch signaling. *ELife* 3, 1–20.

Francisco, L.M., Salinas, V.H., Brown, K.E., Vanguri, V.K., Freeman, G.J., Kuchroo, V.K., and Sharpe, A.H. (2009). PD-L1 regulates the development, maintenance, and function of induced regulatory T cells. *The Journal of Experimental Medicine* 206, 3015–3029.

- Franklin, C., Livingstone, E., Roesch, A., Schilling, B., and Schadendorf, D. (2017). Immunotherapy in melanoma: Recent advances and future directions. *European Journal of Surgical Oncology (EJSO)* 43, 604–611.
- Funk, J.O., Schiller, P.I., Barrett, M.T., Wong, D.J., Kind, P., and Sander, C.A. (1998). p16INK4a expression is frequently decreased and associated with 9p21 loss of heterozygosity in sporadic melanoma. *J Cutan Pathol* 25, 291–296.
- Gao, J., Aksoy, B.A., Dogrusoz, U., Dresdner, G., Gross, B., Sumer, S.O., Sun, Y., Jacobsen, A., Sinha, R., Larsson, E., et al. (2013). Integrative Analysis of Complex Cancer Genomics and Clinical Profiles Using the cBioPortal. *Science Signaling* 6, pl1–pl1.
- Garnett, M.J., and Marais, R. (2004). Guilty as charged: B-RAF is a human oncogene. *Cancer Cell* 6, 313–319.
- Georgantas, R.W., Streicher, K., Luo, X., Greenlees, L., Zhu, W., Liu, Z., Brohawn, P., Morehouse, C., Higgs, B.W., Richman, L., et al. (2014). MicroRNA-206 induces G1 arrest in melanoma by inhibition of CDK4 and Cyclin D. *Pigment Cell Melanoma Res.* 27, 275–286.
- Glendening, J.M., Flores, F., Walker, G.J., Stone, S., Albino, A.P., and Fountain, J.W. (1995). Homozygous Loss of the p15INK4B Gene (and not the p16INK4 Gene) during Tumor Progression in a Sporadic Melanoma Patient. *Cancer Resear* 55, 5531–5535.

- Goel, V.K., Ibrahim, N., Jiang, G., Singhal, M., Fee, S., Flotte, T., Westmoreland, S., Haluska, F.S., Hinds, P.W., and Haluska, F.G. (2009). Melanocytic nevus-like hyperplasia and melanoma in transgenic BRAFV600E mice. *Oncogene* 28, 2289–2298.
- Golan, T., Parikh, R., Jacob, E., Vaknine, H., Zemser-Werner, V., Hershkovitz, D., Malcov, H., Leibou, S., Reichman, H., Sheinboim, D., et al. (2019). Adipocytes sensitize melanoma cells to environmental TGF- β cues by repressing the expression of miR-211. *Sci. Signal.* 12, 1–15.
- Grivennikov, S.I., Greten, F.R., and Karin, M. (2010). Immunity, Inflammation, and Cancer. *Cell* 140, 883–899.
- Guo, H., Ingolia, N.T., Weissman, J.S., and Bartel, D.P. (2010). Mammalian microRNAs predominantly act to decrease target mRNA levels. *Nature* 466, 835–840.
- Haferkamp, S., Tran, S.L., Becker, T.M., Scurr, L.L., Kefford, R.F., and Rizos, H. (2009). The relative contributions of the p53 and pRb pathways in oncogene-induced melanocyte senescence. *Aging* 1, 542–556.
- Halaban, R., Cheng, E., Zhang, Y., Mandigo, C.E., and Miglarese, M.R. (1998). Release of cell cycle constraints in mouse melanocytes by overexpressed mutant E2F1E132, but not by deletion of p16INK4A or p21WAF1/CIP1. *Oncogene* 16, 2489–2501.
- Hammond, S.M. (2001). Argonaute2, a Link Between Genetic and Biochemical Analyses of RNAi. *Science* 293, 1146–1150.

Hannon, G.J., and Beach, D. (1994). p15INK4B is a potential effector of TGF- β -induced cell cycle arrest. *Nature* 371, 257–261.

Happle, R. (2017). Becker's Nevus and Lethal Beta-Actin Mutations. *Journal of Investigative Dermatology* 137, 1619–1621.

Hauswirth, R., Haase, B., Blatter, M., Brooks, S.A., Burger, D., Drögemüller, C., Gerber, V., Henke, D., Janda, J., Jude, R., et al. (2012). Mutations in MITF and PAX3 Cause “Splashed White” and Other White Spotting Phenotypes in Horses. *PLoS Genet* 8, e1002653.

Heilmann, S., Ratnakumar, K., Langdon, E.M., Kansler, E.R., Kim, I.S., Campbell, N.R., Perry, E.B., McMahon, A.J., Kaufman, C.K., van Rooijen, E., et al. (2015). A Quantitative System for Studying Metastasis Using Transparent Zebrafish. *Cancer Research* 75, 4272–4282.

Hejna, M., Jorapur, A., Song, J.S., and Judson, R.L. (2017). High accuracy label-free classification of single-cell kinetic states from holographic cytometry of human melanoma cells. *Sci Rep* 7, 11943.

Helfrich, B.A., Kim, J., Gao, D., Chan, D.C., Zhang, Z., Tan, A.-C., and Bunn, P.A. (2016). Barasertib (AZD1152), a Small Molecule Aurora B Inhibitor, Inhibits the Growth of SCLC Cell Lines In Vitro and In Vivo. *Molecular Cancer Therapeutics* 15, 2314–2322.

Henion, P.D., and Weston, J.A. (1997). Timing and pattern of cell fate restrictions in the neural crest lineage. *Development* 124, 4351.

Herlyn, M., Thurin, J., Balaban, G., Bannicelli, J.L., Bondi, E., Guerry, D., Nowell, P., Clark, W.H., and Koprowski, H. (1985). Characteristics of Cultured Human Melanocytes Isolated from Different Stages of Tumor Progression. *45*, 8.

Hodi, F.S., O'Day, S.J., McDermott, D.F., Weber, R.W., Sosman, J.A., Haanen, J.B., Gonzalez, R., Robert, C., Schadendorf, D., Hassel, J.C., et al. (2010). Improved Survival with Ipilimumab in Patients with Metastatic Melanoma. *N Engl J Med* *363*, 711–723.

Holst, L.M.B., Kaczkowski, B., Glud, M., Futoma-Kazmierczak, E., Hansen, L.F., and Gniadecki, R. (2011). The microRNA molecular signature of atypic and common acquired melanocytic nevi: differential expression of miR-125b and let-7c: Letter to the Editor. *Experimental Dermatology* *20*, 278–280.

Jørgensen, K., and Holm, R. (2003). Expression of Activated Extracellular Signal-Regulated Kinases 1/2 in Malignant Melanomas: Relationship with Clinical Outcome. *Clinical Cancer Research* *9*, 5325–5331.

Judson, R.L., Greve, T.S., Parchem, R.J., and Blalock, R. (2013). MicroRNA-based discovery of barriers to dedifferentiation of fibroblasts to pluripotent stem cells. *Nat Struct Mol Biol* *20*, 1227–1235.

Juhasz, I., Albelda, S.M., Elder, D.E., Murphy, G.F., Adachi, K., Herlyn, D., Valyi-Nagy, I.T., and Herlyn, M. (1993). Growth and invasion of human melanomas in human skin grafted to immunodeficient mice. *Am J Pathol* *143*, 528–537.

- Kanemaru, H., Fukushima, S., Yamashita, J., Honda, N., Oyama, R., Kakimoto, A., Masuguchi, S., Ishihara, T., Inoue, Y., Jinnin, M., et al. (2011). The circulating microRNA-221 level in patients with malignant melanoma as a new tumor marker. *Journal of Dermatological Science* 61, 187–193.
- Kaur, H., Sarma, P., Kaur, S., Kaur, H., Prajapat, M., Mahendiratta, S., Kumar, S., Thota, P., Parsad, D., and Medhi, B. (2019). Therapeutic options for management of Hori's nevus: A systematic review. *Dermatologic Therapy*.
- Keller-Melchior, R., Schmidt, R., and Piepkorn, M. (1998). Expression of the Tumor Suppressor Gene Product p16INK4 in Benign and Malignant Melanocytic Lesions. *Journal of Investigative Dermatology* 110, 932–938.
- Kim, S., Zaghloul, N.A., Bubenshchikova, E., Oh, E.C., Rankin, S., Katsanis, N., Obara, T., and Tsiokas, L. (2011). Nde1-mediated inhibition of ciliogenesis affects cell cycle re-entry. *Nat Cell Biol* 13, 351–360.
- King, R., Hayzen, B.A., Page, R.N., Googe, P.B., Zeagler, D., and Mihm, M.C. (2009). Recurrent nevus phenomenon: a clinicopathologic study of 357 cases and histologic comparison with melanoma with regression. *Mod Pathol* 22, 611–617.
- Krimpenfort, P., Quon, K.C., Mooi, W.J., Loonstra, A., and Berns, A. (2001). Loss of p16Ink4a confers susceptibility to metastatic melanoma in mice. *Nature* 413, 83–86.
- Kumar, S.M., Dai, J., Li, S., Yang, R., Yu, H., Nathanson, K.L., Liu, S., Zhou, H., Guo, J., and Xu, X. (2014). Human skin neural crest progenitor cells are susceptible to BRAFV600E-induced transformation. *Oncogene* 33, 832–841.

Lang, U.E., Cheung, C., Vldar, E.K., Swetter, S.M., and Kim, J. (2016). Loss of primary cilia correlates with cytologic severity in dysplastic melanocytic nevi: Loss of primary cilia correlates with cytologic severity. *J Cutan Pathol* 43, 113–119.

Langmead, B., Trapnell, C., Pop, M., and Salzberg, S.L. (2009). Ultrafast and memory-efficient alignment of short DNA sequences to the human genome. *Genome Biol* 10, 1–10.

Laurençon, A., Dubrulle, R., Efimenko, E., Grenier, G., Bissett, R., Cortier, E., Rolland, V., Swoboda, P., and Durand, B. (2007). Identification of novel regulatory factor X (RFX) target genes by comparative genomics in *Drosophila* species. *Genome Biol* 8, R195.

Law, C.W., Chen, Y., Shi, W., and Smyth, G.K. (2014). voom: precision weights unlock linear model analysis tools for RNA-seq read counts. *Genome Biol* 15, 1–17.

Lee, R.C., Feinbaum, R.L., and Ambros, V. (1993). The *C. elegans* heterochronic gene *lin-4* encodes small RNAs with antisense complementarity to *lin-14*. *Cell* 75, 843–854.

Leonardi, G., Falzone, L., Salemi, R., Zanghì, A., Spandidos, D., Mccubrey, J., Candido, S., and Libra, M. (2018). Cutaneous melanoma: From pathogenesis to therapy (Review). *Int J Oncol*.

Levy, C., Khaled, M., Iliopoulos, D., Janas, M.M., Schubert, S., Pinner, S., Chen, P.-H., Li, S., Fletcher, A.L., Yokoyama, S., et al. (2010). Intronic miR-211 Assumes the Tumor Suppressive Function of Its Host Gene in Melanoma. *Molecular Cell* 40, 841–849.

Lewis, B.P., Shih, I., Jones-Rhoades, M.W., Bartel, D.P., and Burge, C.B. (2003). Prediction of Mammalian MicroRNA Targets. *Cell* 115, 787–798.

Lewis, B.P., Burge, C.B., and Bartel, D.P. (2005). Conserved Seed Pairing, Often Flanked by Adenosines, Indicates that Thousands of Human Genes are MicroRNA Targets. *Cell* 120, 15–20.

Li, L., Fukunaga-Kalabis, M., Yu, H., Xu, X., Kong, J., Lee, J.T., and Herlyn, M. (2010). Human dermal stem cells differentiate into functional epidermal melanocytes. *J Cell Sci* 123, 853–860.

Lin, J.Y., and Fisher, D.E. (2007). Melanocyte biology and skin pigmentation. *Nature* 445, 843–850.

Lister, J.A., Robertson, C.P., Lepage, T., Johnson, S.L., and Raible, D.W. (1999). *nacre* encodes a zebrafish microphthalmia-related protein that regulates neural-crest-derived pigment cell fate. *Development* 126, 3757.

Liu, C., ADAMSONt, E., and Mercola, D. (1996). Transcription factor EGR-1 suppresses the growth and transformation of human HT-1080 fibrosarcoma cells by induction of transforming growth factor (8. *Proc. Natl. Acad. Sci. USA* 6.

Liu, Q., Tan, G., Levenkova, N., Li, T., Rux, J.J., Speicher, D.W., and Pierce, E.A. (2007). The Proteome of the Mouse Photoreceptor Sensory Cilium Complex*□S. *Molecular & Cellular Proteomics* 6, 1299–1317.

- Lohrum, M.A.E., Ashcroft, M., Kubbutat, M.H.G., and Vousden, K.H. (2000). Contribution of two independent MDM2-binding domains in p14ARF to p53 stabilization. *Current Biology* *10*, 539–542.
- Love, M.I., Huber, W., and Anders, S. (2014). Moderated estimation of fold change and dispersion for RNA-seq data with DESeq2. *Genome Biol* *15*, 550.
- Lu, H., Liu, S., Zhang, G., Kwong, L.N., Zhu, Y., Miller, J.P., Hu, Y., Zhong, W., Zeng, J., Wu, L., et al. (2016). Oncogenic BRAF-Mediated Melanoma Cell Invasion. *Cell Reports* *15*, 2012–2024.
- Lu, J., Getz, G., Miska, E.A., Alvarez-Saavedra, E., Lamb, J., Peck, D., Sweet-Cordero, A., Ebert, B.L., Mak, R.H., Ferrando, A.A., et al. (2005). MicroRNA expression profiles classify human cancers. *Nature* *435*, 834–838.
- Lytle, J.R., Yario, T.A., and Steitz, J.A. (2007). Target mRNAs are repressed as efficiently by microRNA-binding sites in the 5' UTR as in the 3' UTR. *Proceedings of the National Academy of Sciences* *104*, 9667–9672.
- Manchi, M., and Canzonieri, V. (2019). Atypical melanocytic lesions: a historical overview. *Pjp* *70*, 26–32.
- Marsh Durban, V., Deuker, M.M., Bosenberg, M.W., Phillips, W., and McMahon, M. (2013). Differential AKT dependency displayed by mouse models of BRAFV600E-initiated melanoma. *J. Clin. Invest.* *123*, 5104–5118.

Masaki, T., Wang, Y., DiGiovanna, J.J., Khan, S.G., Raffeld, M., Beltaifa, S., Hornyak, T.J., Darling, T.N., Lee, C.-C.R., and Kraemer, K.H. (2014). High frequency of PTEN mutations in nevi and melanomas from xeroderma pigmentosum patients. *Pigment Cell Melanoma Res.* 27, 454–464.

Mazar, J., DeYoung, K., Khaitan, D., Meister, E., Almodovar, A., Goydos, J., Ray, A., and Perera, R.J. (2010). The Regulation of miRNA-211 Expression and Its Role in Melanoma Cell Invasiveness. *PLoS ONE* 5, 1–14.

Mazar, J., Qi, F., Lee, B., Marchica, J., Govindarajan, S., Shelley, J., Li, J.-L., Ray, A., and Perera, R.J. (2016). MicroRNA 211 Functions as a Metabolic Switch in Human Melanoma Cells. *Mol. Cell. Biol.* 36, 1090–1108.

McConnell, B.B., Gregory, F.J., Stott, F.J., Hara, E., and Peters, G. (1999). Induced Expression of p16 ^{*INK4a*} Inhibits Both CDK4- and CDK2-Associated Kinase Activity by Reassortment of Cyclin-CDK-Inhibitor Complexes. *Mol. Cell. Biol.* 19, 1981–1989.

McNeal, A.S., Liu, K., Nakhate, V., Natale, C.A., Duperret, E.K., Capell, B.C., Dentchev, T., Berger, S.L., Herlyn, M., Seykora, J.T., et al. (2015). CDKN2B Loss Promotes Progression from Benign Melanocytic Nevus to Melanoma. *Cancer Discovery* 5, 1072–1085.

Melton, C., Judson, R.L., and Blelloch, R. (2010). Opposing microRNA families regulate self-renewal in mouse embryonic stem cells. *Nature* 463, 621–626.

Michaloglou, C., Vredeveld, L.C.W., Soengas, M.S., Denoyelle, C., Kuilman, T., van der Horst, C.M.A.M., Majoor, D.M., Shay, J.W., Mooi, W.J., and Peeper, D.S. (2005).

BRAFE600-associated senescence-like cell cycle arrest of human naevi. *Nature* 436, 720–724.

Mitchison, H.M., and Valente, E.M. (2017). Motile and non-motile cilia in human pathology: from function to phenotypes: Motile and non-motile ciliopathies. *J. Pathol.* 241, 294–309.

Mort, R.L., Jackson, I.J., and Patton, E.E. (2015). The melanocyte lineage in development and disease. 14.

Narita, M., Nuñez, S., Heard, E., Narita, M., Lin, A.W., Hearn, S.A., Spector, D.L., Hannon, G.J., and Lowe, S.W. (2003). Rb-Mediated Heterochromatin Formation and Silencing of E2F Target Genes during Cellular Senescence. *Cell* 113, 703–716.

Natale, C.A., Duperret, E.K., Zhang, J., Sadeghi, R., Dahal, A., O'Brien, K.T., Cookson, R., Winkler, J.D., and Ridky, T.W. (2016). Sex steroids regulate skin pigmentation through nonclassical membrane-bound receptors. *ELife* 5, e15104.

Nemlich, Y., Greenberg, E., Ortenberg, R., Besser, M.J., Barshack, I., Jacob-Hirsch, J., Jacoby, E., Eyal, E., Rivkin, L., Prieto, V.G., et al. (2013). MicroRNA-mediated loss of ADAR1 in metastatic melanoma promotes tumor growth. *J. Clin. Invest.* 123, 2703–2718.

Nishimura, E.K. (2011). Melanocyte stem cells: a melanocyte reservoir in hair follicles for hair and skin pigmentation: Melanocyte stem cells. *Pigment Cell & Melanoma Research* 24, 401–410.

Nogales-Cadenas, R., Abascal, F., Diez-Perez, J., Carazo, J.M., and Pascual-Montano, A. (2009). CentrosomeDB: a human centrosomal proteins database. *Nucleic Acids Research* 37, D175–D180.

Nonaka, D., Chiriboga, L., and Rubin, B.P. (2008). Differential expression of S100 protein subtypes in malignant melanoma, and benign and malignant peripheral nerve sheath tumors. *Journal of Cutaneous Pathology* 35, 1014–1019.

Obata, M., Lee, G.-H., Kanda, H., Kitagawa, T., and Ogawa, K. Loss of heterozygosity at loci on chromosome 4, a common genetic event during the spontaneous immortalization of mouse embryonic fibroblasts. 8.

Okamoto, N., Aoto, T., Uhara, H., Yamazaki, S., Akutsu, H., Umezawa, A., Nakauchi, H., Miyachi, Y., Saida, T., and Nishimura, E.K. (2014). A melanocyte-melanoma precursor niche in sweat glands of volar skin. *Pigment Cell Melanoma Res.* 27, 1039–1050.

Okamura, K., Hagen, J.W., Duan, H., Tyler, D.M., and Lai, E.C. (2007). The Mirtron Pathway Generates microRNA-Class Regulatory RNAs in *Drosophila*. *Cell* 130, 89–100.

Parchem, R.J., Ye, J., Judson, R.L., LaRussa, M.F., Krishnakumar, R., Blelloch, A., Oldham, M.C., and Blelloch, R. (2014). Two miRNA Clusters Reveal Alternative Paths in Late-Stage Reprogramming. *Cell Stem Cell* 14, 617–631.

Park, J.H., and Shin, C. (2014). MicroRNA-directed cleavage of targets: mechanism and experimental approaches. *BMB Reports* 47, 417–423.

Park, J.J., Diefenbach, R.J., Joshua, A.M., Kefford, R.F., Carlino, M.S., and Rizos, H. (2018). Oncogenic signaling in uveal melanoma. *Pigment Cell Melanoma Res* 31, 661–672.

Pasquinelli, A.E., Reinhart, B.J., Slack, F., Martindale, M.Q., Kuroda, M.I., Maller, B., Hayward, D.C., Ball, E.E., Degnan, B., Müller, P., et al. (2000). Conservation of the sequence and temporal expression of let-7 heterochronic regulatory RNA. *Nature* 408, 86–89.

Pavey, S.J., Cummings, M.C., Whiteman, D.C., Castellano, M., Walsh, M.D., Gabrielli, B.G., Green, A., and Hayward, N.K. (2002). Loss of p16 expression is associated with histological features of melanoma invasion. *Melanoma Research* 12.

Pazour, G.J., Dickert, B.L., Vucica, Y., Seeley, E.S., Rosenbaum, J.L., Witman, G.B., and Cole, D.G. (2000). Chlamydomonas IFT88 and Its Mouse Homologue, Polycystic Kidney Disease Gene Tg737, Are Required for Assembly of Cilia and Flagella. *The Journal of Cell Biology* 151, 709–718.

Pazour, G.J., Agrin, N., Leszyk, J., and Witman, G.B. (2005). Proteomic analysis of a eukaryotic cilium. *Journal of Cell Biology* 170, 103–113.

Pencheva, N., Tran, H., Buss, C., Huh, D., Drobnjak, M., Busam, K., and Tavazoie, S.F. (2012). Convergent Multi-miRNA Targeting of ApoE Drives LRP1/LRP8-Dependent Melanoma Metastasis and Angiogenesis. *Cell* 151, 1068–1082.

- Pérez-Guijarro, E., Day, C.-P., Merlino, G., and Zaidi, M.R. (2017). Genetically engineered mouse models of melanoma: Mouse Models of Melanoma. *Cancer* 123, 2089–2103.
- Petersson, S., Shubbar, E., Enerbäck, L., and Enerbäck, C. (2009). Expression patterns of S100 proteins in melanocytes and melanocytic lesions: *Melanoma Research* 19, 215–225.
- Pollock, P.M., Harper, U.L., Hansen, K.S., Yudt, L.M., Stark, M., Robbins, C.M., Moses, T.Y., Hostetter, G., Wagner, U., Kakareka, J., et al. (2003). High frequency of BRAF mutations in nevi. *Nat Genet* 33, 19–20.
- Porcelli, L., Guida, G., Quatrone, A.E., Cocco, T., Sidella, L., Maida, I., Iacobazzi, R.M., Ferretta, A., Stolfi, D.A., Strippoli, S., et al. (2015). Aurora kinase B inhibition reduces the proliferation of metastatic melanoma cells and enhances the response to chemotherapy. *J Transl Med* 13, 26.
- Potterf, S.B., Furumura, M., Dunn, K.J., Arnheiter, H., and Pavan, W.J. (2000). Transcription factor hierarchy in Waardenburg syndrome: regulation of MITF expression by SOX10 and PAX3. *Hum Genet* 107, 1–6.
- Prieto, V.G., and Shea, C.R. (2011). Immunohistochemistry of Melanocytic Proliferations. *Arch Pathol Lab Med* 135, 7.
- Ran, F.A., Hsu, P.D., Lin, C.-Y., Gootenberg, J.S., Konermann, S., Trevino, A.E., Scott, D.A., Inoue, A., Matoba, S., Zhang, Y., et al. (2013). Double Nicking by RNA-Guided CRISPR Cas9 for Enhanced Genome Editing Specificity. *Cell* 154, 1380–1389.

Reed, J.A., Loganzo, F., Shea, C.R., Walker, G.J., Flores, J.F., and Glendening, J.M. Loss of Expression of the p16/Cydin-dependent Kinase Inhibitor 2 Tumor. *Cancer Research* 55, 2713–2718.

Reinhart, B.J., Slack, F.J., Basson, M., Pasquinelli, A.E., Bettinger, J.C., Rougvie, A.E., Horvitz, H.R., and Ruvkun, G. (2000). The 21-nucleotide let-7 RNA regulates developmental timing in *Caenorhabditis elegans*. *Nature* 403, 901–906.

Ren, G., Feng, J., Datar, I., Yeung, A.H., Saladi, S.V., Feng, Y., de la Serna, I., and Yeung, K.C. (2012). A Micro-RNA Connection in BRAf V600E -Mediated Premature Senescence of Human Melanocytes. *International Journal of Cell Biology* 2012, 1–9.

Ridky, T.W., Chow, J.M., Wong, D.J., and Khavari, P.A. (2010). Invasive three-dimensional organotypic neoplasia from multiple normal human epithelia. *Nat Med* 16, 1450–1455.

Robinson, W., Lemon, M., Elefanty, A., Harrison-Smith, M., Markham, N., and Norris, D. (1998). Human acquired naevi are clonal. *Melanoma Research* 8, 499–503.

Rodriguez, A. (2004). Identification of Mammalian microRNA Host Genes and Transcription Units. *Genome Research* 14, 1902–1910.

Roh, M.R., Eliades, P., Gupta, S., and Tsao, H. (2015). Genetics of melanocytic nevi. *Pigment Cell Melanoma Res.* 28, 661–672.

Sahoo, A., Sahoo, S.K., Joshi, P., Lee, B., and Perera, R.J. (2019). MicroRNA-211 Loss Promotes Metabolic Vulnerability and BRAF Inhibitor Sensitivity in Melanoma. *Journal of Investigative Dermatology* 139, 167–176.

Schmiedel, J.M., Klemm, S.L., Zheng, Y., Sahay, A., Blüthgen, N., Marks, D.S., and van Oudenaarden, A. (2015). MicroRNA control of protein expression noise. *Science* 348, 128–132.

Shain, A.H., Yeh, I., Kovalyshyn, I., Sriharan, A., Talevich, E., Gagnon, A., Dummer, R., North, J., Pincus, L., Ruben, B., et al. (2015). The Genetic Evolution of Melanoma from Precursor Lesions. *N Engl J Med* 373, 1926–1936.

Shain, A.H., Joseph, N.M., Yu, R., Benhamida, J., Liu, S., Prow, T., Ruben, B., North, J., Pincus, L., Yeh, I., et al. (2018). Genomic and Transcriptomic Analysis Reveals Incremental Disruption of Key Signaling Pathways during Melanoma Evolution. *Cancer Cell* 34, 45-55.e4.

Sharma, A., Shah, S.R., Illum, H., and Dowell, J. (2012). Vemurafenib: Targeted Inhibition of Mutated BRAF for Treatment of Advanced Melanoma and Its Potential in Other Malignancies. *Drugs* 72, 2207–2222.

Shukla, G.C., Singh, J., and Barik, S. (2012). MicroRNAs: Processing, Maturation, Target Recognition and Regulatory Functions. 14.

Siegel, R.L., Miller, K.D., and Jemal, A. (2017). Cancer statistics, 2017. *CA: A Cancer Journal for Clinicians* 67, 7–30.

- Smith, E.H., Lowe, L., Harms, P.W., Fullen, D.R., and Chan, M.P. (2016). Immunohistochemical evaluation of p16 expression in cutaneous histiocytic, fibrohistiocytic and undifferentiated lesions. *J Cutan Pathol* 43, 671–678.
- Stegmaier, O.C. (1959). Natural Regression of the Melanocytic Nevus. *Journal of Investigative Dermatology* 32, 413–421.
- Steingrímsson, E., Copeland, N.G., and Jenkins, N.A. (2004). Melanocytes and the *Microphthalmia* Transcription Factor Network. *Annu. Rev. Genet.* 38, 365–411.
- Stolz, W., Abmayr, W., Schmoeckel, C., Landthaler, M., Massoudy, P., and Braun-Falco, O. (1991). Ultrastructural Discrimination Between Malignant Melanomas and Benign Nevocytic Nevi Using High-Resolution Image and Multivariate Analyses. *Journal of Investigative Dermatology* 97, 903–910.
- Stubbs, J.L., Oishi, I., Izpisua Belmonte, J.C., and Kintner, C. (2008). The forkhead protein Foxj1 specifies node-like cilia in *Xenopus* and zebrafish embryos. *Nat Genet* 40, 1454–1460.
- Su, M., Miao, F., Jiang, S., Shi, Y., Luo, L., He, X., Wan, J., Xu, S., and Lei, T. (2020). Role of the p53-TRPM1/miR-211-MMP9 axis in UVB-induced human melanocyte migration and its potential in repigmentation. *Int J Mol Med* 4478, 1–10.
- Sviderskaya, E.V. (2002). p16Ink4a in Melanocyte Senescence and Differentiation. *CancerSpectrum Knowledge Environment* 94, 446–454.

Sviderskaya, E.V., Gray-Schopfer, V.C., Hill, S.P., Smit, N.P., Evans-Whipp, T.J., Bond, J., Hill, L., Bataille, V., Peters, G., Kipling, D., et al. (2003). p16/Cyclin-Dependent Kinase Inhibitor 2A Deficiency in Human Melanocyte Senescence, Apoptosis, and Immortalization: Possible Implications for Melanoma Progression. *JNCI Journal of the National Cancer Institute* 95, 723–732.

Talve, L., Sauroja, I., Collan, Y., Punnonen, K., and Ekfors, T. Loss of expression of the p16INK4/CDKN2 gene in cutaneous malignant melanoma correlates with tumor cell proliferation and invasive stage. *Int. J. Cancer (Pred. Oncol.)* 74, 255–259.

Thomson, D.W., Bracken, C.P., Szubert, J.M., and Goodall, G.J. (2013). On Measuring miRNAs after Transient Transfection of Mimics or Antisense Inhibitors. *PLoS ONE* 8, e55214.

Topalian, S.L., Hodi, F.S., Brahmer, J.R., Gettinger, S.N., Smith, D.C., McDermott, D.F., Powderly, J.D., Carvajal, R.D., Sosman, J.A., Atkins, M.B., et al. (2012). Safety, Activity, and Immune Correlates of Anti-PD-1 Antibody in Cancer. *N Engl J Med* 366, 2443–2454.

Torres, R., Lang, U.E., Hejna, M., Shelton, S.J., Joseph, N.M., Shain, A.H., Yeh, I., Wei, M.L., Oldham, M.C., Bastian, B.C., et al. (2020). MicroRNA Ratios Distinguish Melanomas from Nevi. *Journal of Investigative Dermatology* 140, 164-173.e7.

Uribe, P., Andrade, L., and Gonzalez, S. (2006). Lack of Association between BRAF Mutation and MAPK ERK Activation in Melanocytic Nevi. *Journal of Investigative Dermatology* 126, 161–166.

- Venza, M., Visalli, M., Beninati, C., De Gaetano, G.V., Teti, D., and Venza, I. (2015). Cellular Mechanisms of Oxidative Stress and Action in Melanoma. *Oxidative Medicine and Cellular Longevity* 2015, 1–11.
- Vitiello, M., Tuccoli, A., D'Aurizio, R., Sarti, S., Giannecchini, L., Lubrano, S., Marranci, A., Evangelista, M., Peppicelli, S., Ippolito, C., et al. (2017). Context-dependent miR-204 and miR-211 affect the biological properties of amelanotic and melanotic melanoma cells. *Oncotarget* 8, 25395–25417.
- Vitiello, M., D'Aurizio, R., and Poliseno, L. (2018). Biological role of miR-204 and miR-211 in melanoma. *Oncoscience* 5, 248–251.
- Wandler, A., Riber-Hansen, R., Hager, H., Hamilton-Dutoit, S., Schmidt, H., Nielsen, B., Stougaard, M., and Steiniche, T. (2017). Quantification of microRNA-21 and microRNA-125b in melanoma tissue. *Melanoma Research* 27, 417–428.
- Wang, Y.-L., Uhara, H., Yamazaki, Y., Nikaido, T., and Saida, T. (1996). Immunohistochemical detection of CDK4 and 9 16^{INK4} proteins in cutaneous malignant melanoma. *Br J Dermatol* 134, 269–275.
- Watanabe, K., Takeda, K., Katori, Y., Ikeda, K., Oshima, T., Yasumoto, K., Saito, H., Takasaka, T., and Shibahara, S. (2000). Expression of the Sox10 gene during mouse inner ear development. *Molecular Brain Research* 84, 141–145.
- Westerhof, W. (2006). The discovery of the human melanocyte. *Pigment Cell Res* 19, 183–193.

Wigge, P.A., Jensen, O.N., Holmes, S., Souès, S., Mann, M., and Kilmartin, J.V. (1998). Analysis of the *Saccharomyces* Spindle Pole by Matrix-assisted Laser Desorption/Ionization (MALDI) Mass Spectrometry. *Journal of Cell Biology* 141, 967–977.

Wightman, B., Ha, I., and Ruvkun, G. (1993). Posttranscriptional regulation of the heterochronic gene *lin-14* by *lin-4* mediates temporal pattern formation in *C. elegans*. *Cell* 75, 855–862.

Wolfel, T., Hauer, M., Schneider, J., Serrano, M., Wolfel, C., Klehmann-Hieb, E., De Plaen, E., Hankeln, T., Meyer zum Buschenfelde, K., and Beach, D. (1995). A p16INK4a-insensitive CDK4 mutant targeted by cytolytic T lymphocytes in a human melanoma. *Science* 269, 1281.

Yamaguchi, Y., and Hearing, V.J. (2009). Physiological factors that regulate skin pigmentation. *BioFactors* 35, 193–199.

Yamaguchi, Y., and Hearing, V.J. (2014). Melanocytes and Their Diseases. *Cold Spring Harbor Perspectives in Medicine* 4, a017046–a017046.

Yeh, I., von Deimling, A., and Bastian, B.C. (2013). Clonal BRAF Mutations in Melanocytic Nevi and Initiating Role of BRAF in Melanocytic Neoplasia. *JNCI: Journal of the National Cancer Institute* 105, 917–919.

Zeng, H., Jorapur, A., Shain, A.H., Lang, U.E., Torres, R., Zhang, Y., McNeal, A.S., Botton, T., Lin, J., Donne, M., et al. (2018). Bi-allelic Loss of CDKN2A Initiates Melanoma Invasion via BRN2 Activation. *Cancer Cell* 34, 56-68.e9.

Zhang, H.S., Postigo, A.A., and Dean, D.C. (1999). Active Transcriptional Repression by the Rb–E2F Complex Mediates G1 Arrest Triggered by p16INK4a, TGF- β , and Contact Inhibition. *Cell* 97, 53–61.

Zhu, J., Woods, D., McMahon, M., and Bishop, J.M. (1998). Senescence of human fibroblasts induced by oncogenic Raf. *Genes & Development* 12, 2997–3007.

Zuo, L., Weger, J., Yang, Q., Goldstein, A.M., Tucker, M.A., Walker, G.J., Hayward, N., and Dracopoli, N.C. (1996). Germline mutations in the p16INK4a binding domain of CDK4 in familial melanoma. *Nature Genetics* 12, 97–99.

Publishing Agreement

It is the policy of the University to encourage open access and broad distribution of all theses, dissertations, and manuscripts. The Graduate Division will facilitate the distribution of UCSF theses, dissertations, and manuscripts to the UCSF Library for open access and distribution. UCSF will make such theses, dissertations, and manuscripts accessible to the public and will take reasonable steps to preserve these works in perpetuity.

I hereby grant the non-exclusive, perpetual right to The Regents of the University of California to reproduce, publicly display, distribute, preserve, and publish copies of my thesis, dissertation, or manuscript in any form or media, now existing or later derived, including access online for teaching, research, and public service purposes.

DocuSigned by:

Andrew McNeal

FC0C1536344D4A2...

Author Signature

6/3/2020

Date